2.19 Simulation of Ultrasound Fields

MD Verweij, Delft University of Technology, Delft, The Netherlands
BE Treeby, University College London, London, UK
KWA van Dongen, Delft University of Technology, Delft, The Netherlands
L Demi, Eindhoven University of Technology, Eindhoven, The Netherlands

Nomenclature

Operators

$*$	Convolution operator
∇^2	Laplacian
$\nabla_\perp^2$	Laplacian in lateral plane
$\hat{f}$	Temporal Fourier transform of f
$\tilde{f}$	Spatial Fourier transform of f
$\boldsymbol{F}_t\{\}$	Temporal Fourier transformation
$\boldsymbol{F}_t^{-1}\{\}$	Inverse temporal Fourier transformation
$\boldsymbol{F}_x\{\}$	Spatial Fourier transformation
$\boldsymbol{F}_x^{-1}\{\}$	Inverse spatial Fourier transformation
$\|\|\mathbf{a}\|\| = a$	Length of a vector $\mathbf{a}$

Parameters and Functions

b	Exponent of attenuation power law
c	Sound speed
c_0	Ambient sound speed
CFL	Courant–Friedrichs–Lewy number
D	Number of spatial dimensions
f	Frequency
$\boldsymbol{f}$	Volume density of volume force
G	Green's function
h	Spatial impulse response of transducer
$\hat{h}(x,y,z)$	Spatial propagator/point spread function
$\tilde{h}(k_x,k_y,z)$	Spectral propagator
$H(t)$	Heaviside step function
j	Imaginary unit
$k=\omega/c_0$	Wave number
$\boldsymbol{k}=(k_x,k_y,k_z)$	Wave vector
$\mathcal{L}$	Lagrangian density
m	Normalized compliance relaxation function
$\boldsymbol{n}$	Unit normal on a surface
O	Landau order symbol
p	Acoustic pressure
$\bar{p}$	Total pressure
$\tilde{\bar{p}}$	Acoustic pressure in retarded time frame
p_0	Ambient pressure
q	Volume density of volume injection rate
S	Source term
$\mathrm{sinc}(x)$	$\sin(x)/x$
t	Time coordinate
$\boldsymbol{v}$	Perturbation of particle velocity
$\bar{\boldsymbol{v}}$	Total particle velocity
$\boldsymbol{v_0}$	Stationary particle velocity
$\boldsymbol{v}_\perp$	Normal component of particle velocity
$\boldsymbol{x}=(x,y,z)$	Position vector
α	Attenuation coefficient
α_0	Coefficient of attenuation power law
β	Coefficient of nonlinearity/phase coefficient
$\delta(t)$	Dirac delta function
$\gamma=\alpha+j\beta$	Propagation coefficient
λ	Wavelength
κ_0	Ambient compressibility
ρ	Perturbation of density of mass
$\bar{\rho}$	Total density of mass
ρ_0	Ambient density of mass
$\tau=t-z/c_0$	Retarded time
ω	Angular frequency

2.19.1 Introduction

2.19.1.1 Purpose of Simulations

Ultrasound plays a steadily increasing role in diagnostic and therapeutic medicine. The ability to simulate medical ultrasound fields serves several purposes. First, the fabrication of prototypes of novel ultrasound transducers is expensive, and the experimental characterization of the emitted 3-D ultrasound field is elaborate because this requires a tremendous amount of hydrophone measurements in a water tank. The development costs may be reduced when the performance of a new transducer design can be assessed at an early stage by doing simulations. Second, imaging modalities like harmonic imaging and contrast imaging often employ intricate excitation schemes and involve ultrasound fields with a number of harmonics. To demonstrate the effectiveness of these modalities, a preliminary simulation study with medium parameters that mimic real tissue behavior is usually easier to perform than *in vitro* and *in vivo* measurements. Moreover, these simulations yield information about the ultrasound field inside the tissue, which in practice is inaccessible. Third, each treatment that is based on ultrasound heating or ultrasound ablation relies on a predefined treatment plan that provides the sequence of focal positions with corresponding insonification intensities and durations. Diffraction due to tissue heterogeneity and the generation of harmonics caused by nonlinear propagation make it hard to estimate the correct transmit settings for obtaining a desired focal position and intensity. Simulations of the ultrasound field inside a known model of the patient may offer considerable help in generating an accurate treatment plan.

For all of the purposes just mentioned, the ability to deal with sufficiently realistic situations is of prime importance. For diagnostics, the speed of the computations is relatively insignificant because simulated ultrasound fields do not yet play a role in the real-time imaging of patients. The situation may change when wave field inversion techniques are applied for the extraction of quantitative tissue data. These techniques require the repeated computation of the ultrasound field in a complex patient model. Although inversion results need not be available in real time, the simulations should be fast enough to be applicable in a clinical workflow. The same is already required for simulations in the context of therapeutic treatment planning.

2.19.1.2 Variety of Simulation Methods

There exist many methods for the simulation of ultrasound fields in a medical context. One reason that explains the multitude of methods is the large variation in the complexity of the source and the medium involved in the simulations. For example, the field of a round, single-element transducer in a homogeneous and lossless medium like water can be obtained by much simpler methods compared to the field of a phased array in a heterogeneous and attenuative medium like brain tissue. In the first case, the symmetry of the problem reduces the number of spatial dimensions to two, attenuation and dispersion need not be incorporated, and the applied method need not be able to cope with reflections. In the second case, these simplifications do not apply and a more advanced method is required for the simulations. Another reason for the variety of methods is the difference in the computation of time-domain and frequency-domain results. Moreover, various approximations may be applied to reduce the numerical effort. When the results need only be accurate near the axis of the ultrasound beam, one may, for instance, apply the paraxial approximation, and when reflections are not important, forward stepping methods may be applied. Finally, the variety is enlarged by the difference between methods for the simulation of linear wave fields and those for the simulation of nonlinear wave fields. In the linear case, the principle of superposition is valid, and this allows the straightforward use of integral transformations like the Fourier transformation and the Laplace transformation, and integral equation methods like Green's function methods and boundary element methods. In the nonlinear case, the superposition principle no longer holds, and simulation methods have to cope with the fact that many approaches that apply for linear acoustics may no longer be used.

2.19.1.3 Scales Involved in Modeling and Simulation

Like all acoustic waves, ultrasound waves propagate in an acoustic medium and consist of the collective motion of microscopic particles that constitute this medium. Although the microscopic interactions between individual particles may be described by simple laws, it is neither feasible nor necessary to compose an acoustic wave field from the individual particle motions at the microscopic level. Instead, it is commonly assumed that acoustic phenomena occur as an average behavior that is observed at the macroscopic scale and that this behavior may be described by quantities that vary (piecewise) continuously with position. This is the so-called continuum hypothesis. The macroscopic quantities are obtained by averaging over a representative elementary domain that is small compared to the scale on which the macroscopic quantities will change but large enough to contain so many microscopic particles to give (piecewise) continuously varying averages. The huge difference between microscopic intermolecular distances (of the order 10^{-10} m in fluids) and macroscopic ultrasonic wavelengths (of the order $10^{-5} - 10^{-3}$ m in fluids) demonstrates the plausibility of the continuum hypothesis. Averaging the relevant microscopic quantities of the individual particles over the volume of a representative elementary domain yields macroscopic quantities like the particle velocity $\bar{\boldsymbol{v}}(\boldsymbol{x}, t)$ (m s^{-1}) and the density of mass $\bar{\rho}(\boldsymbol{x}, t)$ (kg m^{-3}), while the pressure $\bar{p}(\boldsymbol{x}, t)$ (Pa) follows from averaging the corresponding quantity over the surface of the elementary domain. Here, $\boldsymbol{x}$ (m) denotes position in a fixed coordinate frame, and t (s) denotes time. The symbols are fitted with a bar to indicate that these are absolute or total quantities and to distinguish these from the acoustic quantities that will be introduced later.

The relations between the macroscopic quantities follow from the basic laws of physics, for example, the conservation of mass and the conservation of linear momentum, applied to an arbitrary domain having at least the size of a representative elementary domain. In this article, it is assumed that the arbitrary domain has a fixed shape and does not move. This provides the Eulerian version of the equations of continuum mechanics, and in this context, the arbitrary domain is referred to as a control volume. The obtained equations are in the global

form, that is, they relate the integrated versions of the quantities. By applying Gauss' integral theorem and considering that the global equations must hold for any control volume, the equations can be recast into local form, that is, relating the quantities and their derivatives at a single point. These local equations are then combined into the basic equations of acoustics and are presented in Sections 2.19.2.1–2.19.2.3.

The solution of the basic equations for simple situations can be performed analytically or semianalytically, as will be further explained in Section 2.19.3. However, most practical situations require one of the numerical solution methods that will be explained in Sections 2.19.4 and 2.19.5. Numerical methods can roughly be categorized in three classes: finite-difference (FD) methods, finite-element (FE) methods, and integral equation (IE) methods. FD methods use the local basic equations and replace the mathematical differentiations by numerical finite differences. FE methods integrate a weighted version of the local basic equations over the computational domain. This is discretized into finite volume elements in which the quantities are approximated by simple expansion functions. IE methods express the solution of the actual problem in terms of the analytic solution that holds in a simple background medium. This leads to an integral equation that is discretized by subdividing the integration domain into finite-sized volume elements.

With any numerical method, the acoustic wave field is evaluated on the scale of the numerical discretization. In practice, the numerical discretization ranges from two to several tens of steps per spatial wavelength or temporal period, depending on the applied numerical method. To summarize, Figure 1 shows the entire chain of scales used to translate the behavior of microscopic particles into the discrete numerical representation that is used to simulate the macroscopic ultrasound field.

2.19.1.4 Acoustic Quantities

An acoustic wave consists of the propagation of a disturbance of the macroscopic acoustic quantities from their static values. The quantities of interest are therefore the differences between the actual total quantities and the quantities in the absence of the acoustic wave, that is, in the ambient condition. In view of this, the acoustic pressure $p(\boldsymbol{x},t)$ is defined as

$$p(\boldsymbol{x},t) = \bar{p}(\boldsymbol{x},t) - p_0 \qquad [1]$$

where $\bar{p}(\boldsymbol{x},t)$ is the total acoustic pressure introduced earlier and p_0 is the hydrostatic pressure in the case of fluids or the atmospheric pressure in the case of gases. Likewise, the perturbation of the density of mass is

$$\rho(\boldsymbol{x},t) = \bar{\rho}(\boldsymbol{x},t) - \rho_0 \qquad [2]$$

In the case of the particle velocity,

$$\boldsymbol{v}(\boldsymbol{x},t) = \bar{\boldsymbol{v}}(\boldsymbol{x},t) - \boldsymbol{v}_0 \qquad [3]$$

where the static value $\boldsymbol{v}_0$ is the stationary particle velocity, which for a medium without flow is zero. In most practical situations, the disturbances are relatively small and are considered to be small-signal quantities.

2.19.1.5 Transformed Quantities

To aid the analysis or numerical computation, the acoustic quantities will often be subjected to a temporal or spatial Fourier transformation. Throughout this article, the following conventions will be used. The temporal Fourier transformation of a function $f(t)$ is defined by

$$\hat{f}(\omega) = F_t\{f(t)\} = \int_{-\infty}^{\infty} f(t)\exp(-j\omega t)\,\mathrm{d}t \qquad [4]$$

where ω is the temporal angular frequency. The inverse transformation is

$$f(t) = F_t^{-1}\left\{\hat{f}(\omega)\right\} = \frac{1}{2\pi}\int_{-\infty}^{\infty} \hat{f}(\omega)\exp(j\omega t)\,\mathrm{d}\omega \qquad [5]$$

The spatial Fourier transformation of a function $f(x)$ is defined by

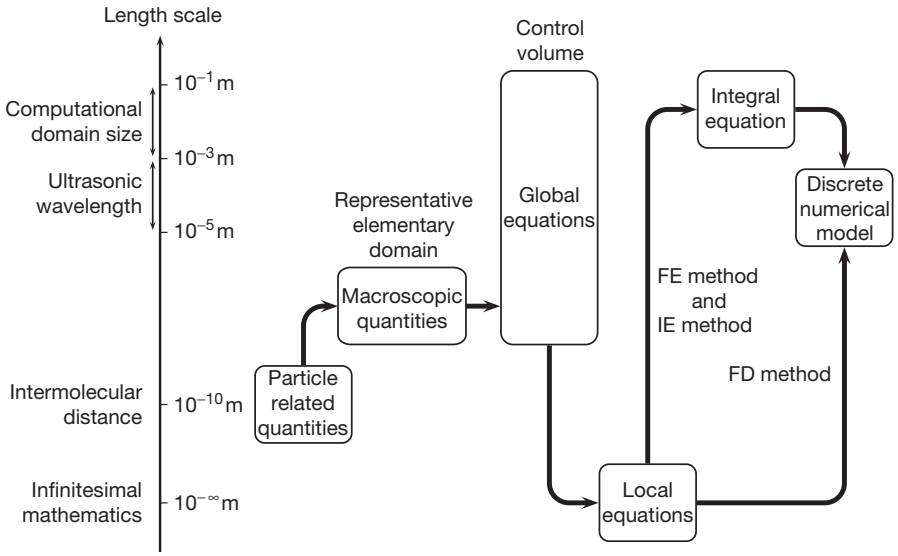

Figure 1 The different scales that are applied on the route from microscopic particle behavior to the discrete numerical model of the acoustic wave field.

$$\tilde{f}(k) = F_x\{f(x)\} = \int_{-\infty}^{\infty} f(x)\exp(jkx)\,\mathrm{d}k \qquad [6]$$

where k is the spatial angular frequency. The inverse transformation is

$$f(x) = F_x^{-1}\left\{\tilde{f}(k)\right\} = \frac{1}{2\pi}\int_{-\infty}^{\infty} \tilde{f}(k)\exp(-jkx)\,\mathrm{d}k \qquad [7]$$

These transformations can be evaluated numerically by invoking fast Fourier transformation (FFT) routines from numerical packages like MATLAB. When using these routines for evaluating the expressions from this article, one should take care that the same convention for the sign in the exponential function is used.

2.19.2 Basic Acoustic Equations

This section describes the basic equations of acoustic wave propagation. These equations give the local relations that physics imposes on the basic quantities of the acoustic wave field. Mathematically, the basic acoustic equations, together with appropriate boundary conditions, form a complete system of equations that may be solved by an appropriate numerical method. The basic acoustic equations will first be presented for a lossless, homogeneous, and source-free part of the medium, and later on, discussion will be given on how losses, heterogeneities, and sources may be accounted for. As mentioned in **Section 2.19.1.3**, all equations in this article will be given in their Eulerian form. Much of the theory presented in this section can also be found in books by authors like Pierce (1989), De Hoop (1995), and Temkin (2001) about acoustics in general; Hamilton and Blackstock (2008) about nonlinear acoustics; and Cobbold (2007) about medical ultrasound.

2.19.2.1 General Equations

The following basic equations for the total quantities $\bar{p} = \bar{p}(\boldsymbol{x}, t)$, $\bar{\rho} = \bar{\rho}(\boldsymbol{x}, t)$, and $\bar{\boldsymbol{v}} = \bar{\boldsymbol{v}}(\boldsymbol{x}, t)$ serve as the foundation for all acoustic field simulations: the continuity equation, the equation of motion, and the state equation of the medium. The entropy variable will be suppressed in the equations because, in the absence of losses and for the frequencies involved with medical ultrasound, the isentropic condition applies, that is, the entropy stays constant (Pierce, 1989, 34–36).

The continuity equation is

$$\frac{\partial\bar{\rho}}{\partial t} + \bar{\boldsymbol{v}}\cdot\nabla\bar{\rho} + \bar{\rho}\nabla\cdot\bar{\boldsymbol{v}} = 0 \qquad [8]$$

which expresses the conservation of mass. In the lossless and isentropic case, the equation of motion is the Euler equation:

$$\bar{\rho}\left[\frac{\partial\bar{\boldsymbol{v}}}{\partial t} + (\bar{\boldsymbol{v}}\cdot\nabla)\bar{\boldsymbol{v}}\right] = -\nabla\bar{p} \qquad [9]$$

This equation represents the conservation of linear momentum. The state equation provides the relation between the pressure $\bar{p}$ and the density of mass $\bar{\rho}$ and describes the behavior of the medium. Although different formulations exist, the Taylor expansion

$$\bar{p}(\bar{\rho}) = p_0 + \left(\frac{\partial\bar{p}}{\partial\bar{\rho}}\right)_0(\bar{\rho}-\rho_0) + \frac{1}{2!}\left(\frac{\partial^2\bar{p}}{\partial\bar{\rho}^2}\right)_0(\bar{\rho}-\rho_0)^2 + \frac{1}{3!}\left(\frac{\partial^3\bar{p}}{\partial\bar{\rho}^3}\right)_0(\bar{\rho}-\rho_0)^3 + \cdots \qquad [10]$$

provides a general description that can capture nearly all specific forms that occur in a lossless and homogeneous medium. The subscript '0' of the partial derivatives designates that these are evaluated at the ambient state, that is, at a static density of mass ρ_0 and entropy s_0. The first derivative defines the ambient isentropic sound speed c_0 (m s^{-1}) through

$$\left(\frac{\partial\bar{p}}{\partial\bar{\rho}}\right)_0 = c_0^2 \qquad [11]$$

2.19.2.2 Nonlinear Small-Signal Equations

To find the first-order differential equations for the small-signal quantities $p = p(\boldsymbol{x},t)$ and $\boldsymbol{v} = \boldsymbol{v}(\boldsymbol{x},t)$, eqns [1]–[3] are substituted into the basic eqns [8]–[10], and the terms that only consist of static quantities are removed. Assuming that all terms of order three and higher in the small-signal quantities are sufficiently small to be discarded, the continuity equation, the equation of motion, and the state equation turn into equations that are accurate up till second order in the small-signal quantities. Next, the state equation is combined with the continuity equation, and terms of third and higher order in the small-signal quantities are again neglected. The result of these manipulations is a set of two first-order nonlinear differential equations (cf. **Chapter 2.16**, eqns [21] and [22]) derived by Aanonsen et al. (1984) and given here as

$$\nabla\cdot\boldsymbol{v} + \kappa_0\frac{\partial p}{\partial t} = \frac{\beta}{\rho_0^2 c_0^4}\frac{\partial p^2}{\partial t} + \kappa_0\frac{\partial\mathcal{L}}{\partial t} \qquad [12]$$

$$\nabla p + \rho_0\frac{\partial\boldsymbol{v}}{\partial t} = -\nabla\mathcal{L} \qquad [13]$$

Here, $\kappa_0 = 1/(\rho_0 c_0^2)$ (Pa^{-1}) is the compressibility under ambient conditions, and

$$\beta = 1 + \frac{B}{2A} \qquad [14]$$

is the coefficient of nonlinearity. Moreover, $\mathcal{L}$ denotes the Lagrangian density:

$$\mathcal{L} = \frac{1}{2}\rho_0 v^2 - \frac{1}{2}\kappa_0 p^2 \qquad [15]$$

where $v = \sqrt{\boldsymbol{v}\cdot\boldsymbol{v}}$ is the length of the vector $\boldsymbol{v}$. Further combination of these equations and again neglecting terms of order three and higher in the small quantities yields the second-order nonlinear differential equation:

$$\nabla^2 p - \frac{1}{c_0^2}\frac{\partial^2 p}{\partial t^2} = -\frac{\beta}{\rho_0 c_0^4}\frac{\partial^2 p^2}{\partial t^2} - \left(\nabla^2 + \frac{1}{c_0^2}\frac{\partial^2}{\partial t^2}\right)\mathcal{L} \qquad [16]$$

which is the lossless nonlinear wave equation for the acoustic pressure. From this equation, it is obvious that acoustic wave propagation is inherently nonlinear. As explained by Aanonsen et al. (1984), the nonlinear behavior manifests itself in both local and global (i.e., cumulative) effects. Local nonlinear effects may usually be neglected for quasiplanar, propagating waves when these are more than one wavelength away

from the source. Fortunately, this situation arises quite often, for instance, with the directional sound beams applied in medical ultrasound. In this case, the Lagrangian density may be omitted, which results in the second-order nonlinear differential equation (see Chapter 2.16, eqn [25]):

$$\nabla^2 p - \frac{1}{c_0^2}\frac{\partial^2 p}{\partial t^2} = -\frac{\beta}{\rho_0 c_0^4}\frac{\partial^2 p^2}{\partial t^2} \qquad [17]$$

This equation is known as the lossless Westervelt (1963) equation, and it often serves as the basis for simulations of nonlinear ultrasound fields in medical applications. When the Lagrangian density may not be neglected, for example, for standing waves or in the case of scattering of sound by sound, local nonlinearity might be important and the Westervelt equation is less appropriate.

2.19.2.3 Linear Small-Signal Equations

When the acoustic perturbations are sufficiently small, the effects of nonlinearity become unnoticeable. In this case, the first-order differential equations for the small-signal quantities $p=p(\boldsymbol{x},t)$ and $\boldsymbol{v}=\boldsymbol{v}(\boldsymbol{x},t)$ may be simplified by neglecting the second-order terms in eqns [12] and [13]. This yields

$$\nabla\cdot\boldsymbol{v} + \kappa_0\frac{\partial p}{\partial t} = 0 \qquad [18]$$

$$\nabla p + \rho_0\frac{\partial \boldsymbol{v}}{\partial t} = 0 \qquad [19]$$

which are the linearized first-order differential equations for the acoustic wave field. Substitution of the time derivative of eqn [18] into the divergence of eqn [19] gives

$$\nabla^2 p - \frac{1}{c_0^2}\frac{\partial^2 p}{\partial t^2} = 0 \qquad [20]$$

which is the linearized second-order wave equation for the acoustic pressure. This equation can also be obtained by directly linearizing eqn [16] or [17].

2.19.2.4 Attenuation and Dispersion

In practice, an acoustic wave will gradually lose energy during propagation. This phenomenon, called attenuation or loss, is caused by absorption and scattering. Absorption occurs because mechanical energy that is carried by the acoustic wave is irreversibly converted into other forms of energy like heat. Scattering is due to the reflection of the propagating wave in random directions by tiny particles inside the medium. Consequently, the amplitudes of the acoustic field quantities will be reduced in comparison with the lossless case. There exists a vast amount of literature about the attenuation of ultrasound in biomedical tissue. Bamber (1998, 2004) provides an extensive overview of the physical background, the measurement principles, and the literature pertaining to this topic.

2.19.2.4.1 Attenuation coefficient

The quantitative effect of attenuation is most easily explained for a homogeneous medium carrying a plane wave, that is, a wave that neither diverges nor converges and therefore does not show a decrease or increase of its acoustic field quantities due to geometric spreading or focusing. Consider a plane wave that enters a fictitious slab of material of width $\mathrm{d}x$ with amplitude $P(x)$, as indicated in Figure 2. For a slab without attenuation, the amplitude remains the same, so upon leaving the slab, it is found that $P(x+\mathrm{d}x)=P(x)$. In case of attenuation, the amplitude will change by an amount $\mathrm{d}P$ when traveling through the slab, and upon exit, it has become $P(x+\mathrm{d}x)=P(x)+\mathrm{d}P$. Because $\mathrm{d}P$ is a decrease that will be proportional to both the initial amplitude and the width of the slab, it may be written as

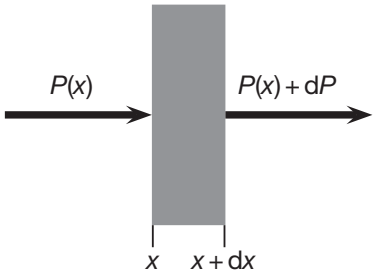

Figure 2 Change in the acoustic pressure due to attenuation in a slab of material.

$$\mathrm{d}P = -\alpha P(x)\,\mathrm{d}x \qquad [21]$$

The constant α (Np m^{-1}) is called the attenuation coefficient and represents the attenuative behavior of the medium. Often, the attenuation coefficient is expressed in decibels per meter instead of nepers per meter, with $\alpha_{\mathrm{dB}}=8.686\,\alpha_{\mathrm{Np}}$. Solving eqn [21] then yields

$$P(x) = P(0)\exp(-\alpha x) \qquad [22]$$

where $P(0)$ is the amplitude imposed by the source at $x=0$. Equation [22] shows that attenuation causes an exponential decay of the amplitude of the acoustic wave.

Below 10 MHz, in most types of biological tissue, acoustic attenuation is dominated by the effects of absorption, with only a small contribution from scattering. Although measurements on these individual phenomena have been performed (Nassiri and Hill, 1986), it is hard to obtain accurate coefficients for the separate absorption and scattering processes (Bamber, 1998, 74–76; Bamber, 2004, 146–148). Because of this difficulty, both phenomena are usually combined and only the total attenuation is considered.

Measurements show that the acoustic attenuation in biological tissues depends on the frequency of the ultrasound wave. The attenuation coefficient of most soft tissues satisfies an empirical frequency power law of the form (Bamber, 1998, 74–76; Bamber, 2004, 149; Wells, 1975)

$$\alpha = \alpha_0 f^b \qquad [23]$$

Here, α_0 (Np m MHz^{-b}) and b (1) are parameters that depend on the medium under consideration, and f (MHz) is the frequency. Virtually all tissues have $1\le b\le 2$, while below 10 MHz for most tissues, it is found that b is slightly larger than unity.

Parameters for attenuation in water, blood, and some types of human tissue are given in Table 1. More extensive data on

Table 1 Medium parameters for water, blood, and different types of human tissue, obtained from Duck (1990) for frequencies below 10 MHz

Medium type	c_0 (m s^{-1})	ρ_0 (kg m^{-3})	β (1)	α_0 (Np cm^{-1} MHz^{-b})	b (1)
Water	1482	998	3.48	2.5×10^{-4}	2.0
Blood	1584	1060	4.00	1.6×10^{-2}**	1.21**
Brain	1562	1035	4.28	6.7×10^{-2}**	1.3**
Fat	1430	928	6.14	3.4×10^{-1}**	1.0*
Liver	1578	1050	4.38	5.2×10^{-2}**	1.05
Muscle (skeletal)	1580	1041	4.72	6.3×10^{-2}**	1.0*

*Assumed value.
**Mean value.

these media may be found in Duck (1990), Bamber (1998, 2004), and Mast (2000). An extensive investigation into the attenuation of blood has also been presented by Treeby et al. (2011).

2.19.2.4.2 Thermoviscous approach

There are several ways to account for attenuation in the basic acoustic equations. One common approach is to consider the medium to be a thermoviscous fluid with shear viscosity μ (kg m^{-1} s^{-1}), bulk viscosity μ_B (kg m^{-1} s^{-1}), and thermal conductivity K (W m^{-1} K^{-1}). This approach is elaborated by Aanonsen et al. (1984) and Hamilton and Morfey (2008). With respect to the lossless case, this causes two changes. First, assuming the medium to be homogeneous, eqn [9] should be replaced by the Navier–Stokes equation for $\bar{\rho}$, $\bar{p}$, and $\bar{\boldsymbol{v}}$:

$$\bar{\rho}\left[\frac{\partial\bar{\boldsymbol{v}}}{\partial t}+(\bar{\boldsymbol{v}}\cdot\nabla)\bar{\boldsymbol{v}}\right]=-\nabla\bar{p}+\mu\nabla^2\bar{\boldsymbol{v}}+\left(\mu_B+\frac{1}{3}\mu\right)\nabla(\nabla\cdot\bar{\boldsymbol{v}}) \quad [24]$$

Second, small perturbations of the entropy and temperature should be accounted for by the inclusion of a small-signal entropy term in the state equation and the introduction of a thermodynamic equation that relates small entropy and small temperature fluctuations. As a result of these changes, eqn [16] gains an additional diffusivity term and becomes

$$\nabla^2 p-\frac{1}{c_0^2}\frac{\partial^2 p}{\partial t^2}+\frac{\delta}{c_0^4}\frac{\partial^3 p}{\partial t^3}=-\frac{\beta}{\rho_0 c_0^4}\frac{\partial^2 p^2}{\partial t^2}-\left(\nabla^2+\frac{1}{c_0^2}\frac{\partial^2}{\partial t^2}\right)\mathcal{L} \quad [25]$$

with a similar term appearing in eqns [17] and [20]. The constant

$$\delta=\frac{1}{\rho_0}\left[\frac{4}{3}\mu+\mu_B+K\left(\frac{1}{c_v}+\frac{1}{c_p}\right)\right] \quad [26]$$

is the diffusivity of sound, with c_v (J kg^{-1} K^{-1}) and c_p (J kg^{-1} K^{-1}) being the specific heats at constant volume and at constant pressure, respectively. Thermoviscous loss approximately corresponds to power-law attenuation (see eqn [23]) with $\alpha_0=2\pi^2\delta/c_0^3$ and $b=2$ provided that $\alpha\ll1/\lambda$, with $\lambda=f/c_0$ being the wavelength. A drawback of the thermoviscous loss model is that it can only describe media with quadratic ($b=2$) power-law attenuation. While water satisfies a quadratic power law and is well described by thermoviscous loss, most soft tissues have a near linear ($b\approx1$) power-law attenuation and are not well captured by the thermoviscous loss model.

2.19.2.4.3 Relaxation approach

One possibility to account for more general forms of attenuation, including frequency power laws with exponents $1<b\leq2$, is to explicitly introduce relaxation in the medium behavior. This approach represents the underlying physics in a natural way and can deal with a great variety of loss models. Relaxation can be incorporated by replacing the lossless linear equation [18] by Verweij (1995) and Demi et al. (2011)

$$\nabla\cdot\boldsymbol{v}(\boldsymbol{x},t)+\kappa_0\frac{\partial}{\partial t}[m(t)*_t p(\boldsymbol{x},t)]=0 \quad [27]$$

The function $m(t)$ (s^{-1}) describes the attenuative behavior of the medium and is called the normalized memory or compliance relaxation function, and the symbol $*_t$ denotes a temporal convolution. The relaxation function $m(t)$ may be separated according to

$$m(t)=\delta(t)+A(t) \quad [28]$$

where the Dirac delta function $\delta(t)$ represents the instantaneous medium behavior, and the relaxation function $A(t)$ represents the delayed reaction of the medium to events that happened in the past. The former term is associated with the lossless propagation of the wave, and the latter term represents the occurrence of attenuation and the corresponding dispersion. Because of its physical role, the relaxation function $A(t)$ is real-valued. Moreover, it should not 'predict the future' and it should not contribute to the instantaneous medium behavior. This implies that $A(t)$ is a causal function, that is, $A(t)=0$ for $t<0$, and it does not include a function $\delta(t)$ or its derivatives. In the nonlinear case, relaxation may be introduced by replacing the second term in eqn [12] by the second term in eqn [27]. The last term in eqn [12] need not be changed as long as the attenuation is weak, that is, when introduction of the relaxation function will only cause a small perturbation from the lossless situation. In this case, the changes in the last term of eqn [12] only generate third-order terms that may be neglected.

It is usually assumed that the inertia shows negligible relaxation effects. For this reason, eqns [13] and [19] remain unchanged.

The introduction of relaxation also causes the wave equations to change. In the linear case, eqn [20] is replaced by

$$\nabla^2 p(\boldsymbol{x},t)-\frac{1}{c_0^2}\frac{\partial^2}{\partial t^2}[m(t)*_t p(\boldsymbol{x},t)]=0 \quad [29]$$

and similar changes apply to the left-hand sides of eqns [16] and [17].

For a medium with several distinct relaxation processes with relaxation times τ_i, a suitable choice for the function $m(t)$ is

$$m(t) = \delta(t) + H(t)\sum_i k_i \exp\left(\frac{-t}{\tau_i}\right) \quad [30]$$

in which the Heaviside or unit step function is defined as $H(t) = \left\{0, \frac{1}{2}, 1\right\}$ for $\{t<0, t=0, t>0\}$. The strength of each individual relaxation process is represented by the respective constant k_i. The time-domain series in eqn [30] may be found, for example, in Cleveland et al. (1996), and a frequency-domain version is presented in Pierce (1989) and Nachman et al. (1990).

To model a medium with attenuation following a frequency power law, the relaxation function $m(t)$ may most easily be described by its counterpart $\hat{m}(\omega)$ in the frequency domain. An appropriate choice for $\hat{m}(\omega)$ is

$$\hat{m}(\omega) = \left(1 + \frac{c_0\alpha_1 (j\omega)^{b-1}}{\cos\left(\frac{1}{2}\pi b\right)}\right)^2 \quad [31]$$

where $\alpha_1 = (2\pi)^{-b}\alpha_0$ and $1<b\leq 2$. The relation between this relaxation function and the attenuation coefficient follows from its substitution into the frequency-domain counterpart of, for instance, eqn [20]. This gives

$$\nabla^2\hat{p} + \frac{\omega^2}{c_0^2}\hat{m}(\omega)\hat{p} = 0 \quad [32]$$

This equation corresponds to the Helmholtz equation:

$$\nabla^2\hat{p} - \gamma^2(\omega)\hat{p} = 0 \quad [33]$$

in which

$$\gamma(\omega) = \alpha(\omega) + j\beta(\omega) \quad [34]$$

is the propagation coefficient of the acoustic wave at angular frequency ω. The real part of γ (m^{-1}) is the attenuation coefficient α, which describes the decay of the acoustic wave, and the imaginary part is the phase coefficient β, which describes the progress of the acoustic wave. Combination of eqns [31]–[34] shows that the relaxation function in eqn [31] yields the attenuation coefficient

$$\alpha(\omega) = \alpha_1|\omega|^b \quad [35]$$

and the phase coefficient

$$\beta(\omega) = \frac{\omega}{c_0} + \alpha_1 \tan\left(\frac{1}{2}\pi b\right)\omega|\omega|^{b-1} \quad [36]$$

These are the same attenuation and phase coefficients as obtained by Szabo (1995), who also presents the time-domain counterpart of eqn [31]. For positive frequencies, the attenuation coefficient in eqn [35] is equal to $\alpha = \alpha_0 f^b$, which is exactly the frequency power law of eqn [23]. The phase coefficient in eqn [36] relates to the propagation or phase speed $c(\omega)$ of the acoustic wave, according to

$$\beta(\omega) = \frac{\omega}{c(\omega)} \quad [37]$$

From eqns [36] and [37], it may be deduced that

$$\frac{1}{c(\omega)} = \frac{1}{c_0} + \alpha_1 \tan\left(\frac{1}{2}\pi b\right)|\omega|^{b-1} \quad [38]$$

which implies that the wave propagation exhibits dispersion for $1<b<2$. Dispersion is the phenomenon where the phase speed is frequency-dependent. Attenuation and dispersion are intrinsically related (O'Donnell et al., 1981). As shown earlier, dispersion is automatically taken into account when attenuation is modeled by explicitly introducing the relaxation of the medium. Equation [38] shows that quadratic power-law losses, as, for example, encountered in thermoviscous fluids, are dispersion-free.

2.19.2.5 Heterogeneous Media

Table 1 shows that different tissues in general have different medium parameters. To simulate the propagation of ultrasound waves through a volume containing different types of tissues, a heterogeneous medium must be considered.

2.19.2.5.1 Spatially dependent medium parameters

The description of heterogeneous media involves spatially dependent parameters like the density of mass $\rho_0(\boldsymbol{x})$, speed of sound $c_0(\boldsymbol{x})$, attenuation parameters $\alpha_0(\boldsymbol{x})$ and $b(\boldsymbol{x})$, and the coefficient of nonlinearity $\beta(\boldsymbol{x})$. Spatial changes in the medium parameters cause phenomena like refraction and reflection of the acoustic wave field. Especially when there are considerable variations in the density of mass and/or the speed of sound, these phenomena may become significant and it becomes important to employ a simulation method that is capable of capturing these phenomena.

2.19.2.5.2 Boundary conditions

When there is a spatial jump in one or more acoustic medium parameters, one or more acoustic field quantities may become mathematically discontinuous at the location of the jump. In that case, one or more of the spatial derivatives that occur in the basic acoustic equations may not be defined. This implies that it is not possible to deduce the behavior of the acoustic field at the jump from the basic acoustic equations. To remedy this difficulty, additional boundary conditions are provided that describe the behavior of the acoustic field quantities at a jump in the medium parameters. Assuming that the jump appears over a surface $\mathcal{S}$ with a local unit normal vector $\boldsymbol{n}$, the boundary conditions are the following:

- The acoustic pressure p should be continuous at $\mathcal{S}$.
- The normal component $\boldsymbol{v}_\perp = (\boldsymbol{v}\cdot\boldsymbol{n})\boldsymbol{n}$ of the particle velocity should be continuous at $\mathcal{S}$.

The first condition follows from the demand that the surface $\mathcal{S}$ should only have a finite acceleration, and the second condition is imposed by the requirement that no mixing or separation of the media joining at $\mathcal{S}$ should occur.

Two special cases may occur when considering boundary conditions. For a perfectly rigid boundary $\mathcal{S}$, the boundary condition is:

- The normal component $\boldsymbol{v}_\perp = (\boldsymbol{v}\cdot\boldsymbol{n})\boldsymbol{n} = 0$ at $\mathcal{S}$,

and the pressure at the boundary should not be specified to avoid possible ambiguity. For a perfectly compliant boundary $\mathcal{S}$, the boundary condition is:

- The acoustic pressure $p = 0$ at $\mathcal{S}$,

and the normal velocity at the boundary must be left unspecified.

2.19.2.6 Sources

The features of an emitted ultrasound field depend strongly on the actual geometry of the transducer and the motion of its active parts. It is therefore paramount to incorporate the source behavior into the simulation of an ultrasound field.

2.19.2.6.1 Boundary condition representations

One way to account for the source is to consider it as being a part of the boundary of the computational domain. The action of the source may then be included by imposing the pressure or the normal particle velocity at the source surface as boundary conditions on the computational domain. The subsequent propagation of the ultrasound field is then computed with the source-free basic acoustic equations.

2.19.2.6.2 Monopole and dipole representations

A different approach to include the source is to extend the basic acoustic equations with source terms. An acoustic source may be modeled as a monopole source or a dipole source. Examples of both source types are depicted in Figure 3. A monopole source has the ability to displace the surrounding medium by changing its volume, and is represented by its volume density of volume injection rate $q(\boldsymbol{x},t)$ (s^{-1}). A dipole source has the ability to move the surrounding medium by exerting a force on it, and is represented by its volume density of volume force $\boldsymbol{f}(\boldsymbol{x},t)$ ($\mathrm{N\,m}^{-3}$). The physical effect of these manifestations of the source may easily be accounted for in the basic acoustic equations. For example, the source-free linear eqns [18] and [19] may be extended to

$$\nabla\cdot\boldsymbol{v}+\kappa_0\frac{\partial p}{\partial t}=q \qquad [39]$$

$$\nabla p+\rho_0\frac{\partial \boldsymbol{v}}{\partial t}=\boldsymbol{f} \qquad [40]$$

and substitution of eqn [39] into eqn [40] shows that the corresponding wave equation is

$$\nabla^2 p-\frac{1}{c_0^2}\frac{\partial^2 p}{\partial t^2}=\nabla\cdot\boldsymbol{f}-\rho_0\frac{\partial q}{\partial t} \qquad [41]$$

In eqns [39]–[41], the nonzero right-hand sides represent the action of the source. Similar extensions may be made to the corresponding nonlinear equations.

When a source generates a normal velocity $v_{\perp,\mathrm{source}}(\boldsymbol{x},t)$ on a part $\mathcal{A}$ of an otherwise perfectly rigid plane, its effect may be modeled by an infinitely thin volume injection source that radiates in free space. Suppose that the source plane is located at $z=0$, then the appropriate source is

$$q(\boldsymbol{x},t)=\begin{cases}2v_{\perp,\mathrm{source}}(\boldsymbol{x},t)\,\delta(z) & \text{for}\quad \boldsymbol{x}\in\mathcal{A}\\ 0 & \text{for}\quad \boldsymbol{x}\notin\mathcal{A}\end{cases} \qquad [42]$$

where $\delta(z)$ is the Dirac delta function. This monopole source will cause exactly the same acoustic wave field for $z>0$ as imposing the normal velocity $v_{\perp,\mathrm{source}}(\boldsymbol{x},t)$ on part $\mathcal{A}$ of the boundary of the computational domain. Similarly, when a source generates a pressure $p_{\mathrm{source}}(\boldsymbol{x},t)$ on a part $\mathcal{A}$ of an otherwise perfectly compliant plane, its effect may be modeled by an infinitely thin force source that radiates in free space. For a source plane that is located at $z=0$, the appropriate source is

$$\boldsymbol{f}(\boldsymbol{x},t)=\begin{cases}2p_{\mathrm{source}}(\boldsymbol{x},t)\,\delta(z) & \text{for}\quad \boldsymbol{x}\in\mathcal{A}\\ 0 & \text{for}\quad \boldsymbol{x}\notin\mathcal{A}\end{cases} \qquad [43]$$

This dipole source will cause exactly the same acoustic wave field for $z>0$ as imposing the pressure $p_{\mathrm{source}}(\boldsymbol{x},t)$ on part $\mathcal{A}$ of the boundary of the computational domain.

2.19.3 Semianalytical Methods

In relatively simple situations, explicit mathematical expressions may be obtained for the ultrasound field that is generated by a transducer. For linear wave propagation in homogeneous media, there exist integral expressions for the acoustic wave fields emitted by sources in one-, two-, and three-dimensional configurations. Because the expressions are integrals of analytical functions, these will be qualified as being semianalytical. Such expressions form the basis of some semianalytical field simulation packages. This section will deal with the semianalytical simulation of linear wave propagation. For nonlinear wave propagation, semianalytical expressions (in the form of infinite series of analytical functions) only exist in the one-dimensional case. For the semianalytical simulation of nonlinear wave propagation, the reader is referred to the chapter on nonlinear acoustics (see Chapter 2.16).

2.19.3.1 Green's Function Approach

In a homogeneous medium without attenuation, the acoustic pressure field $p=p(\boldsymbol{x},t)$ is described by the wave equation in eqn [41], that is,

$$\nabla^2 p-\frac{1}{c_0^2}\frac{\partial^2 p}{\partial t^2}=-S_{\mathrm{tr}} \qquad [44]$$

The action of the ultrasound transducer is represented by the source term

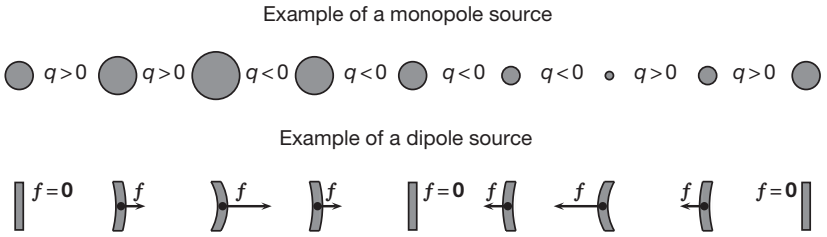

Figure 3 The operating principle of a monopole source and a dipole source.

$$S_{\text{tr}} = -\nabla\cdot\boldsymbol{f} + \rho_0 \frac{\partial q}{\partial t} \qquad [45]$$

which contains the source's density of volume force $\boldsymbol{f}=\boldsymbol{f}(\boldsymbol{x},t)$ and its volume injection rate $q=q(\boldsymbol{x},t)$. To obtain a unique solution, the wave equation must be complemented with boundary conditions that describe how the field behaves at the boundaries of the domain of interest. These conditions follow from the physics of the configuration. In the case of an infinite medium, the boundary condition is that the field should only propagate outward towards infinity. The case of an infinite medium is usually referred to as free space, and the behavior of the wave towards infinity is more specifically called a radiation condition.

The wave equation with an explicit source term may be solved in a semianalytical way by using the Green's function, as will be demonstrated later. Detailed information about the approach can be found in mathematically oriented works by authors like Barton (1995). The approach is based on the fact that eqn [44] has much resemblance with the equation

$$\nabla^2 G - \frac{1}{c_0^2}\frac{\partial^2 G}{\partial t^2} = -\delta(x)\delta(t) \qquad [46]$$

which defines the Green's function $G=G(\boldsymbol{x},t)$. The right-hand side of this equation represents an impulsive point source that acts at position $\mathbf{x}=\mathbf{0}$ and time instant $t=0$. Consequently, G is the spatiotemporal impulse response of the linear wave problem. For an infinite medium without attenuation, the analytic expressions for the Green's function in several dimensions are

$$G(x,t) = \frac{c_0}{2} H\left(t - \frac{|x|}{c_0}\right), \qquad (1\text{D}) \qquad [47]$$

$$G(\boldsymbol{x},t) = \frac{1}{2\pi\sqrt{t^2 - (||\boldsymbol{x}||/c_0)^2}} H\left(t - \frac{||\boldsymbol{x}||}{c_0}\right), \qquad (2\text{D}) \qquad [48]$$

$$G(\boldsymbol{x},t) = \frac{1}{4\pi||\boldsymbol{x}||}\delta\left(t - \frac{||\boldsymbol{x}||}{c_0}\right) \qquad (3\text{D}) \qquad [49]$$

Recall that $H(t)$ is the Heaviside step function and $\delta(t)$ is the Dirac delta pulse.

By virtue of the superposition theorem, both sides of eqn [46] may be convolved with $S_{\text{tr}}(\boldsymbol{x},t)$ over the entire space and all times. This yields

$$\nabla^2(G*_{\boldsymbol{x},t}S_{\text{tr}}) - \frac{1}{c_0^2}\frac{\partial^2}{\partial t^2}(G*_{\boldsymbol{x},t}S_{\text{tr}}) = -[\delta(\boldsymbol{x})\delta(t)]*_{\boldsymbol{x},t}S_{\text{tr}} \qquad [50]$$

where $*_{\boldsymbol{x},t}$ denotes the spatiotemporal convolution of the adjacent functions, for instance,

$$G*_{\boldsymbol{x},t}S_{\text{tr}} = \int_{-\infty}^{\infty}\iiint_{\mathbb{R}^3} G\left(\boldsymbol{x}-\boldsymbol{x}',t-t'\right)S_{\text{tr}}\left(\boldsymbol{x}',t'\right)\mathrm{d}\boldsymbol{x}'\,\mathrm{d}t' \qquad [51]$$

The convolution on the right-hand side of eqn [50] gives

$$[\delta(\boldsymbol{x})\delta(t)]*_{\boldsymbol{x},t}S_{\text{tr}} = \int_{-\infty}^{\infty}\iiint_{\mathbb{R}^3}\delta\left(\boldsymbol{x}-\boldsymbol{x}'\right)\delta\left(t-t'\right)S_{\text{tr}}\left(\boldsymbol{x}',t'\right)\mathrm{d}\boldsymbol{x}'\,\mathrm{d}t' = S_{\text{tr}}(\boldsymbol{x},t) \qquad [52]$$

Substitution of this result in eqn [50] and comparison with eqn [44] leads to the conclusion that

$$p(\boldsymbol{x},t) = G*_{\boldsymbol{x},t}S_{\text{tr}} \qquad [53]$$

Any practical source is limited in both space and time, and the result of the convolution will not change when the integrations are restricted to the spatial domain $\mathcal{D}$ occupied by the source and the temporal interval $\mathcal{T}$ during which it is active. This means that the acoustic pressure for an arbitrary source in an infinite homogeneous medium is given by the integral expression

$$p(\boldsymbol{x},t) = G*_{\boldsymbol{x},t}S_{\text{tr}} = \int_{\mathcal{T}}\iiint_{\mathcal{D}} G\left(\boldsymbol{x}-\boldsymbol{x}',t-t'\right)S_{\text{tr}}\left(\boldsymbol{x}',t'\right)\mathrm{d}\boldsymbol{x}'\,\mathrm{d}t' \qquad [54]$$

In the temporal frequency domain, a similar approach may be used to find the frequency-domain acoustic pressure $\hat{p}=\hat{p}(\boldsymbol{x},\omega)$ generated by a frequency-domain source $\hat{S}_{\text{tr}}(\boldsymbol{x},\omega)$ in an infinite homogeneous medium without attenuation. In this case, the equation that must be satisfied is

$$\nabla^2\hat{p} + k^2\hat{p} = -\hat{S}_{\text{tr}} \qquad [55]$$

in which $k=\omega/c_0$ is the wave number. The counterparts of eqns [47]–[49] are the frequency-domain Green's functions:

$$\hat{G}(x,\omega) = \frac{\exp(-jk|x|)}{2jk}, \qquad (1\text{D}) \qquad [56]$$

$$\hat{G}(\boldsymbol{x},\omega) = -\frac{j}{4}H_0^{(2)}(k||\boldsymbol{x}||), \qquad (2\text{D}) \qquad [57]$$

$$\hat{G}(\boldsymbol{x},\omega) = \frac{\exp(-jk||\boldsymbol{x}||)}{4\pi||\boldsymbol{x}||}, \qquad (3\text{D}) \qquad [58]$$

where $H_0^{(2)}$ denotes the Hankel function of the second kind and order zero.

Unlike the time-domain Green's functions, the frequency-domain Green's functions can easily be adapted to apply to an infinite homogeneous medium with attenuation. This is achieved by replacing the real wave number $k=\omega/c_0$ by the complex wave number $k(\omega)=-j\gamma(\omega)$, in which $\gamma(\omega)$ is the propagation coefficient that has been introduced in eqn [34] (Huijssen et al., 2008).

Using the appropriate Green's function, the frequency-domain acoustic pressure for an arbitrary source in a homogeneous medium is obtained as

$$\hat{p}(\boldsymbol{x},\omega) = \hat{G}*_{\boldsymbol{x}}\hat{S}_{\text{tr}} = \iiint_{\mathcal{D}}\hat{G}\left(\boldsymbol{x}-\boldsymbol{x}',\omega\right)\hat{S}_{\text{tr}}\left(\boldsymbol{x}',\omega\right)\mathrm{d}\boldsymbol{x}' \qquad [59]$$

2.19.3.2 Rayleigh Integral

As an alternative to using an explicit source term S_{tr}, the action of a transducer can also be represented by prescribing the pressure or the normal velocity that it imposes on the boundary of the computational domain. When this is the case, an alternative to the Green's function formulations in eqns [54] and [59] exists, as will be shown later for the three-dimensional case.

The conventional derivation (Cobbold, 2007; Pierce, 1989) starts with the equation for the frequency-domain acoustic pressure $\hat{p}(\boldsymbol{x})=\hat{p}(\boldsymbol{x},\omega)$

$$\nabla^2\hat{p}(\boldsymbol{x}) + k^2\hat{p}(\boldsymbol{x}) = -\hat{S}_{\text{tr}}(\boldsymbol{x}) \qquad [60]$$

and the corresponding equation for the Green's function $\hat{G}(\boldsymbol{x},\boldsymbol{x}')=\hat{G}(\boldsymbol{x},\boldsymbol{x}',\omega)$

$$\nabla^2\hat{G}\left(\boldsymbol{x},\boldsymbol{x}'\right)+k^2\hat{G}\left(\boldsymbol{x},\boldsymbol{x}'\right)=-\delta\left(\boldsymbol{x}-\boldsymbol{x}'\right) \quad [61]$$

The notation $\hat{G}(\boldsymbol{x},\boldsymbol{x}')$ is generally used to indicate the field at location $\boldsymbol{x}$ due to a point source at location $\boldsymbol{x}'$. Note that the transducer need not be located in free space and that the boundary conditions on $\hat{p}$ and $\hat{G}$ are not restricted to the radiation condition, as was the case in Section 2.19.3.1.

Multiplication of eqn [60] by $\hat{G}(\boldsymbol{x},\boldsymbol{x}')$ and eqn [61] by $\hat{p}(\boldsymbol{x})$, followed by subtraction of the results, yields

$$\begin{aligned}&\hat{G}\left(\boldsymbol{x},\boldsymbol{x}'\right)\nabla^2\hat{p}(\boldsymbol{x})-\hat{p}(\boldsymbol{x})\nabla^2\hat{G}\left(\boldsymbol{x},\boldsymbol{x}'\right)\\&\quad=\hat{p}(\boldsymbol{x})\delta\left(\boldsymbol{x}-\boldsymbol{x}'\right)-\hat{G}\left(\boldsymbol{x},\boldsymbol{x}'\right)\hat{S}_{\mathrm{tr}}(\boldsymbol{x})\end{aligned} \quad [62]$$

Next, the role of $\boldsymbol{x}$ and $\boldsymbol{x}'$ is interchanged, giving

$$\begin{aligned}&\hat{G}\left(\boldsymbol{x}',\boldsymbol{x}\right)\nabla'^2\hat{p}\left(\boldsymbol{x}'\right)-\hat{p}\left(\boldsymbol{x}'\right)\nabla'^2\hat{G}\left(\boldsymbol{x}',\boldsymbol{x}\right)\\&\quad=\hat{p}\left(\boldsymbol{x}'\right)\delta\left(\boldsymbol{x}'-\boldsymbol{x}\right)-\hat{G}\left(\boldsymbol{x}',\boldsymbol{x}\right)\hat{S}_{\mathrm{tr}}\left(\boldsymbol{x}'\right)\end{aligned} \quad [63]$$

where ∇' involves derivatives with respect to the primed coordinates. Integration with respect to $\boldsymbol{x}'$ over the domain $\mathcal{D}$ in Figure 4 results in

$$\begin{aligned}&\iiint_{\mathcal{D}}\hat{G}\left(\boldsymbol{x}',\boldsymbol{x}\right)\nabla'^2\hat{p}\left(\boldsymbol{x}'\right)-\hat{p}\left(\boldsymbol{x}'\right)\nabla'^2\hat{G}\left(\boldsymbol{x}',\boldsymbol{x}\right)\mathrm{d}\boldsymbol{x}'\\&=\iiint_{\mathcal{D}}\hat{p}\left(\boldsymbol{x}'\right)\delta\left(\boldsymbol{x}'-\boldsymbol{x}\right)-\hat{G}\left(\boldsymbol{x}',\boldsymbol{x}\right)\hat{S}_{\mathrm{tr}}\left(\boldsymbol{x}'\right)\mathrm{d}\boldsymbol{x}'\end{aligned} \quad [64]$$

Using Green's second identity, the left-hand side may be recast into an integral over the boundary $\mathcal{S}=\mathcal{S}_0+\mathcal{S}_\infty$ of $\mathcal{D}$. The right-hand side may be simplified in view of the sifting property of the Dirac delta function and the fact that $\hat{S}_{\mathrm{tr}}=0$ inside $\mathcal{D}$ because the source is only represented by a boundary condition on $\mathcal{S}$. It is thus found that

$$\hat{p}(\boldsymbol{x})=\oiint_{\mathcal{S}}\left[\hat{G}\left(\boldsymbol{x}',\boldsymbol{x}\right)\nabla'\hat{p}\left(\boldsymbol{x}'\right)-\hat{p}\left(\boldsymbol{x}'\right)\nabla'\hat{G}\left(\boldsymbol{x}',\boldsymbol{x}\right)\right]\cdot\boldsymbol{n}\,\mathrm{d}\boldsymbol{x}' \quad [65]$$

where $\boldsymbol{n}$ is the outward pointing unit normal on $\mathcal{S}$. The surface $\mathcal{S}$ consists of the source plane $\mathcal{S}_0$ containing the finite source aperture $\mathcal{A}$ and a hemispherical surface $\mathcal{S}_\infty$ at infinity. On $\mathcal{S}_\infty$, the same radiation condition applies as in the free-space case. The integration over $\mathcal{S}_\infty$ yields a zero contribution because for an increasing radius R of the hemisphere, the integrand in eqn [65] decreases faster than the increase of the hemispherical surface area.

Next, it is assumed that $\mathcal{S}_0$ is a rigid boundary with a prescribed normal surface velocity $\hat{\boldsymbol{v}}\cdot\boldsymbol{n}=-\hat{v}_\perp$ on $\mathcal{A}$ (taking $\hat{v}_\perp$ positive inward) and $\hat{\boldsymbol{v}}\cdot\boldsymbol{n}=0$ outside $\mathcal{A}$. With the aid of eqn [19], the boundary conditions for the normal particle velocity translate into the boundary conditions $\left[\nabla'\hat{p}\left(\boldsymbol{x}'\right)\right]\cdot\boldsymbol{n}=j\omega\rho_0\hat{v}_\perp$ on $\mathcal{A}$ and $\left[\nabla'\hat{p}\left(\boldsymbol{x}'\right)\right]\cdot\boldsymbol{n}=0$ outside $\mathcal{A}$ for the acoustic pressure. In the current context, $\hat{G}\left(\boldsymbol{x}',\boldsymbol{x}\right)$ must also satisfy similar boundary conditions. As long as $\boldsymbol{x}\neq\boldsymbol{x}'$, the Green's function will not have its source point on $\mathcal{S}_0$ and the boundary condition is that $\left[\nabla'\hat{G}\left(\boldsymbol{x}',\boldsymbol{x}\right)\right]\cdot\boldsymbol{n}=0$ everywhere on $\mathcal{S}_0$. Here, it is important to realize that, as far as the Green's function is concerned, the swapping of $\boldsymbol{x}$ and $\boldsymbol{x}'$ implies that $\boldsymbol{x}'$ has the role of observation point and $\boldsymbol{x}$ has the role of source point. The condition $\boldsymbol{x}\neq\boldsymbol{x}'$ is satisfied as long as $p(\boldsymbol{x})$ is not evaluated in the source plane. The facts just mentioned make that eqn [65] turns into

$$\hat{p}(\boldsymbol{x})=j\omega\rho_0\iint_{\mathcal{A}}\hat{G}\left(\boldsymbol{x}',\boldsymbol{x}\right)\hat{v}_\perp\left(\boldsymbol{x}'\right)\mathrm{d}\boldsymbol{x}' \quad [66]$$

To find the explicit Green's function, the swapping of $\boldsymbol{x}$ and $\boldsymbol{x}'$ is discarded for a while. In case of a flat, rigid boundary, the Green's function $\hat{G}(\boldsymbol{x},\boldsymbol{x}')$ with boundary condition $\left[\nabla\hat{G}(\boldsymbol{x},\boldsymbol{x}')\right]\cdot\boldsymbol{n}=0$ on $\mathcal{S}_0$ may be obtained by adding the free-space Green's functions for a point source $\delta(\boldsymbol{x}-\boldsymbol{x}')$, and for its mirror source $\delta(\boldsymbol{x}-\boldsymbol{x}'')$, see Figure 5. The resulting Green's function is

$$\hat{G}\left(\boldsymbol{x},\boldsymbol{x}'\right)=\frac{\exp\left(-jk||\boldsymbol{x}-\boldsymbol{x}'||\right)}{4\pi||\boldsymbol{x}-\boldsymbol{x}'||}+\frac{\exp\left(-jk||\boldsymbol{x}-\boldsymbol{x}''||\right)}{4\pi||\boldsymbol{x}-\boldsymbol{x}''||} \quad [67]$$

When $\boldsymbol{x}'$ is located on $\mathcal{S}_0$, as is the case in eqn [66], it will happen that $\boldsymbol{x}'=\boldsymbol{x}''$. In this case, eqn [67] yields

$$\hat{G}\left(\boldsymbol{x},\boldsymbol{x}'\right)=\frac{\exp\left(-jk||\boldsymbol{x}-\boldsymbol{x}'||\right)}{2\pi||\boldsymbol{x}-\boldsymbol{x}'||} \quad [68]$$

which shows that as far as the actual Green's function is concerned, the swapping of $\boldsymbol{x}$ and $\boldsymbol{x}'$ is irrelevant because $\hat{G}(\boldsymbol{x},\boldsymbol{x}')=\hat{G}(\boldsymbol{x}',\boldsymbol{x})$. As explained by Pierce (1989, 195–199), this is a general property of Green's functions and is a manifestation of the reciprocity principle. Now, eqn [66] can be written as

$$\hat{p}(\boldsymbol{x})=j\omega\rho_0\iint_{\mathcal{A}}\frac{\exp\left(-jk||\boldsymbol{x}-\boldsymbol{x}'||\right)\hat{v}_\perp\left(\boldsymbol{x}'\right)}{2\pi||\boldsymbol{x}-\boldsymbol{x}'||}\,\mathrm{d}\boldsymbol{x}' \quad [69]$$

The time-domain equivalent of this equation is found by using the known identities for the Fourier transformation from Section 2.19.1.5, giving

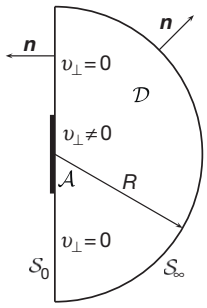

Figure 4 Configuration for the analysis of the acoustic pressure due to a source with aperture $\mathcal{A}$. The figure applies to the specific case of a rigid boundary $\mathcal{S}_0$ with a prescribed normal velocity on $\mathcal{A}$.

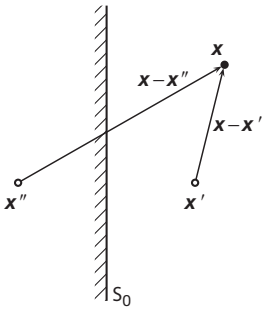

Figure 5 Point source and its mirror image in the plane $\mathcal{S}_0$. The combined field of both sources has a zero normal velocity at $\mathcal{S}_0$.

$$p(\boldsymbol{x},t)=\rho_0\int\int_{\mathcal{A}}\frac{1}{2\pi||\boldsymbol{x}-\boldsymbol{x}'||}\frac{\partial}{\partial t}v_\perp\left(\boldsymbol{x}',t-\frac{||\boldsymbol{x}-\boldsymbol{x}'||}{c_0}\right)\mathrm{d}\boldsymbol{x}' \quad [70]$$

In recognition of the first derivation of a similar result by Rayleigh (1945, 107), this expression is called the Rayleigh integral.

The same expression may be found in an alternative and more direct way by combining eqn [42] with eqns [45], [49], and [59]. In this case, the free-space Green's function may be used because the boundary condition in the source plane is implied by the use of the volume source. This approach is briefly discussed by Pierce (1989, 214).

A special case arises for nonapodized sources, that is, sources with a normal surface velocity that is independent of the position. Many single-element transducers belong to this class of sources. In this case,

$$v_\perp(\boldsymbol{x},t)=v_\perp(t) \quad [71]$$

and eqn [70] may be written as

$$p(\boldsymbol{x},t)=h(\boldsymbol{x},t)*_t\left(\rho_0\frac{\partial v_\perp(t)}{\partial t}\right) \quad [72]$$

where

$$h(\boldsymbol{x},t)=\int\int_{\mathcal{A}}\frac{1}{2\pi||\boldsymbol{x}-\boldsymbol{x}'||}\delta\left(t-\frac{||\boldsymbol{x}-\boldsymbol{x}'||}{c_0}\right)\mathrm{d}\boldsymbol{x}' \quad [73]$$

is called the spatial impulse response of the transducer (Harris, 1981; Stepanishen, 1971).

An alternative to eqns [69] and [70] exists for the case in which $\mathcal{S}_0$ is a compliant boundary with a prescribed surface pressure $\hat{p}$ on $\mathcal{A}$ and $p=0$ outside $\mathcal{A}$. Applying the proper boundary conditions, a similar analysis as presented earlier yields

$$\hat{p}(\boldsymbol{x})\approx\frac{j\omega}{c_0}\int\int_{\mathcal{A}}\frac{\exp(-jk||\boldsymbol{x}-\boldsymbol{x}'||)\hat{p}(\boldsymbol{x}')}{2\pi||\boldsymbol{x}-\boldsymbol{x}'||}\cos(\varphi)\,\mathrm{d}\boldsymbol{x}' \quad [74]$$

in which φ is the angle between $\boldsymbol{x}-\boldsymbol{x}'$ and the normal on the transducer surface. The approximation is valid provided that $||\boldsymbol{x}-\boldsymbol{x}'||\gg 1/k$. The time-domain counterpart of eqn [74] is

$$p(\boldsymbol{x},t)\approx\frac{1}{c_0}\int\int_{\mathcal{A}}\frac{1}{2\pi||\boldsymbol{x}-\boldsymbol{x}'||}\frac{\partial}{\partial t}p\left(\boldsymbol{x}',t-\frac{||\boldsymbol{x}-\boldsymbol{x}'||}{c_0}\right)\cos(\varphi)\,\mathrm{d}\boldsymbol{x}' \quad [75]$$

2.19.3.3 Field II

Developed in the 1990s, Field II is probably still the most employed program for the simulation of medical ultrasound. It can be used for tasks ranging from the computation of acoustic fields from simple transducers to the assessment of intricate imaging scenarios. The theoretical background of the program is described in Jensen and Svendsen (1992), and a description of the structure and features may be found in Jensen (2001) and Jensen (2011). Field II assumes that the propagation medium consists of a homogeneous, linear background with point scatterers, and it only provides an attenuation model with a linear frequency dependence. Therefore, Field II is not a logical choice for simulations involving large-scale medium heterogeneities, general power-law attenuation, or nonlinear propagation. The spatial impulse response in eqn [73] forms the theoretical foundation of the program. The computations are performed in a core program that has been written in C. The C program communicates with MATLAB through a number of m-functions, which perform one of the following tasks:

- Initializing the program
  These functions perform the start-up and termination of the Field II program and set parameters like the speed of sound, attenuation, and the temporal sampling rate.
- Defining the transducer
  Functions are available for defining a score of transducer types, for example, single-element, 1-D, and 2-D arrays (either flat or curved) and associated features like focusing, apodization (tapering), and excitation.
- Calling for a specific type of simulation
  These functions start the actual computation. General options are calculation of the spatial impulse response, emitted field, or pulse-echo field.

By using MATLAB as a front end, a standardized way of sending data to and collecting data from the program has been achieved. Moreover, the approach allows the user to employ the features of MATLAB for preprocessing tasks such as the generation of apodization and dynamic focusing settings or the rendering of a distribution of point scatterers, and for postprocessing tasks like signal processing and visualization of the computed data.

2.19.3.3.1 Computation of spatial impulse response

The most fundamental data that Field II can compute are the spatial impulse response $h(\boldsymbol{x},t)$ given in eqn [73]. This expression applies to a transducer in a flat, rigid wall and is exact for flat transducers. In case of a curved transducer, an additional term should be added, but this term is neglected under the assumption that the curvature is small and the transducer is large compared to the wavelength. The original procedure for computing $h(\boldsymbol{x},t)$ is described in Jensen and Svendsen (1992), and an extended version of the procedure is presented in Jensen (1999). These procedures are based on earlier work described in Stepanishen (1971) and Harris (1981).

To explain the original procedure for computing the spatial impulse response as a function of t, a receive scenario is considered first. Here, it is supposed that a point source at $\boldsymbol{x}=(x,y,z)$ emits an impulsive wave at $t=0$. At time t, the emitted spherical wave front with center $\boldsymbol{x}$ will have a radius $R=c_0t$. The intersection of the wave front with the transducer surface, assumed here to be at $z=0$, will be a circular arc $\mathcal{C}(R)$ with center of curvature $\boldsymbol{x}_c=(x,y,0)$, radius of curvature $r=\sqrt{R^2-z^2}$, and endpoints that are defined by the edges of the transducer as shown in Figure 6. In reception, $\mathcal{C}(R)=\mathcal{C}(c_0t)$ holds all the points that at time t receive the emitted impulsive wave. It might therefore be expected that the total signal received by the transducer depends on the length $||\mathcal{C}(c_0t)||$ of the circular arc $\mathcal{C}(c_0t)$. This is indeed the case, as follows from integration over the transducer surface of the time-domain equivalent of the Green's function $\hat{G}(\boldsymbol{x}',\boldsymbol{x})$ from eqn [68]. This gives the so-called spatial impulse response in reception:

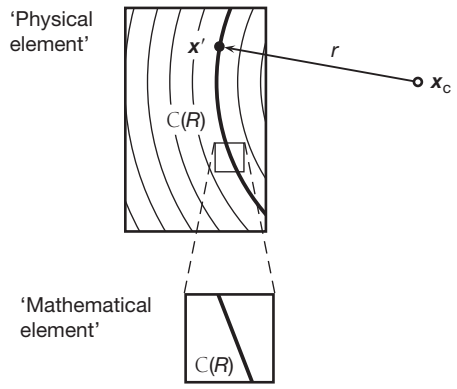

Figure 6 A 'physical element' being hit by the wave front from an impulsive point source. The intersection of the wave front with the source plane $z=0$ yields the circular arc $\mathcal{C}(R)$. Within the smaller 'mathematical element,' $\mathcal{C}(R)$ can be approximated by a straight line.

$$\begin{aligned} h_{\mathrm{r}}(\boldsymbol{x},t) &= \int\int_{\mathcal{A}} \frac{1}{2\pi||\boldsymbol{x}'-\boldsymbol{x}||}\,\delta\left(t-\frac{||\boldsymbol{x}'-\boldsymbol{x}||}{c_0}\right)\mathrm{d}\boldsymbol{x}' \\ &= \int_{r_{\min}}^{r_{\max}}\int_{\mathcal{C}(R)} \frac{1}{2\pi R}\,\delta\left(t-\frac{R}{c_0}\right)\mathrm{d}l\,\mathrm{d}r \\ &= \int_{R_{\min}}^{R_{\max}}\int_{\mathcal{C}(R)} \mathrm{d}l\,\frac{1}{2\pi R}\,\delta\left(t-\frac{R}{c_0}\right)\frac{\mathrm{d}r}{\mathrm{d}R}\mathrm{d}R \\ &= \int_{R_{\min}}^{R_{\max}} \frac{||\mathcal{C}(R)||}{2\pi R}\,c_0\delta(c_0t-R)\frac{1}{\sin[\varphi(R)]}\,\mathrm{d}R \\ &= \frac{||\mathcal{C}(c_0t)||}{2\pi t\sin[\varphi(c_0t)]} \end{aligned} \qquad [76]$$

In this derivation, the integration over the Cartesian coordinates x' and y' in the first line has been replaced in the second line by an integration over the radius r and the length l along $\mathcal{C}(R)$. Moreover, $\varphi(R)$ is the angle between $\boldsymbol{x}-\boldsymbol{x}'$ and the normal on the transducer surface. As shown in Figure 6, it might also happen that $\mathcal{C}(R)$ consists of more than one circular segment. In that case, $||\mathcal{C}(R)||$ is the total length of all segments.

In case of transmission, $\mathcal{C}(R)=\mathcal{C}(c_0t)$ contains all the points that emit pulses that at time t arrive simultaneously at $\boldsymbol{x}$. The total emitted wave arriving at point $\boldsymbol{x}$ due to the impulsive transducer again depends on the length $||\mathcal{C}(c_0t)||$. This follows from integration over the transducer surface of the time-domain equivalent of $\hat{G}(\boldsymbol{x},\boldsymbol{x}')$ from eqn [68]. Using similar steps as in the derivation of eqn [76], the so-called spatial impulse response in transmission is obtained as

$$\begin{aligned} h_{\mathrm{t}}(\boldsymbol{x},t) &= \int\int_{\mathcal{A}} \frac{1}{2\pi||\boldsymbol{x}-\boldsymbol{x}'||}\,\delta\left(t-\frac{||\boldsymbol{x}-\boldsymbol{x}'||}{c_0}\right)\mathrm{d}\boldsymbol{x}' \\ &= \int_{r_{\min}}^{r_{\max}}\int_{\mathcal{C}(R)} \frac{1}{2\pi R}\,\delta\left(t-\frac{R}{c_0}\right)\mathrm{d}l\,\mathrm{d}r \\ &= \frac{||\mathcal{C}(c_0t)||}{2\pi t\sin[\varphi(c_0t)]} \end{aligned} \qquad [77]$$

Equations [76] and [77] show that the spatial impulse responses of a transducer in transmission and in reception are identical. In other words, the pressure signal received by the transducer from an impulsive point source in some location is equal to the pressure that arrives in the same location when the transmitter sends an impulsive signal. This fact is a demonstration of acoustic reciprocity and makes that only one spatial impulse response $h(\boldsymbol{x},t)$ needs to be defined for a given transducer.

In general, a procedure in which the integral in eqn [73] is replaced by a straightforward summation over discrete grid points is not preferred because at some time instants, the spatial impulse response will change abruptly and an inefficiently dense grid will be necessary to retain accuracy. Instead, Field II uses a procedure based on the arc length, as outlined earlier, for the numerical evaluation of $h(\boldsymbol{x},t)$. To approximate the actual geometry, the 'physical' elements that make up the transducer are usually subdivided into smaller 'mathematical' elements. These mathematical elements may have a rectangular, triangular, or polygonal shape. For each mathematical element, the spatial impulse response is determined analytically. For the rectangular elements, this is done under the assumption that the element dimensions are much smaller than the distance to the point $\boldsymbol{x}$. In this far-field approximation, the arcs may be replaced by straight lines, as shown in Figure 6, and the spatial impulse response has a trapezoidal shape that may be computed with little numerical effort. For the triangular and polygonal elements, the exact spatial impulse response is obtained at the expense of an increased numerical effort. In view of this, to obtain a given accuracy, it is often more efficient to subdivide the transducer surface into many rectangular elements instead of using a few triangular or polygonal elements. The occurrence of fast changes in the spatial impulse response implies the occurrence of high frequencies and calls for a high temporal sampling rate (Jensen, 2001). However, the spectrum of the acoustic pulse and the emit and receive transfer functions of the transducer usually do not contain these high frequencies. Therefore, instead of using a high sampling rate, it makes more sense to lower the sampling rate while preserving the total energy in the signal. This fact is employed in Field II by computing the time-integrated spatial impulse responses of the mathematical elements and adding the results on a relatively coarse temporal grid. Afterward, the spatial impulse response is obtained by simple numerical differentiation.

2.19.3.3.2 Computation of emitted field

Knowing the spatial impulse response $h(\boldsymbol{x},t)$ of a nonapodized transducer and the normal velocity $v_{\perp}(t)$ at its surface, the acoustic pressure is found as (cf. eqn [72])

$$p(\boldsymbol{x},t) = h(\boldsymbol{x},t)*_{\mathrm{t}}\left(\rho_0\frac{\partial v_{\perp}(t)}{\partial t}\right) \qquad [78]$$

2.19.3.3.3 Computation of pressure from a point scatterer

A point scatterer is an infinitely small object that causes the same reflected field as a small volume with medium properties that differ from the background medium. Suppose that around $\boldsymbol{x}_{\mathrm{sc}}$, there is a volume ΔV in which the wave speed equals $c\neq c_0$. In this case, the wave equation in the domain ΔV is

$$\nabla^2 p - \frac{1}{c_0^2}\frac{\partial^2 p}{\partial t^2} = -\left(\frac{1}{c_0^2}-\frac{1}{c^2}\right)\frac{\partial^2 p}{\partial t^2} \qquad [79]$$

The wave equation for the total computational domain is then

$$\nabla^2 p - \frac{1}{c_0^2}\frac{\partial^2 p}{\partial t^2} = -S_{sc} \quad [80]$$

with the so-called contrast source term

$$S_{sc} = S_{sc}(\boldsymbol{x}, t) = \begin{cases} \left(\frac{1}{c_0^2} - \frac{1}{c^2}\right)\frac{\partial^2 p(\boldsymbol{x}, t)}{\partial t^2} & \text{for } \boldsymbol{x} \in \Delta V, \\ 0 & \text{for } \boldsymbol{x} \notin \Delta V. \end{cases} \quad [81]$$

Assuming that the scattering takes place in free space, the field p_{sc} scattered by ΔV may formally be found by convolution of S_{sc} with the free-space Green's function G in eqn [49]. However, when the dimensions of the volume ΔV are much smaller than a wavelength, the same scattered field is obtained when the Green's function is convolved with the point source

$$S_{sc}(\boldsymbol{x}, t) = a\,\delta(\boldsymbol{x} - \boldsymbol{x}_{sc})\frac{\partial^2 p(\boldsymbol{x}_{sc}, t)}{\partial t^2} \quad [82]$$

with $a = (c_0^{-2} - c^{-2})\Delta V$. It may be shown that local deviations of the density of mass can be represented in a similar way. Equation [82] defines a point scatterer with strength a. In Field II, configurations with several hundred thousands of point scatterers are used to mimic biological tissue.

The scattered acoustic pressure due to the scattering by a point scatterer located at $\boldsymbol{x}_{sc}$ is

$$\begin{aligned} p_{sc}(\boldsymbol{x}, t) &= S_{sc}(\boldsymbol{x}, t) *_{\boldsymbol{x}, t} G(\boldsymbol{x}, t) \\ &= a\frac{\partial^2 p(\boldsymbol{x}_{sc}, t)}{\partial t^2} *_t G(\boldsymbol{x} - \boldsymbol{x}_{sc}, t) \end{aligned} \quad [83]$$

which, with the aid of eqn [78], can be written as

$$p_{sc}(\boldsymbol{x}, t) = a\rho_0 \frac{\partial v_\perp(t)}{\partial t} *_t \frac{\partial^2 h(\boldsymbol{x}_{sc}, t)}{\partial t^2} *_t G(\boldsymbol{x} - \boldsymbol{x}_{sc}, t) \quad [84]$$

In case of more point scatterers, the total scattered field is computed by adding the fields of the individual point scatterers as obtained from eqn [84]. This implies that in eqn [82], p is taken to be the incident field from the transducer and multiple scattering is not taken into account. This approach is known as the Born approximation.

2.19.3.3.4 Computation of pulse-echo signal

Suppose that an acoustic pressure wave is incident on the same transducer as used for transmission. Indicating a point on the surface of the transducer by $\boldsymbol{x}'$, the received signal is

$$s_r(t) = \int\int_{\mathcal{A}} p_{sc}\left(\boldsymbol{x}', t\right) \mathrm{d}\boldsymbol{x}' \quad [85]$$

Substitution of eqn [84] yields

$$s_r(\boldsymbol{x}, t) = a\rho_0 \frac{\partial v_\perp(t)}{\partial t} *_t \frac{\partial^2 h(\boldsymbol{x}_{sc}, t)}{\partial t^2} *_t \int\int_{\mathcal{A}} G\left(\boldsymbol{x}' - \boldsymbol{x}_{sc}, t\right) \mathrm{d}\boldsymbol{x}' \quad [86]$$

However, in view of eqns [49] and [73], it follows that

$$\int\int_{\mathcal{A}} G\left(\boldsymbol{x}' - \boldsymbol{x}_{sc}, t\right) \mathrm{d}\boldsymbol{x}' = \frac{1}{2} h(\boldsymbol{x}_{sc}, t) \quad [87]$$

and eqn [86] may be written as

$$s_r(\boldsymbol{x}, t) = \frac{1}{2} a\rho_0 \frac{\partial v_\perp(t)}{\partial t} *_t \frac{\partial^2 H(\boldsymbol{x}_{sc}, t)}{\partial t^2} \quad [88]$$

with

$$H(\boldsymbol{x}_{sc}, t) = h(\boldsymbol{x}_{sc}, t) *_t h(\boldsymbol{x}_{sc}, t) \quad [89]$$

being the pulse-echo spatial impulse response (Jensen, 1991). In case of multiple point scatterers, the pulse-echo responses of individual scatterers are added.

2.19.3.3.5 Attenuation

In Field II, only attenuation with a linear frequency dependency is implemented. The user can set the parameters α_0, α_1, and f_0 of an attenuation coefficient of the form

$$\alpha(f) = \alpha_0 + \alpha_1(f - f_0) \quad [90]$$

In Jensen et al. (1993), it is explained that two steps are used to obtain the attenuated version of the spatial impulse response $h(\boldsymbol{x},t)$ in the far field. First, the frequency-dependent part $\alpha_1(f-f_0)$ of the attenuation coefficient is combined with an imaginary part that accounts for the corresponding dispersion. The result is used as the argument of an exponential function that provides a frequency-dependent attenuation/dispersion factor. To avoid a spatial convolution, the mean distance $||\boldsymbol{x}_{mean}||$ between the points on the transducer surface and the point $\boldsymbol{x}$ is used instead of the actual distances. The complex attenuation/dispersion factor is subsequently multiplied by the temporal Fourier transform of $h(\boldsymbol{x},t)$, and the result is transformed back to the time domain. Second, the intermediate result is multiplied by the frequency-independent attenuation factor $\exp(-\alpha_0||\boldsymbol{x}_{mean}||)$ to yield the final attenuated spatial impulse response in the far field.

2.19.3.3.6 Apodization and focusing

Multielement sources can often be described by a normal surface velocity that is separable into an apodization (tapering) function $A(\boldsymbol{x})$ and source signature function $v(t)$. The apodization function is used to model the tapering of the surface excitation towards the edge of the transducer or the on–off switching of elements. Moreover, the ultrasound beam may be steered and focused by giving the elements of a transducer a different time delay $\tau(\boldsymbol{x})$. Both effects can be accounted for by the introduction of a normal surface velocity

$$v_\perp(\boldsymbol{x}, t) = A(\boldsymbol{x})v[t - \tau(\boldsymbol{x})] \quad [91]$$

Substitution into eqn [70] yields that the emitted acoustic pressure may still be written in the form of eqn [72], but now the spatial impulse response becomes

$$h(\boldsymbol{x}, t) = \int\int_{\mathcal{A}} \frac{A\left(\boldsymbol{x}'\right)}{2\pi||\boldsymbol{x} - \boldsymbol{x}'||}\,\delta\left[t - \frac{||\boldsymbol{x} - \boldsymbol{x}'||}{c_0} - \tau\left(\boldsymbol{x}'\right)\right] \mathrm{d}\boldsymbol{x}' \quad [92]$$

These changes can easily be accounted for when it is assumed that the apodization and the time delay are constant over the physical elements of the transducer. In that case, apodization implies multiplication of the spatial impulse response of a physical element, and time delay means shifting the spatial impulse response of a physical element in time before adding it to the spatial impulse responses of the other elements.

When transducer apodization, beam steering, and beam focusing are dynamically controlled, it may not always be a

good idea to recompute the spatial impulse response of a transducer for each scanning scenario. Usually, a better option is to first compute the pulse-echo responses for each physical element and account for the apodization and delay later on. This synthetic aperture strategy may save a lot of numerical effort, particularly in the case of pulse-echo simulations involving a huge amount of static point scatterers. A discussion of this issue is given in Jensen and Nikolov (2000).

2.19.3.4 FOCUS

FOCUS can be considered as a modern successor of Field II and is organized and used in roughly the same way. A description of the program may be found in the FOCUS Quick Start Guide (2013). FOCUS is built on two different numerical techniques: the fast near-field method (FNM) and the angular spectrum approach (ASA). Most computations are performed in core programs that have been written in C++. These programs communicate with MATLAB through m-functions, which can be used to set the medium parameters, define the transducer, or start a particular type of computation. The choice of using the MATLAB environment brings the same benefits as mentioned for the Field II program. Noticeable differences between Field II and FOCUS are the following:

- FOCUS aims at high-accuracy computations, in particular in the near field.
- Field II can compute pulse-echo scenarios.

2.19.3.4.1 Fast near-field method

The basis of this method is derived from the exact integral expressions for the frequency-domain versions of the spatial impulse response of some basic transducer shapes, for example, a rectangular, circular, or triangular piston. Although impulse response calculations contain only single integrals over a finite domain, their numerical evaluation is difficult because the integrand typically has a singularity on the integration interval. As demonstrated in McGough (2004), McGough et al. (2004), and Kelly and McGough (2006), the FNM uses one or more of the following techniques to improve the numerical evaluation of the pressure:

- Rewriting the integrals in another form that does not involve a singular integrand
- Combining integrals that share the same integrands
- Evaluating the integrals using Gauss quadrature
- Adapting the number of abscissas to the local need (grid sectoring)
- Avoiding repeated computation of the same quantities
- Representing functions with a mixed space–time argument, for example, $v(t-z/c_0)$, by a sum of terms $f_n(t)g_n(z/c_0)$ that consist of a temporal function multiplied by a spatial function (time–space decomposition)

In this way, the pressure may be obtained with less effort and/or with increased accuracy as compared to a straightforward evaluation of the classical expressions. Because no far-field approximations are made, the results are also much more accurate in the near field.

2.19.3.4.2 Angular spectrum approach

This general approach is used to propagate the frequency-domain field in the transducer plane towards other parallel planes. This axial propagation is performed in the so-called angular spectrum domain, which is arrived at after applying a transformation with respect to the lateral coordinates. The approach may be found in, for example, Christopher and Parker (1991b), Zemp et al. (2003), Varslot and Taraldsen (2005), and Varslot and Måsøy (2006). In the context of FOCUS, the evaluation of the ASA by Zeng and McGough (2008) is relevant.

In FOCUS, the starting field in the transducer plane is obtained by the FNM. Suppose that in the transducer plane $z=0$, the normal surface velocity $\hat{v}_\perp(x,y,0)=\hat{v}_\perp(x,y,0,\omega)$ is given. This field may be used in eqn [70] to obtain

$$\hat{p}(x,y,z)=j\omega\rho_0\,\hat{v}_\perp(x,y,0)*_{x,y}\hat{h}(x,y,z) \qquad [93]$$

where

$$\hat{h}(x,y,z)=\hat{h}(\boldsymbol{x})=\frac{\exp(-jk||\boldsymbol{x}||)}{2\pi||\boldsymbol{x}||} \qquad [94]$$

is the so-called spatial propagator.

Application of the two-dimensional Fourier transformation with respect to x and y yields the angular spectral domain alternative to eqn [93]:

$$\tilde{p}(k_x,k_y,z)=j\omega\rho_0\tilde{v}_\perp(k_x,k_y,0)\tilde{h}(k_x,k_y,z) \qquad [95]$$

Here, k_x and k_y are the lateral spatial frequencies, and the tilde has been used to indicate quantities in the spatial frequency domain. The function

$$\tilde{h}(k_x,k_y,z)=\begin{cases}\dfrac{\exp\left(-jz\sqrt{k^2-k_x^2-k_y^2}\right)}{j\sqrt{k^2-k_x^2-k_y^2}} & \text{for } k_x^2-k_y^2\le k^2,\\[2ex] \dfrac{\exp\left(-z\sqrt{k^2-k_x^2-k_y^2}\right)}{\sqrt{k^2-k_x^2-k_y^2}} & \text{for } k_x^2-k_y^2>k^2,\end{cases} \qquad [96]$$

is called the spectral propagator. The first line indicates the undecaying motion of propagating plane wave components with lateral spectral frequencies that satisfy $k_x^2-k_y^2\le k^2$, and the second line represents the exponential decay of evanescent plane wave components with $k_x^2-k_y^2>k^2$. The spectral propagator approach can be numerically implemented by using two-dimensional FFTs. However, care should be taken to avoid aliasing and wraparound errors. These difficulties can be overcome by applying spectral filtering and zero-padding techniques, as will be further explained in Section 2.19.5.3.

2.19.4 Numerical Methods for Linear Ultrasound Fields

2.19.4.1 Background and Common Numerical Methods

In many practical cases, the equations governing the propagation of ultrasound waves do not have an analytical or semi-analytical solution. For example, the acoustic medium may have a spatially varying sound speed, or the acoustic

absorption may be governed by a particular spatial distribution of relaxation processes. For these cases, numerical methods must instead be used. The solution of partial differential equations by numerical calculations is now commonplace, both in academia and in industry. This ubiquity can be attributed to the continued expansion of low-cost computer systems over the last two decades. Large-scale, tissue-realistic ultrasound simulations that are possible using desktop machines today would have been very difficult 10 years ago and almost unthinkable 20 years ago!

The general idea behind the numerical solution of partial differential equations is to take a continuous system, which has an infinite number of degrees of freedom, and approximate this by a discrete system that can be analyzed using a computer. Some of the most commonly encountered techniques for discretizing differential equations in space are the finite difference (FD) method, the pseudospectral method, the finite element (FE) method, the boundary element method, and the integral equation (IE) method. For time-dependent problems, the time derivatives must also be discretized. This is commonly achieved using an FD approach. The different methods will be briefly discussed here before giving a more detailed (and gentle) introduction to the FD and pseudospectral methods in Sections 2.19.4.2 and 2.19.4.3.

Throughout this section, the numerical methods will be presented in the context of simulating linear ultrasound propagation. However, most methods can be easily adapted to also deal with nonlinear ultrasound.

2.19.4.1.1 Finite difference method

In the FD method, the region of interest is first divided up into an evenly distributed mesh of grid points as illustrated in Figure 7(a). The grid points represent the discrete positions in space at which the solution values are obtained. The continuous derivatives in the governing equations are then replaced with FD approximations. These are obtained by interpolating between the discrete values of the function over a small neighborhood of grid points using a series of overlapping polynomials. The derivative of the function at each grid point can then be computed using the derivative of the polynomials. The FD method is frequently used in acoustics and ultrasound, as it is well suited to broadband and time-domain problems and is relatively simple to formulate and implement.

2.19.4.1.2 Pseudospectral method

In the pseudospectral method, instead of approximating derivatives locally using the function values at a small number of neighboring grid points, the complete field is decomposed into a finite sum of basis functions that vary globally over the grid. For wave problems, the most common choice is to use a Fourier basis. After the basis function weights are calculated (e.g., using the Fourier transform), derivatives can then be computed using a weighted sum of the derivatives of the chosen basis functions. Compared to the FD method, the pseudospectral method can significantly reduce the number of grid points per wavelength needed for accurate simulations. This makes it well suited to modeling wave propagation in large domains.

2.19.4.1.3 Finite element method

In the FE method, the region of interest is also divided into a mesh of grid points. However, in contrast to the FD method, the grid is usually unstructured, which allows fine geometric details to be resolved (an example is given in Figure 7(b)). Before discretization, the governing equations are rewritten as an integral equation (called the weak formulation), which is then solved numerically. The variation of the unknown field variables (like the acoustic pressure and particle velocity) is described by a set of nonoverlapping polynomials that vary locally over each element. To model time-domain problems, the calculation of spatial derivatives using the FE method is normally combined with the calculation of temporal derivatives using the FD method. One advantage of the FE method is that the solution can be obtained by minimizing an error function. This means the mesh can be adaptively refined in order to control the accuracy of the solution. The method has found particular use in modeling piezoelectric ultrasound transducers, and there are currently several commercial packages available, including PZFlex, LMS SYSNOISE, and COMSOL Multiphysics. However, a disadvantage of the FE method is that it becomes inefficient for solving many time-domain problems, particularly when the ultrasound signals are broadband.

2.19.4.1.4 Boundary element method

In the boundary element method, the discretization of the complete region of interest is replaced by a discretization of

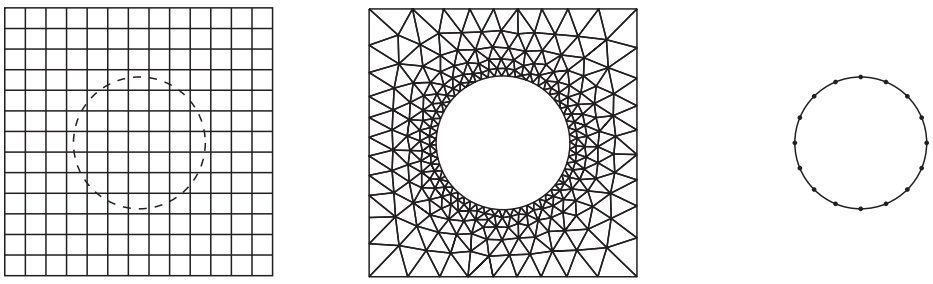

Figure 7 Examples of the computational grids used by different numerical methods for calculating the acoustic scattering from a rigid cylinder in 2-D. (a) The finite-difference method uses a structured mesh. (b) The finite-element method uses an unstructured mesh. (c) The boundary element method uses a boundary discretization rather than a volume discretization.

the boundaries within the domain (see Figure 7(c)). The resulting integral equation is then solved numerically, where the variation of both the field variables and the boundary geometry over each boundary element is described by shape functions. The solution is obtained in two steps, first by computing the acoustic pressure on the boundary surface and then by using this to compute the pressure field elsewhere in the domain. The main advantage of this approach is that only the boundary surfaces need to be discretized, which reduces the dimensionality of the problem. This also alleviates the need to truncate the computational grid in the far field. The method is particularly useful for modeling acoustic scattering problems in otherwise homogeneous media. For example, Gélat et al. (2011) used the boundary element method to study the aberration of a therapeutic ultrasound beam by the rib cage, where the ribs were modeled as rigid scatterers. The main disadvantage of the boundary element method is that it is restricted to piecewise homogeneous media and cannot easily account for the power-law acoustic attenuation behavior that is observed in biological tissue.

2.19.4.1.5 Integral equation method

The IE method is based on the concept of a so-called background medium for which the Green's function is known in analytical form. The deviations of the actual medium from the (necessarily simple) background medium are accounted for by contrast sources. Such deviations can occur in one or more medium parameters. In the background medium, two different acoustic wave fields are formally distinguished: the incident field that is directly caused by the transducer and the scattered field that is caused by the contrast sources. The scattered field can be written as a convolution of the background Green's function and the contrast sources. When both fields are added, this results in an integral equation, which may be solved by various iterative methods (Kleinman and Van den Berg, 1991). Each iteration step involves a convolution over space and time, which can be performed efficiently by transforming to the spatial and temporal frequency domain. This approach enables the application of a spatiotemporal grid with only two points per wavelength and period (Verweij and Huijssen, 2009). Another benefit of IE methods is that domain truncation is in general not necessary. An extensive discussion of the IE method for linear acoustics is given by Fokkema and Van den Berg (1993). In Section 2.19.5.4, a more detailed presentation of the IE method is given in the context of nonlinear acoustics.

2.19.4.2 Finite Difference Methods

2.19.4.2.1 Finite difference schemes and Taylor series

Of all the numerical methods used to model ultrasound waves, FD methods are probably encountered the most often. Before considering how these methods can be used to derive numerical solutions to the acoustic equations discussed in Section 2.19.2, it will be constructive to discuss more generally how they can be used to calculate derivatives of discretely sampled functions, that is, functions whose values are known only at a particular set of points. For most of this section, the analysis will be restricted to functions that vary in one or two space dimensions. However, analogous results for other dimensions easily follow.

Consider a function of two space variables $f(x,y)$. Provided this function is sufficiently smooth, the variation at some point $(x+\Delta x, y)$ can be written as a sum of derivatives at (x,y) using a Taylor series, where

$$f(x+\Delta x,y) = f(x,y) + \Delta x \frac{\partial f(x,y)}{\partial x} + \frac{\Delta x^2}{2!}\frac{\partial^2 f(x,y)}{\partial x^2} + \frac{\Delta x^3}{3!}\frac{\partial^3 f(x,y)}{\partial x^3} + \cdots \quad [97]$$

Dividing this expansion by Δx and only retaining the first two terms in the series then yields an expression for the partial derivative of $f(x,y)$ in the x-direction using the value of the function at two points separated by Δx:

$$\frac{\partial f(x,y)}{\partial x} = \frac{f(x+\Delta x,y) - f(x,y)}{\Delta x} + \mathrm{O}(\Delta x) \quad [98]$$

This expression is a simple example of an FD formula. It is called a forward difference approximation as the derivative at (x,y) is found with the help of the function values at $(x+\Delta x,y)$, that is, offset in the forward or positive x-direction. This particular expression can be traced back to Newton, and the limit as $\Delta x \to 0$ is often seen in the formal definition of the derivative.

The symbol O in eqn [98] is the Landau symbol. It is used to describe the error in the expansion that is introduced from the truncation of the Taylor series to a finite number of terms. The notation $\mathrm{O}(\Delta x^n)$ (sometimes called the big-O notation) states that the error in the FD approximation as $\Delta x \to 0$ is bounded by a constant value multiplied by $(\Delta x)^n$. For eqn [98], because the error is proportional to Δx (where $n=1$), the FD scheme is referred to as first-order accurate or simply first-order. Practically, this means that if the grid spacing Δx is reduced by a factor of 2, the truncation error will also approximately reduce by a factor of 2. Note, the Landau symbol describes the error introduced from a single application of the FD formula. It does not account for the cumulative or total error if the formula is applied several times in succession. This is discussed in more detail in Section 2.19.4.2.5.

When dealing with discrete functions rather than continuous ones, it is common to write FD formulas using subscript notation, where the function value at a particular grid point (i,j) in two dimensions is denoted $f_{i,j}$. The grid points represent the discrete set of spatial points where the values of the input function are known. In most cases, these points will be distributed uniformly such that $x_i = i\Delta x$ and $y_j = j\Delta y$ where $i = 0, 1, \ldots, N_x - 1$ and $j = 0, 1, \ldots, N_y - 1$, and the function values will be stored as a matrix. An example of a uniform mesh in 2-D is given in Figure 7(a). Using subscript notation, the first-order forward difference approximation given in eqn [98] can be written in the form

$$\left.\frac{\partial f}{\partial x}\right|_{i,j} = \frac{f_{i+1,j} - f_{i,j}}{\Delta x} + \mathrm{O}(\Delta x) \quad [99]$$

Computationally, this can be implemented by looping over the complete set of grid points. The derivative at each position is then calculated using the function values at the neighboring points. The pattern that is formed by connecting the grid neighbors required to calculate the derivative at any

particular position is called the FD stencil. A discussion of how to deal with the edges of the domain is postponed until Section 2.19.4.2.6.

Following the same procedure used earlier, the variation of a function at a point $(x-\Delta x, y)$ offset in the negative or backward direction can also be expanded as a sum of derivatives at (x,y) using a Taylor series:

$$f(x-\Delta x,y) = f(x,y) - \Delta x\frac{\partial f(x,y)}{\partial x} + \frac{\Delta x^2}{2!}\frac{\partial^2 f(x,y)}{\partial x^2} - \frac{\Delta x^3}{3!}\frac{\partial^3 f(x,y)}{\partial x^3} + \cdots \quad [100]$$

Again, this leads to an FD formula, in this case a first-order accurate backward difference approximation:

$$\left.\frac{\partial f}{\partial x}\right|_{i,j} = \frac{f_{i,j} - f_{i-1,j}}{\Delta x} + \mathrm{O}(\Delta x) \quad [101]$$

The expansions for forward and backward differences can also be combined to give a central difference formula, where the function values on either side of the point of interest are used. Subtracting eqn [100] from eqn [97] and dividing by the grid spacing yields

$$\left.\frac{\partial f}{\partial x}\right|_{i,j} = \frac{f_{i+1,j} - f_{i-1,j}}{2\Delta x} + \mathrm{O}(\Delta x^2) \quad [102]$$

As the $\partial^2/\partial x^2$ terms and other even-order derivatives in the two Taylor series expansions cancel, the truncation error is reduced, giving second-order accuracy. Practically, this can be significant, as reducing the grid spacing by a factor of 2 will now reduce the truncation error by approximately a factor of 4. A visualization of the backward, forward, and central FD schemes in one-dimension is shown in Figure 8. In the particular example shown, it is clear that the central difference approximation gives a closer estimate of the derivative at f_i.

By combining the Taylor series expansions for different points in different ways, it is possible to derive a complete library of FD schemes with varying accuracy and for different order derivatives. For example, the Taylor series expansions for $f(x\pm\Delta x, y)$ and $f(x\pm 2\Delta x, y)$ can be combined in such a way that the $\partial^3/\partial x^3$ terms and even-order derivatives cancel. This yields a fourth-order accurate central difference approximation:

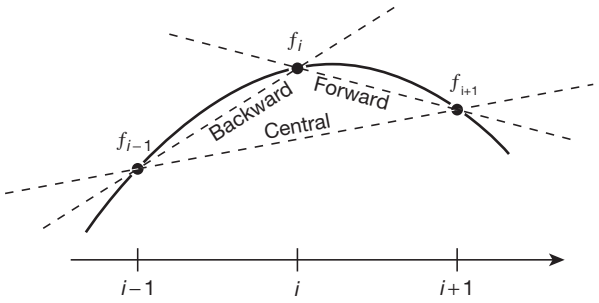

Figure 8 Illustration of forward, backward, and centered finite difference schemes used to numerically compute the derivative of a one-dimensional function from its discrete values (shown with filled circles). The slope of dashed lines indicate the value of the calculated derivatives.

$$\left.\frac{\partial f}{\partial x}\right|_{i,j} = \frac{f_{i-2,j} - 8f_{i-1,j} + 8f_{i+1,j} - f_{i+2,j}}{12\Delta x} + \mathrm{O}(\Delta x^4) \quad [103]$$

Similarly, summing eqns [97] and [100] such that the $\partial/\partial x$ terms cancel gives a second-order accurate central difference approximation for the second derivative:

$$\left.\frac{\partial^2 f}{\partial x^2}\right|_{i,j} = \frac{f_{i+1,j} - 2f_{i,j} + f_{i-1,j}}{\Delta x^2} + \mathrm{O}(\Delta x^2) \quad [104]$$

Other approximations can be formed in a similar fashion. A comprehensive list of FD weights for different accuracy and derivative orders is given by Fornberg (1988, 1996).

2.19.4.2.2 Finite difference schemes and polynomials

In the previous section, the derivation of FD formulas is considered using the machinery of the Taylor series. This approach is particularly instructive as the accuracy of different approximations can be directly extracted via the truncation error. It is also possible to derive equivalent FD schemes by fitting polynomials of a given degree to the discrete function values. For example, consider a linear polynomial $P(x)$ that interpolates between the values of the discrete function f at the neighboring points x_i and x_{i+1}. The equation for this polynomial may be written in general form as

$$P_j(x) = \left(\frac{x-x_i}{\Delta x}\right)f_{i+1,j} - \left(\frac{x-x_{i+1}}{\Delta x}\right)f_{i,j} \quad \text{where} \quad x_i \le x \le x_{i+1} \quad [105]$$

The derivative of the function f can then be approximated by using the derivative of the interpolating polynomial, that is,

$$\left.\frac{\partial f}{\partial x}\right|_{i,j} \approx \frac{\partial P_j(x)}{\partial x} = \frac{f_{i+1,j} - f_{i,j}}{\Delta x} \quad [106]$$

This formula is equivalent to the first-order forward difference approximation given in eqn [99] derived using a Taylor series. For central differences, a general formula for the FD scheme of order $2M$ can be written as (Hesthaven et al., 2007)

$$\left.\frac{\partial f}{\partial x}\right|_{i,j} \approx \sum_{m=1}^{M} \alpha_m^M \left(\frac{f_{i+m,j} - f_{i-m,j}}{2m\Delta x}\right) \quad [107]$$

where

$$\alpha_m^M = -2(-1)^m \frac{(M!)^2}{(M-m)!(M+m)!} \quad [108]$$

Other schemes can similarly be derived by fitting the appropriate interpolating polynomial to the discrete function values at more grid points (Fornberg, 1988). The derivative of the function (and consequently the FD scheme) can then be obtained using the derivative of the polynomial.

There are several benefits to considering the relationship between FD schemes and their corresponding interpolating polynomials. In particular, it is clear using this formulation that FD approximations will give exact results if the variation of the underlying function between the grid points follows a polynomial of the same degree as that used in the numerical scheme. For example, if there is a quadratic variation between three grid nodes, then a second-order FD will calculate the derivative exactly. In all other cases, the expressions are approximate.

2.19.4.2.3 Solution of the linearized acoustic equations

Now that the basic components of the FD method have been introduced, these can be used to derive a numerical solution to the acoustic equations described in Section 2.19.2. First, consider the homogeneous wave equation for the acoustic pressure in eqn [20]. This can be written in the form

$$\frac{\partial^2 p}{\partial t^2} = c_0^2 \nabla^2 p \qquad [109]$$

The general approach to solving partial differential equations of this kind is to replace the continuous derivatives with discrete FD approximations. In this case, there are both temporal and spatial derivatives that must be discretized. As discussed in Sections 2.19.4.2.1 and 2.19.4.2.2, there are a large number of possible approximations that may be used. Perhaps, the simplest approach is to use a second-order accurate central difference approximation for both the temporal and the spatial derivatives. In two dimensions, this leads to

$$\frac{p_{i,j}^{n+1} - 2p_{i,j}^{n} + p_{i,j}^{n-1}}{\Delta t^2} = c_0^2 \frac{p_{i+1,j}^{n} + p_{i,j+1}^{n} - 4p_{i,j}^{n} + p_{i-1,j}^{n} + p_{i,j-1}^{n}}{\Delta x^2} \qquad [110]$$

(recall that in 2-D, $\nabla^2 = \partial^2/\partial x^2 + \partial^2/\partial y^2$). Here, n corresponds to the temporal index, where $p_{i,j}^{n-1}$, $p_{i,j}^{n}$, and $p_{i,j}^{n+1}$ signify the acoustic pressure values at the previous, current, and next time points, respectively, and the grid is assumed to be evenly spaced, where $\Delta x = \Delta y$. Rearranging this expression gives an explicit update equation that may be used to calculate the evolution of the pressure field at each grid point in a time-stepping fashion:

$$p_{i,j}^{n+1} = 2p_{i,j}^{n} - p_{i,j}^{n-1} + \Delta t^2 c_0^2 \frac{p_{i+1,j}^{n} + p_{i,j+1}^{n} - 4p_{i,j}^{n} + p_{i-1,j}^{n} + p_{i,j-1}^{n}}{\Delta x^2} \qquad [111]$$

A similar formula can easily be developed using a second-order accurate central difference for the temporal derivative and a fourth-order accurate central difference for the spatial derivative (sometimes called a 2–4 scheme) (Strikwerda, 2004). This formulation is widely used in practice as discussed in Section 2.19.4.2.7.

Notice that in eqn [111], the calculation of the pressure field at the next time step requires the values at two previous time steps. To allow this scheme to get started, initial conditions for the pressure field and its temporal derivative at $t = 0$ are required, where

$$p_{i,j}^{0} = \phi_{i,j} \qquad [112]$$

$$\frac{\partial p_{i,j}^{0}}{\partial t} = \psi_{i,j} \qquad [113]$$

Using the second-order accurate central difference formula from eqn [102], the second initial condition can be rewritten as $p_{i,j}^{-1} = p_{i,j}^{1} + 2\Delta t \psi_{i,j}$. Substituting this and eqn [112] into eqn [111] then gives an expression for $p_{i,j}^{1}$ based on the initial conditions $\phi_{i,j}$ and $\psi_{i,j}$.

In addition to solving the wave equation, it is also possible to use the FD method to directly solve the linearized acoustic equations written as a set of coupled first-order partial differential equations. The coupled equations [18] and [19] for the acoustic pressure p and the acoustic particle velocity $\boldsymbol{v}$ can be written as

$$\frac{\partial \boldsymbol{v}}{\partial t} = -\frac{1}{\rho_0} \nabla p \qquad [114]$$

$$\frac{\partial p}{\partial t} = -\frac{1}{\kappa_0} \nabla \cdot \boldsymbol{v} \qquad [115]$$

To derive an equivalent second-order accurate FD scheme, the spatial and temporal derivatives must now be discretized using the second-order accurate central difference scheme for the first derivative given in eqn [102]. Considering for a moment the one-dimensional case and assuming the velocity is updated first followed by the pressure, this leads to the following set of discrete equations:

$$\frac{v_i^{n+1} - v_i^{n-1}}{2\Delta t} = -\frac{1}{\rho_0} \frac{p_{i+1}^{n} - p_{i-1}^{n}}{2\Delta x} \qquad [116]$$

$$\frac{p_i^{n+2} - p_i^{n}}{2\Delta t} = -\frac{1}{\kappa_0} \frac{v_{i+1}^{n+1} - v_{i-1}^{n+1}}{2\Delta x} \qquad [117]$$

An interesting pattern appears if the progression of this scheme is mapped out as shown in Figure 9(a). First, the pressure and the velocity are only evaluated at alternating time points. Second, two independent simulations will progress (shown with the white and black markers) without any interaction. If only one of these is retained, and the temporal and spatial grid spacing are halved (which reduces the truncation error by a factor of 4), the discrete equations can be rewritten as

$$\frac{v_{i+1/2}^{n+1/2} - v_{i+1/2}^{n-1/2}}{\Delta t} = -\frac{1}{\rho_0} \frac{p_{i+1}^{n} - p_i^{n}}{\Delta x} \qquad [118]$$

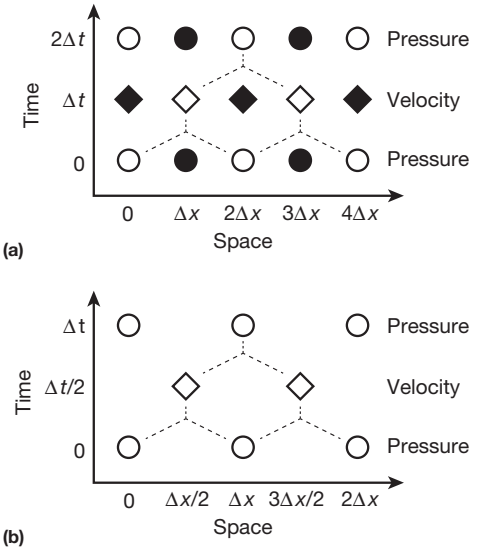

Figure 9 (a) Pattern that arises from the application of second-order accurate central differences to solve the acoustic equations expressed as first-order partial differential equations. The dashed lines show the connections between the grid points used to calculate the spatial derivatives. (b) Equivalent staggered grid scheme.

$$\frac{p_i^{n+1} - p_i^n}{\Delta t} = -\frac{1}{\kappa_0}\frac{v_{i+1/2}^{n+1/2} - v_{i-1/2}^{n+1/2}}{\Delta x} \qquad [119]$$

Using this scheme, the acoustic particle velocity is now computed on a staggered spatial and temporal grid as shown in Figure 9(b). This particular scheme was first proposed by Yee (1966) for solving the electromagnetic equations. The main advantage of using a staggered grid scheme compared to a nonstaggered scheme with forward or backward differences is that additional accuracy can be obtained without increasing the number of grid points in the domain or the FD stencil width. Again, two initial conditions are required to get the scheme started (one for the pressure and one for the particle velocity).

If the particle velocity is eliminated from the discrete equations given in eqns [118] and [119], the second-order accurate scheme for the wave equation given in eqn [111] is obtained. Thus, the two schemes can be considered equivalent. One advantage of solving coupled equations for the pressure and particle velocity is that a split-field perfectly matched layer (PML) can be used to absorb the waves at the edge of the domain. This is discussed in more detail in Section 2.19.4.2.6. There are also differences in the amount of computer memory required to implement the schemes. Solving the wave equation directly requires three matrices the size of the computational domain to store three time levels of p. In comparison, solving the coupled equations requires $1+D$ matrices (where D is the number of spatial dimensions in the simulation) to store the acoustic pressure and the Cartesian components of the particle velocity vector.

The discrete equations given in eqn [111] and eqns [118] and [119] are both examples of explicit FD schemes. This means the field variables at the next time step are calculated directly from values at the previous time steps, and the simulation proceeds in a time-stepping fashion. An alternative approach is to use implicit FD schemes, where the approximations for the spatial derivatives also use values of the field variables at the next time step, which are not yet known. In this case, the complete solution must be written as a system of linear equations and solved using matrix inversion methods. In comparison, implicit methods often have better stability properties than explicit methods. However, for large problems, they are computationally less efficient. It is for this reason they are not often used for modeling ultrasound fields in higher dimensions, where the number of grid points can become very large.

There are many other aspects of the FD method that have not been touched on here, for example, compact schemes (where higher-order accuracy is achieved using a smaller FD stencil) and multistage or Runge–Kutta schemes (where higher-order accuracy is achieved by introducing intermediate stages into each time step). For further details, the interested reader is directed to one of the many available books on FD methods, for example, Thomas (2010) or Strikwerda (2004).

2.19.4.2.4 Consistency, convergence, and stability

In Section 2.19.4.2.3, different explicit FD models are constructed from the partial differential equations describing the propagation of ultrasound waves. Here, the conditions under which these numerical models provide the correct solution to the governing equations are considered. This is assessed using three related concepts: consistency, convergence, and stability. A numerical model is consistent if it mathematically reduces to the continuous governing equations in the limit that the spatial and temporal steps reduce to zero, in the same way that $[f(x+\Delta x)-f(x)]/\Delta x \to \partial f/\partial x$ as $\Delta x \to 0$. This is straightforward to show, and provided that the appropriate FD approximations have been used when discretizing the equations, the models will be consistent. A numerical model is convergent if the numerical solution approaches the exact solution as the size of the discrete spatial and temporal steps used in the model is reduced. Similarly, a numerical model is stable if the errors in the numerical solution are bounded, that is, they do not grow as the simulation progresses. Convergence is normally difficult to prove via direct analysis of the discrete equations. However, a consistent and stable numerical scheme can be proved to be convergent (this is known as the Lax equivalence theorem). Thus, if a model is known to be consistent, it is sufficient to show it is convergent by proving that it is stable.

To examine the stability of an FD scheme, a von Neumann stability analysis can be performed (Charney et al., 1950). This begins by assuming that the solution for a 1-D problem can be written in the form $p_m^n = \lambda^n \exp(-jkm\Delta x)$. Here, m has been used as the spatial grid index to avoid any confusion with the imaginary unit. The factor λ accounts for the time dependence of the solution and is sometimes called the amplification factor. The exponential term accounts for the spatial dependence, where k is the spatial frequency or wave number. Choosing a solution of this form can be motivated by considering the acoustic wave field as a superposition of plane waves or Fourier modes, where the overall behavior under linear conditions can be determined by examining the behavior of a single mode. Provided the true solution to the partial differential equation is not growing, the FD scheme will be stable if $|\lambda| \leq 1$ for all possible values of k.

To illustrate how the analysis is performed, consider the second-order accurate central difference scheme constructed in Section 2.19.4.2.3. In 1-D, this can be written as

$$\frac{p_m^{n+1} - 2p_m^n + p_m^{n-1}}{\Delta t^2} = c_0^2 \frac{p_{m+1}^n - 2p_m^n + p_{m-1}^n}{\Delta x^2} \qquad [120]$$

Substituting the solution $p_m^n = \lambda^n \exp(-jkm\Delta x)$ and dividing by $\lambda^n \exp(-jkm\Delta x)$ then gives

$$\begin{aligned} \lambda - 2 + \lambda^{-1} &= \left(\frac{c_0\Delta t}{\Delta x}\right)^2 [\exp(-jk\Delta x) - 2 + \exp(jk\Delta x)] \\ \Rightarrow \lambda + \lambda^{-1} &= 2 + 2\left(\frac{c_0\Delta t}{\Delta x}\right)^2 [\cos(k\Delta x) - 1] \end{aligned} \qquad [121]$$

Denoting the right-hand side of the second equation as a and then multiplying by the amplification factor λ yields the characteristic quadratic equation $\lambda^2 - a\lambda + 1 = 0$, for which the solution is $\lambda = \left(a \pm \sqrt{a^2 - 4}\right)/2$. The requirement that $|\lambda| \leq 1$ is satisfied when $-2 \leq a \leq 2$, that is, when

$$-2 \leq 2 + 2\left(\frac{c_0\Delta t}{\Delta x}\right)^2 [\cos(k\Delta x) - 1] \leq 2 \qquad [122]$$

As the sound speed and spatial and temporal step sizes are positive quantities and the $\cos(k\Delta x) - 1$ term is bounded

between −2 and 0, the right condition is always satisfied. The remaining stability condition can then be reduced to

$$\frac{c_0\Delta t}{\Delta x} \leq 1 \qquad [123]$$

This condition can be used to select an appropriate time step given the spatial step and sound speed in the medium. The number $c_0\Delta t/\Delta x$ is called the Courant–Friedrichs–Lewy (CFL) number (Courant et al., 1967). In the acoustic case, this can be interpreted as the distance a wave can travel in a single time step relative to the spatial grid spacing. The stability condition is often given as a restriction on the CFL number. For example, the stability condition in eqn [123] can also be written as $\text{CFL} \leq 1$.

A simple example of the effect of the time step (or CFL number) on the stability of a numerical simulation is shown in Figure 10. Here, the propagation of a Gaussian initial pressure distribution is modeled using the second-order accurate central difference scheme given in eqn [120]. The time step is chosen to be $\Delta t = \text{CFL}\,\Delta x/c_0$. When the stability condition is met, two identical waves propagate across the domain in opposite directions as expected. When the stability condition is not met, errors in the numerical solution start to appear and continue to grow until the solution is completely corrupted.

In general, the stability condition will depend on both the accuracy of the FD scheme and the dimensionality of the problem. For example, in 2-D and 3-D, the stability condition for the second-order accurate central difference scheme becomes $\text{CFL} \leq 1/\sqrt{D}$, where D is the number of spatial dimensions. For an FD scheme that is second-order accurate in time, and fourth-order accurate in space, the CFL condition is instead $\text{CFL} \leq \sqrt{3/4D}$. More generally, when the wave equation is solved using centered FDs, the stability condition is given by $\text{CFL} \leq \sqrt{a_1/a_2}$, where a_1 and a_2 are the sum of the absolute values of the FD coefficients used to calculate $\partial^2/\partial t^2$ and ∇^2, respectively (Lines et al., 1999).

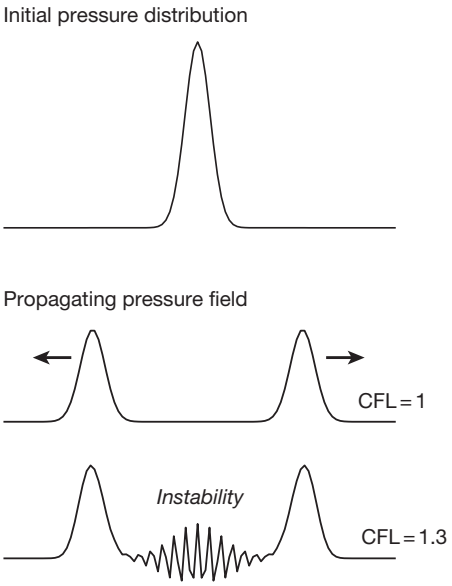

Figure 10 Example of instability in the propagation of Gaussian pressure pulse in 1-D using the FD scheme from eqn [120]. The jagged region in the pressure profile for a Courant–Friedrichs–Lewy number of 1.3 illustrates the instability. This error will continue to grow until the solution is completely corrupted.

2.19.4.2.5 Accuracy and numerical dispersion

In the previous section, the concepts of consistency, convergence, and stability are introduced. The effect of truncation errors in the FD approximations on the overall accuracy of the numerical solution must now also be considered. Consider the discretization of the one-dimensional wave equation using the second-order accurate central difference scheme given in eqn [120]. The exact solutions to the corresponding continuous wave equation subject to the initial condition $p(x,0) = \exp(-jkx)$ are waves traveling to the left and the right that are given by $p(x,t) = \exp[-jk(x \pm c_0 t)]$. Taking the forward traveling wave $p(x,t) = \exp[-jk(x - c_0 t)]$ and substituting this into the FD approximation for the spatial derivative leads to

$$\begin{aligned}\frac{\partial^2}{\partial x^2}p(x,t) &\approx \frac{\exp(-jk\Delta x) - 2 + \exp(jk\Delta x)}{\Delta x^2}\exp[-jk(x - c_0 t)] \\ &= -\text{sinc}^2(k\Delta x/2)k^2\exp[-jk(x - c_0 t)]\end{aligned} \qquad [124]$$

In comparison, the analytical value of the derivative is given by

$$\frac{\partial^2}{\partial x^2}p(x,t) = -k^2\exp[-jk(x - c_0 t)] \qquad [125]$$

Thus, the FD approximation can be seen to introduce an error of $\text{sinc}^2(k\Delta x/2)$ into the value of the derivative compared to the exact solution. Similarly, if a second-order accurate central difference scheme is used to discretize the temporal derivative, an error of $\text{sinc}^2(c_0 k\Delta t/2)$ is introduced. Combining these results, the continuous equation that is exactly solved by the FD scheme can be written as

$$\frac{\partial^2 p}{\partial t^2} = c(k)^2\frac{\partial^2 p}{\partial x^2} \quad \text{where } c(k) = \frac{\text{sinc}(k\Delta x/2)}{\text{sinc}(c_0 k\Delta t/2)}c_0 \qquad [126]$$

Notice the sound speed in the numerical model is now dependent on the wave number k. This illustrates that the FD approximations used to calculate the continuous derivatives introduce phase error or numerical dispersion into the solution. (Dispersion can be both physical and numerical and refers to a dependence of the phase velocity or sound speed on frequency.) Practically, this means that waves will become increasingly distorted compared to the true solution as they propagate across the computational grid. The error in the sound speed introduced by the FD approximation of the spatial derivative against normalized wave number is illustrated in Figure 11.

It is interesting to note from eqn [126], if $\Delta x = c_0\Delta t$ (i.e., the CFL is set to 1), the phase errors introduced by the temporal and spatial FD schemes will exactly cancel. In this case, the numerical solution will be exact for all frequencies up to the Nyquist limit of two grid points per wavelength (this is the minimum number of discrete points per wavelength that can be used to sample a sinusoidal signal without ambiguity in the frequency). Unfortunately, in higher dimensions, stability dictates a maximum CFL value of less than 1, and thus, the introduction of numerical dispersion cannot be avoided. The practical implication of this is a restriction on the number of

grid points per wavelength that must be used at the maximum frequency of interest. From Figure 11, it is clear that at the Nyquist limit of two points per wavelength (where $k\Delta x = \pi$), even the higher-order schemes introduce a significant phase error. However, at $k\Delta x = \pi/4$ (which corresponds to eight points per wavelength), the error in the sound speed for the fourth- and sixth-order schemes is less than 1%. Considering the phase error introduced by both the temporal and the spatial FD schemes, a common choice is typically between 10 and 20 grid points per acoustic wavelength at the maximum frequency of interest. However, this strongly depends on the size of the computational domain and the order of accuracy used. For lower-order schemes and large domains, a finer discretization is required to avoid the accumulation of phase errors. A good approach to check the accuracy of a simulation is to continue to halve the size of both the spatial and the time steps until the numerical solution reaches a steady value.

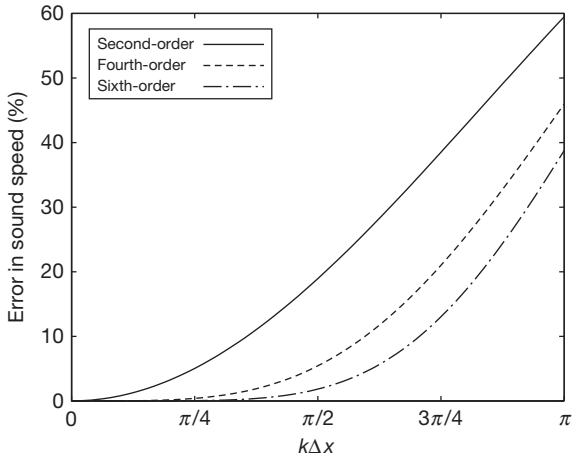

Figure 11 Numerical dispersion introduced by centered FD approximations of $\partial^2 p/\partial x^2$ against normalized wave number. The Nyquist frequency is given by $k\Delta x = \pi$.

2.19.4.2.6 Free-space propagation using a perfectly matched layer

Up to now, strategies to deal with the edges of the computational grid have not been discussed. From an implementation perspective, if centered differences are used to compute the spatial derivatives, these can be replaced with the appropriate forward and backward difference schemes of the same order near the boundaries. Both Neumann (sound-hard or rigid) and Dirichlet (sound-soft or compliant) boundary conditions can then be enforced at the edges of the grid by setting the appropriate values to zero. However, in most practical cases, it is advantageous to choose the size of the computational grid based on a particular region of interest within physical space, not based on the location of physical boundaries within the domain (which are unlikely to be rectangular in any case). Thus, a method to simulate free-field conditions in which acoustic waves are able to exit from the computational grid without being reflected is required.

The simplest way to model free-field conditions is to increase the size of the grid such that the waves never reach the boundaries. However, this carries an obvious computational penalty. A more apposite approach is to use a PML. This is a thin absorbing layer that encloses the region of interest and is governed by a nonphysical set of equations that cause anisotropic absorption (see Figure 12). The properties of the layer are chosen based on two requirements: (1) only components of the wave field traveling within the PML and normal to the boundary are absorbed and (2) reflections from the interface between the interior of the domain and the matching layer are minimized. There are several different forms of the PML based on two distinct ideologies. The split-field PML and related variants are based on solving a different set of governing equations within the absorbing layer (Bérenger, 1994). The uniaxial PML is instead based on solving the original equations everywhere but with anisotropic absorbing medium properties within the PML (Sacks et al., 1995). Both approaches introduce additional complexity; the split-field PML requires the pressure to be artificially split into Cartesian components based on derivatives of the particle velocity, while the uniaxial PML requires the introduction of auxiliary variables (Bérenger, 2007).

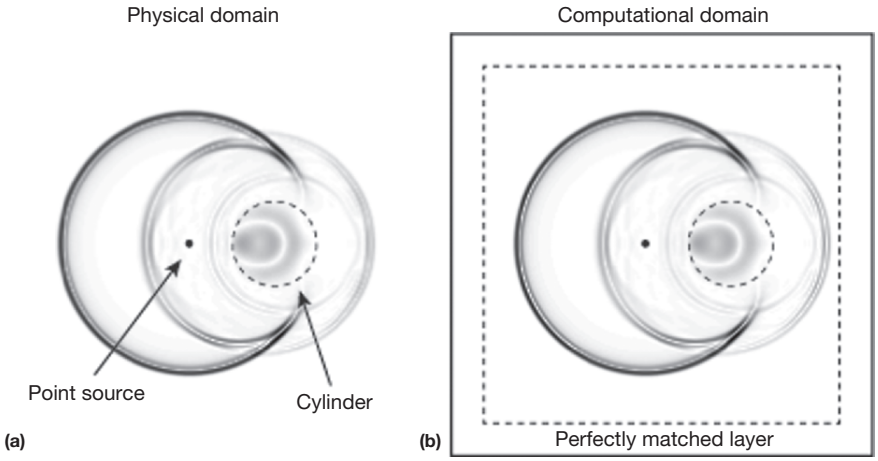

Figure 12 A perfectly matched layer (PML) can be used to simulate free-field conditions using a finite-sized grid by absorbing the waves within a thin layer that terminates the computational domain. (a) Physical domain in the free field. (b) Computational domain truncated by a PML.

The split-field PML, originally formulated for the electromagnetic equations (Bérenger, 1994), works by splitting the acoustic pressure into Cartesian components, where $p = p_x + p_y + p_z$. The field splitting is based on the derivatives of the vector particle velocity. Consequently, this particular PML can only be applied to the acoustic equations expressed as a coupled system of first-order partial differential equations. In two dimensions, the coupled equations for the acoustic pressure and particle velocity given in eqns [114] and [115] including a PML are written as (Qi and Geers, 1998)

$$\frac{\partial v_x}{\partial t} = -\frac{1}{\rho_0}\frac{\partial}{\partial x}(p_x + p_y) - \alpha_x v_x \qquad [127]$$

$$\frac{\partial v_y}{\partial t} = -\frac{1}{\rho_0}\frac{\partial}{\partial y}(p_x + p_y) - \alpha_y v_y \qquad [128]$$

$$\frac{\partial p_x}{\partial t} = -\frac{1}{\kappa_0}\frac{\partial v_x}{\partial x} - \alpha_x p_x \qquad [129]$$

$$\frac{\partial p_y}{\partial t} = -\frac{1}{\kappa_0}\frac{\partial v_y}{\partial y} - \alpha_y p_y \qquad [130]$$

The parameters α_x and α_y specify the PML absorption in units of nepers per second. Both α_x and α_y are zero outside the PML, α_x is nonzero within the PML that terminates the computational domain in the x-direction, and α_y is nonzero within the PML that terminates the domain in the y-direction. To allow for stronger PML absorption values without introducing instability, these equations are sometimes reformulated as (Yuan et al., 1999)

$$\left(\frac{\partial}{\partial t} + \alpha\right) f + Q \rightarrow \frac{\partial}{\partial t}(\exp(\alpha t) f) + \exp(\alpha t) Q \qquad [131]$$

An example of the equations that result from the reformulation of eqns [127]–[130] using eqn [131] is given by Tabei et al. (2002).

In the continuous case, it would seem intuitive to maximize the absorption values within the PML so the size of the layer can be minimized. However, when the equations are discretized, a sharp change in absorption at the interface between the matching layer and the rest of the domain will cause undesired acoustic reflections. To overcome this, a variable absorption parameter is normally used that gradually increases inside the PML. A common choice is

$$\alpha_m = \alpha_{\max}\left(\frac{m}{M}\right)^b \qquad [132]$$

where m is the relative grid point index inside the PML given by $m = 1, 2, \ldots, M$, M is the thickness of the PML in grid points, $\alpha_{\max}$ is the maximum value of absorption within the PML, and b is a shaping parameter normally chosen to be between 2 and 4.

2.19.4.2.7 Application of finite difference methods to ultrasound simulation

There are many studies in the literature that apply the FD techniques described here to different problems in biomedical ultrasound. To give just a small number of examples, Manry and Broschat (1996) used a second-order in time and fourth-order in space discretization of the coupled acoustic equations in 2-D to investigate the effect of fat lobes in the breast on the shape of an ultrasound beam. Mast et al. (1997) used a two-step MacCormack scheme of the same order accuracy to study the aberration of ultrasound pulses by the abdominal wall. Huang et al. (2005) used a similar model to investigate the propagation of photoacoustic waves in the breast. Aubry et al. (2003) used an FD discretization of the second-order acoustic wave equation for a heterogeneous and absorbing medium in 3-D to model aberration and adaptive focusing of ultrasound waves through the skull. Pinton et al. (2009) used a second-order in time and fourth-order in space discretization of the wave equation to simulate beam patterns and B-mode ultrasound images. Finally, Karamalis et al. (2010) used a similar model accelerated using a graphical processing unit to simulate B-mode images from synthetic scattering phantoms.

2.19.4.3 Pseudospectral Methods

2.19.4.3.1 Spectral collocation methods

In Section 2.19.4.2, numerical solutions of the wave equation are obtained by discretizing the derivative operators using FDs. Recall the general principle of the FD method is that for each grid point, an interpolating polynomial is fitted to the function values across a chosen number of neighboring grid points. The derivative of the function is then estimated using the derivative of the polynomial. This can be considered as a local approximation of the derivative, as the calculation only uses the function values at a small number of neighboring grid points. To reduce the phase error introduced by the FD approximation, higher-order schemes can be used, where polynomials of higher degree are fitted to a greater number of grid neighbors. Spectral methods take this idea to the limit and approximate the function at all of the grid points simultaneously using a finite sum of basis functions. This decomposition can be written in the form

$$f(x) \approx \sum_{k=1}^{N} a_k \Phi_k(x) \qquad [133]$$

where $\Phi_k(x)$ are the basis functions and a_k are the basis function weights. Once the basis function weights are known, the derivative of the function can be calculated using the derivative of the basis functions.

The primary advantage of spectral methods compared to FDs is their exponential error convergence. This can be understood by considering an equivalent FD scheme that uses all of the grid points within the domain. As the number of grid points in the domain is increased, the order of the FD scheme using all the points must also be increased, while the distance between the points is reduced. The truncation error will thus scale as $O(N^{-N})$, where N is the number of grid points in the domain. The practical significance of this is that spectral methods are memory-minimizing. That is, they will afford the coarsest possible grid spacing for a given level of accuracy. This can have a significant impact on the tractability of many large-scale problems.

For wave problems, the most common choice of basis function is trigonometric polynomials (in this case, a Fourier series), where the function is expanded as a sum of complex exponentials:

$$f(x) \approx \sum_{k=-N_x/2}^{N_x/2} a_k \exp(-jkx) \qquad [134]$$

This expansion can again be motivated by considering the decomposition of the wave field into a sum of plane waves. The derivative of each basis function $\exp(-jkx)$ is simply $-jk\exp(-jkx)$, and the basis function weights a_k can be computed efficiently using the FFT. This leads to the spectral formula for the spatial derivative

$$\frac{\partial^n}{\partial x^n} f(x) \approx F_x^{-1}\{(-jk_x)^n F_x\{f(x)\}\} \quad [135]$$

where $F_x\{\}$ and $F_x^{-1}\{\}$ denote the forward and inverse Fourier transforms over the x dimension. Assuming the number of grid points is an even number, the discrete set of wave numbers k_x is given by

$$k_x = -\frac{\pi}{\Delta x}, -\frac{\pi}{\Delta x}+\frac{2\pi}{\Delta x N_x}, -\frac{\pi}{\Delta x}+\frac{4\pi}{\Delta x N_x}, \ldots, \frac{\pi}{\Delta x}-\frac{2\pi}{\Delta x N_x} \quad [136]$$

The expression given in eqn [135] is known as the Fourier collocation spectral method or the Fourier pseudospectral method. The term collocation refers to the fact that the truncated sum of basis functions agrees with the discrete function values exactly at each point on the grid (known as the collocation points). It is also possible to determine the basis function weights using tau and Galerkin methods (Boyd, 2001). However, the collocation approach is considerably simpler and benefits from increased computational efficiency.

To derive a solution to the acoustic equations, the spectral calculation of spatial derivatives must still be combined with the FD calculation of temporal derivatives. This approach is often referred to as the pseudospectral time-domain (PSTD) method. Using a second-order accurate central difference approximation for the temporal derivative, the resulting discretization of the 2-D wave equation given in eqn [109] can now be written as

$$\frac{p^{n+1}-2p^n+p^{n-1}}{\Delta t^2} = c_0^2 F_{x,y}^{-1}\{-k^2 F_{x,y}\{p^n\}\} \quad [137]$$

where $k^2 = \boldsymbol{k}\cdot\boldsymbol{k} = k_x^2 + k_y^2$. Compared to eqn [110], the usual grid point subscripts i, j have been omitted as the derivative at all of the grid points is calculated simultaneously. Following a similar analysis to that given in Section 2.19.4.2.4, this scheme can be shown to be stable for CFL $\leq 2/(\pi\sqrt{D})$.

The benefit of the PSTD method compared to the FD method is that the phase error introduced by the approximation of the spatial derivative is eliminated. Again, considering the solution to the 1-D wave equation $p(x,t) = \exp[-jk(x-c_0t)]$ introduced in Section 2.19.4.2.5, it is clear from eqn [135] that the pseudospectral derivative calculation will give the correct solution for all spatial frequencies up to the Nyquist limit. The continuous equation that is solved exactly by eqn [137] can thus be written as

$$\frac{\partial^2 p}{\partial t^2} = c(k)^2 \frac{\partial^2 p}{\partial x^2} \quad \text{where } c(k) = \frac{c_0}{\operatorname{sinc}(ck\Delta t/2)} \quad [138]$$

Compared to eqn [126], the numerical dispersion is now only dependent on the FD approximation of the temporal derivative.

The PSTD method can similarly be used to discretize the linearized continuum equations written as a set of coupled first-order partial differential equations. Using a second-order accurate central difference approximation for the temporal derivative in conjunction with the staggered grid scheme discussed in Section 2.19.4.2.3, the discrete equations in 2-D can be written as

$$\frac{v_x^{n+1/2}-v_x^{n-1/2}}{\Delta t} = -\frac{1}{\rho_0} F_x^{-1}\{-jk_x \exp(-jk_x\Delta x/2) F_x\{p^n\}\} \quad [139]$$

$$\frac{v_y^{n+1/2}-v_y^{n-1/2}}{\Delta t} = -\frac{1}{\rho_0} F_y^{-1}\{-jk_y \exp(-jk_y\Delta y/2) F_y\{p^n\}\} \quad [140]$$

$$\frac{p_i^{n+1}-p_i^n}{\Delta t} = -\frac{1}{\kappa_0}\left(F_x^{-1}\left\{-jk_x \exp(jk_x\Delta x/2) F_x\left\{v_x^{n+1/2}\right\}\right\} + F_y^{-1}\left\{-jk_y \exp(jk_y\Delta y/2) F_y\left\{v_y^{n+1/2}\right\}\right\}\right) \quad [141]$$

The exponential terms $\exp(\pm jk_x\Delta x/2)$ and $\exp(\pm jk_y\Delta y/2)$ that appear within the spatial derivative calculations are spatial shift operators that translate the results by half the grid point spacing for use with the staggered grid. Again, the primary advantage of solving the acoustic equations in this form is the ability to implement a split-field PML as discussed in Section 2.19.4.2.6. A similar PSTD formulation is used in the commercial package SPFlex (Wojcik et al., 1997).

It is useful to note that spectral methods using other polynomial basis functions are also possible. A common choice for nonperiodic problems is to use Chebyshev polynomials. However, a significant disadvantage of the Chebyshev pseudospectral method for solving wave problems using explicit methods is that the time step required for stability scales with N^{-2}, where N is the number of grid points in each Cartesian direction given a fixed domain size (Gottlieb and Hesthaven, 2001). In comparison, the time step for the Fourier spectral method scales with N^{-1}, which is significantly cheaper, particularly for large-scale problems. The Chebyshev spectral method also requires the grid points to be clustered closer together near the boundaries to avoid the Runge phenomenon (Boyd, 2001). This means, for the same maximum grid point spacing, a larger number of grid points is needed. For example, a common choice when using a Chebyshev basis is cosine-spaced points. Compared to using equispaced points, this requires $(\pi/2)^D$ more grid points for a simulation in D spatial dimensions. For 3-D simulations, this increases the memory consumption by almost four times.

2.19.4.3.2 The k-space pseudospectral method

The use of the Fourier pseudospectral method to solve the acoustic equations eliminates the phase error introduced by the FD approximation of the spatial derivatives. However, unwanted numerical dispersion is still introduced in the temporal domain as shown in eqn [138]. Fortunately, as the form of the numerical dispersion introduced by the second-order accurate central difference scheme is known, it is possible to counteract it by introducing a correction to the pseudospectral calculation of the spatial derivative. For the wave equation, this leads to the following discretization:

$$\frac{p^{n+1}-2p^n+p^{n-1}}{\Delta t^2} = c_0^2 F_{x,y}^{-1}\{-k^2 \operatorname{sinc}^2(c_0k\Delta t/2) F_{x,y}\{p^n\}\} \quad [142]$$

This approach is known as the *k*-space pseudospectral method, or simply the *k*-space method, and was first introduced for acoustics by Bojarski (1982, 1985). In the case of a homogeneous medium, this scheme completely eliminates the unwanted phase error introduced by the discretization of both the spatial and the temporal derivatives and thus solves the wave equation exactly without the introduction of numerical dispersion. This is similar to the case discussed in Section 2.19.4.2.5 where the phase error introduced by the spatial and temporal FD schemes in 1-D can be made to exactly cancel by using a CFL of 1.

The *k*-space approach can similarly be used to discretize the linearized continuum equations written as a set of coupled first-order partial differential equations. Using the staggered grid scheme shown in eqns [139]–[141], the phase error introduced by the FD approximation of the temporal derivative is given by $\mathrm{sinc}(c_0 k\Delta t/2) \equiv \vartheta$. The corresponding *k*-space pseudospectral discretization including a correction term can thus be written as

$$\frac{v_x^{n+1/2} - v_x^{n-1/2}}{\Delta t} = -\frac{1}{\rho_0} F_{x,y}^{-1}\{-jk_x\vartheta \exp(-jk_x\Delta x/2) F_{x,y}\{p^n\}\} \quad [143]$$

$$\frac{v_y^{n+1/2} - v_y^{n-1/2}}{\Delta t} = -\frac{1}{\rho_0} F_{x,y}^{-1}\{-jk_y\vartheta \exp(-jk_y\Delta y/2) F_{x,y}\{p^n\}\} \quad [144]$$

$$\frac{p_i^{n+1} - p_i^n}{\Delta t} = -\frac{1}{\kappa_0}\left(F_{x,y}^{-1}\left\{-jk_x\vartheta \exp(jk_x\Delta x/2) F_{x,y}\left\{v_x^{n+1/2}\right\}\right\} + F_{x,y}^{-1}\left\{-jk_y\vartheta \exp(jk_y\Delta y/2) F_{x,y}\left\{v_y^{n+1/2}\right\}\right\}\right) \quad [145]$$

For homogeneous media, the *k*-space schemes given in eqns [142]–[145] are equivalent and can be shown to be unconditionally stable (Tabei et al., 2002).

The main advantage of using the *k*-space pseudospectral method compared to conventional FD and pseudospectral methods is that numerical dispersion is eliminated (or significantly reduced as discussed later). This is critical for many problems in ultrasound where the acoustic waves must travel over large distances. Figure 13(a) illustrates the effect of numerical dispersion on the shape of a monopolar wave in a homogeneous medium after propagating a distance of 200 wavelengths. The temporal input pulse is defined as

$$s(t) = \begin{cases} \sin^3(2\pi f_s t) & \text{for } 0 \le t \le 1/(2f_s) \\ 0 & \text{otherwise} \end{cases} \quad [146]$$

with the medium discretized using 20 grid points per wavelength at f_s. Even using a CFL of 0.05, the shape of the pulse when using the FD method is severely distorted. When the pseudospectral scheme is used, the accuracy with which spatial derivatives are computed is significantly improved, and thus, the dispersion is reduced. However, as the domain size is increased, small CFL numbers must still be used to counteract the accumulation of phase errors introduced by the FD time step. In comparison, when the *k*-space pseudospectral method is used, no dispersion is introduced regardless of the CFL number.

It is important to note that when the sound speed is spatially varying, the *k*-space pseudospectral method is no longer exact, and the phase correction term will no longer completely eliminate numerical dispersion (Treeby et al., 2012b). This is because the correction term is applied in the spatial frequency domain, which means the value of the sound speed used in the correction must be scalar, that is, a single constant value. Consequently, in a heterogeneous medium, there will be regions where the local value of the sound speed in the medium does not match the sound speed used within the phase correction term, and numerical dispersion will still be introduced into the solution. However, for weakly heterogeneous media like soft biological tissue, the difference

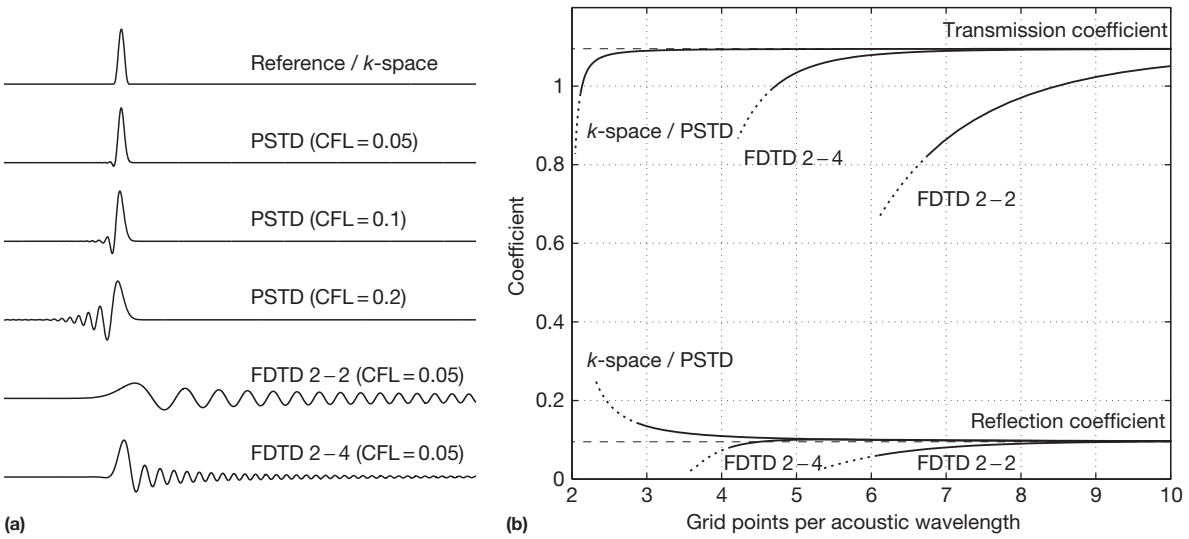

Figure 13 (a) Effect of numerical dispersion on the propagation of a monopolar pulse using different finite-difference time-domain (FDTD), pseudospectral time-domain (PSTD), and *k*-space PSTD schemes. (b) Modeled reflection and transmission coefficients for a 10% step increase in sound speed and density using different numerical schemes. The exact values are shown with the dashed lines.

in sound speeds is generally small, and thus, the *k*-space approach can still significantly reduce numerical dispersion (Treeby et al., 2012b).

For a homogeneous medium, the *k*-space and pseudospectral methods allow spatial derivatives to be computed exactly down to the Nyquist limit of two grid points per wavelength. They also allow a reduction in the number of points per wavelength required to accurately account for the effect of heterogeneous interfaces. This is illustrated in **Figure 13(b)**, which shows the computed reflection and transmission coefficients for a plane wave traveling through a 10% step increase in sound speed and density. Compared to the FD method, the *k*-space and PSTD methods allow a considerable reduction in the number of required points per wavelength for accurate solutions.

2.19.4.3.3 *The* k-Wave *toolbox*

The *k*-space pseudospectral method described in the previous section is implemented in k-Wave, an open source acoustics toolbox written for MATLAB and C++. The simulation functions in k-Wave use the *k*-space method to solve an extended version of the first-order continuum equations discussed in this article (Treeby and Cox, 2010a; Treeby et al., 2012a,b). In particular, power-law acoustic attenuation is accounted for using a linear integrodifferential operator based on the fractional Laplacian (Treeby and Cox, 2010b). The simulation functions are implemented in 1-D, 2-D, and 3-D and allow for an arbitrary distribution of heterogeneous material parameters (sound speed, density, nonlinearity, and attenuation). The functions include the ability to model pressure and velocity sources, photoacoustic sources, and diagnostic and therapeutic ultrasound transducers. They also allow arbitrary detection surfaces to be specified, with options to record acoustic pressure, particle velocity, and acoustic intensity. Further details are given in the k-Wave manual (Treeby et al., 2012a).

2.19.5 Numerical Methods for Nonlinear Ultrasound Fields

2.19.5.1 Background and Common Numerical Methods

Because medical ultrasound fields from practical transducers vary in more than one direction, their nonlinear propagation cannot be simulated by direct application of one of the semi-analytical approaches from **Chapter 2.16**. As a consequence, realistic nonlinear ultrasound fields can only be simulated by numerical methods.

A difficulty encountered with the development of these simulation methods is that in the nonlinear regime, the superposition principle cannot be used. Consequently, the idea of solving the entire wave propagation problem in the frequency domain and finally transforming the result back to the time domain does not work here. Another consequence is that the Green's function of a nonlinear propagation problem is a useless concept, and this fact inhibits the straightforward use of volume and boundary integral equations. As will be shown later, integral transformations and Green's functions are used in nonlinear simulation methods but only in steps that in themselves are linear. A numerical aspect is that the creation of higher harmonics asks for a much finer sampling in space and time as compared to the linear case in which these harmonics remain absent.

Although in this section methods will be presented in the context of nonlinear ultrasound, most methods are also useful in case of linear ultrasound propagation.

2.19.5.1.1 Time- and frequency-domain methods

There is a clear distinction between nonlinear time-domain and nonlinear frequency-domain methods. Time-domain methods are more suitable for the simulation of short propagating pulses or bursts, that is, fields with a dense frequency spectrum. On the other hand, frequency-domain methods perform better for periodic waves with only a few frequency components, that is, a sparse frequency spectrum. Although frequency-domain methods may be applied when a periodic repetition of pulses is used for mimicking single pulse propagation (Baker and Humphrey, 1992), the necessity of computing many frequency components forms a drawback of this approach.

2.19.5.1.2 Split-step and KZK methods

Another distinction between nonlinear methods is whether assumptions about directional behavior of the acoustic wave field are employed. If an ultrasound field propagates mainly in a direction perpendicular to the transducer surface and reflections are unimportant, the directionality of the field enables the use of forward stepping methods. The general principle of these methods is that they start with a given field at the source plane, for example, at $z=0$, and propagate this field forward over a succession of parallel planes that are separated by a distance Δz; see **Figure 14**. The forward stepping approach is computationally efficient because it is not bound to the Nyquist criterion and yields accurate results even with step sizes Δz that are much larger than half the wavelength.

There exist many forward stepping methods, each having their own particular approach in performing the steps. In general, the propagating ultrasound field undergoes changes due to diffraction, attenuation, and nonlinear distortion. If the steps Δz are small enough, these changes may be computed in succession. This approach is used in split-step methods. For highly directive ultrasound fields like narrow beams, the Westervelt equation may be subjected to a parabolic

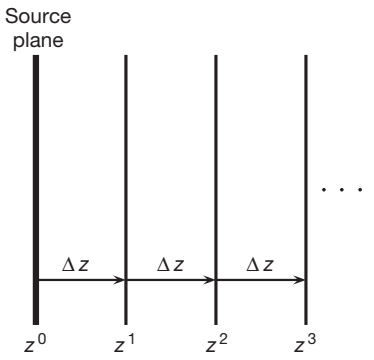

Figure 14 Schematic representation of a forward stepping method. Starting in the source plane, the field is stepped forward with increments Δz.

approximation before performing any numerical steps. The resulting Khokhlov–Zabolotskaya–Kuznetsov (KZK) equation is again solved using the split-step approach. Because split-step methods and KZK methods are often used for the simulation of nonlinear ultrasound, these will be presented in Sections 2.19.5.2 and 2.19.5.3, respectively.

2.19.5.1.3 Omnidirectional methods

A method that can simulate ultrasound fields independently of their direction relative to the computational domain is called omnidirectional. Such methods are relevant when reflections are important or when fields have quite different directions, for example, when an array emits a main and a grating lobe.

One way of getting omnidirectional methods for solving nonlinear acoustic wave problems is to take the first-order basic acoustic equations or the Westervelt equation and numerically solve these by FD, FE, or pseudospectral methods. Examples of nonlinear FD methods may be found in Sparrow and Raspet (1991), Yano and Inoue (1996), Hallaj and Cleveland (1999), and Pinton et al. (2009). A description of a nonlinear FE method is given by Hoffelner et al. (2001). FD and FE methods usually operate directly in the space–time domain and compute the spatial acoustic field distribution at successive time steps. With these methods, the temporal and spatial steps will be chosen much smaller than the step sizes prescribed by the Nyquist criterion, that is, much smaller than half the period and half the wavelength of the highest occurring frequency. Typically, over 20 points per period and per wavelength are required to get accurate results and in particular to battle numerical dispersion. Especially when multiple higher harmonics must be taken into account, these dense grids soon lead to a large storage demand. Numerical stability problems may be prevented by the introduction of (artificial) damping (Ginter et al., 2002; Sparrow and Raspet, 1991). Numerical dispersion and storage problems can be significantly relieved by solving the problem in the spatial frequency domain by means of a Fourier pseudospectral method. Pseudospectral methods for simulating nonlinear ultrasound are, for example, described by Wojcik et al. (1997) and Treeby et al. (2012b). These methods allow a reduction of the spatial grid to only two points per wavelength as demanded by the Nyquist criterion. The temporal grid still needs to be rather dense. Because FD, FE, and pseudospectral methods have been described extensively in Section 2.19.4, these will not be treated in more detail here.

Another way to arrive at omnidirectional methods for computing nonlinear acoustic propagation is to use the IE method. An example of this is the iterative nonlinear contrast source (INCS) method described by Huijssen and Verweij (2010), which will be described in Section 2.19.5.4. The IE approach enables the application of a spatiotemporal grid with only two points per wavelength and period.

A comparison between two omnidirectional methods, the INCS method and a nonlinear version of the *k*-space method, will be presented in Section 2.19.5.5.

2.19.5.2 Split-Step Methods

If a directional ultrasound field is stepped forward with sufficiently small steps Δz, the effects of diffraction, attenuation, and nonlinear distortion need not be computed in one simultaneous process, but may be accounted for in successive substeps. This is the principle behind split-step methods. The mathematical foundation of this method is described by Varslot and Taraldsen (2005). The split-step approach is an approximation that is based on operator splitting. If the diffraction, attenuation, and nonlinearity substeps are applied over the same step Δz, as depicted in Figure 15(a), the obtained method is order $O(\Delta z)$ accurate. However, if the attenuation and nonlinearity substeps over Δz are preceded and followed by 'half' diffraction substeps over $\Delta z/2$, as shown in Figure 15(b), the resulting method is order $O(\Delta z^2)$ accurate (Tavakkoli et al., 1998). Each substep may be performed in the time domain, the temporal frequency domain, and sometimes also the spatial frequency domain. Moreover, each substep may be performed for either the acoustic pressure or the particle velocity. Another distinction is whether normal time or retarded time is applied. Because this gives rise to many possible combinations of substeps, there are also many different split-step methods. Some substeps will be presented later, and some more substeps will be discussed as part of a KZK method.

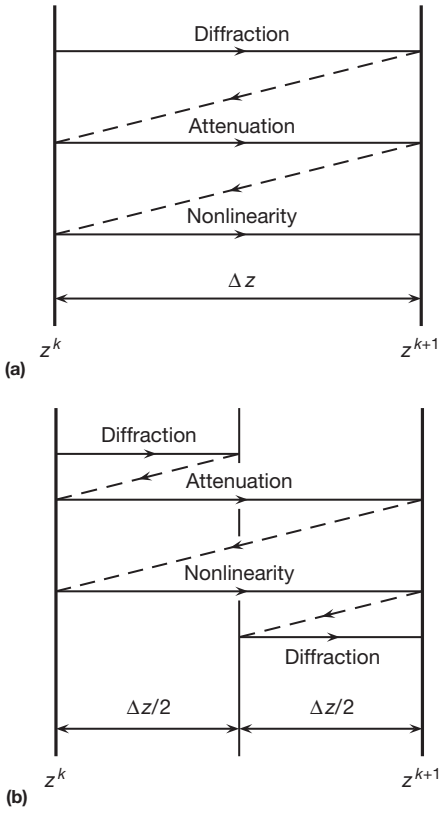

Figure 15 Schematic representation of a single step in the split-step method. (a) When the diffraction, attenuation, and nonlinearity substeps are all performed over the same interval Δz, the method has order $O(\Delta z)$ accuracy. (b) When the attenuation and nonlinearity substeps are preceded and followed by diffraction substeps over $\Delta z/2$, the method has order $O(\Delta z^2)$ accuracy.

2.19.5.2.1 Diffraction substep

If no further assumptions on the directionality of the acoustic wave field are made, the diffraction substep may be based on the time-domain lossless linear wave equation of eqn [20] or on its frequency-domain counterpart. A third alternative is to apply a spatial Hankel transformation with respect to the radial lateral coordinate r (Christopher and Parker, 1991a,b) in the case of circularly symmetric fields, or spatial Fourier transformations with respect to the Cartesian lateral coordinates x and y (Varslot and Måsøy, 2006; Zemp et al., 2003) in less symmetric cases. This results in the angular spectrum approach, which, for example, is used for the diffraction substep in the simulation package Abersim (Frijlink et al., 2008).

Subjecting eqn [20] to Fourier transformations with respect to time and with respect to the lateral coordinates x and y leads to the angular spectrum representation:

$$\frac{\partial^2 \tilde{p}}{\partial z^2} + k_z^2 \tilde{p} = 0 \qquad [147]$$

where the tilde has been used to indicate angular spectrum domain quantities. Further,

$$k_z = \begin{cases} \sqrt{k^2 - k_x^2 - k_y^2} & \text{for } k_x^2 + k_y^2 \le k^2 \\ -j\sqrt{k_x^2 + k_y^2 - k^2} & \text{for } k_x^2 + k_y^2 > k^2 \end{cases} \qquad [148]$$

is the axial propagation coefficient, where k_x and k_y are the lateral spatial frequencies. The first line of eqn [148] is associated with propagating waves and the second line is related with evanescent waves. As before, $k = \omega/c_0$ is the wave number. The diffraction substep is most easily performed in the angular spectrum domain. The solutions of eqn [147] are of the form $\exp(\pm jk_z z)$, where the positive sign applies to waves in the negative z-direction, and vice versa. Stepping $\tilde{p}$ over a positive distance Δz is therefore achieved by

$$\tilde{p}(k_x, k_y, z + \Delta z, \omega) = \tilde{h}(k_x, k_y, \Delta z, \omega)\tilde{p}(k_x, k_y, z, \omega) \qquad [149]$$

in which

$$\tilde{h}(k_x, k_y, \Delta z, \omega) = \exp(-jk_z \Delta z) \qquad [150]$$

is called the spectral operator or spatial frequency transfer function.

In the frequency domain, the diffraction substep is obtained by computing (Zemp et al., 2003)

$$\hat{p}(x, y, z + \Delta z, \omega) = \iint_{\mathcal{A}} \hat{h}\left(x - x', y - y', \Delta z, \omega\right) \times \hat{p}\left(x', y', z, \omega\right) \mathrm{d}x' \, \mathrm{d}y' \qquad [151]$$

where $\hat{h}(x, y, \Delta z, \omega)$ is the counterpart of $\tilde{h}(k_x, k_y, \Delta z, \omega)$. This is a convolution of the so-called point spread function $\hat{h}$ and the pressure $\hat{p}$ over the lateral plane. The integration domain $\mathcal{A}$ should span the area where $\hat{p}$ is significant. The point spread function is

$$\hat{h}(x, y, \Delta z, \omega) = \frac{\Delta z \exp(-jkR)}{2\pi R^2}\left(\frac{1}{R} + jk\right) \qquad [152]$$

where $R = \sqrt{x^2 + y^2 + \Delta z^2}$. After application of a Fourier or Hankel transformation with respect to the lateral coordinates, the convolution can be performed as a multiplication in the relevant transform domain.

The time-domain version of eqn [151] is

$$p(x, y, z + \Delta z, t) = \int_{-\infty}^{\infty} \iint_{\mathcal{A}} h\left(x - x', y - y', \Delta z, t - t'\right) \times p\left(x', y', z, t'\right) \mathrm{d}x' \, \mathrm{d}y' \, \mathrm{d}t' \qquad [153]$$

with

$$h(x, y, \Delta z, t) = \frac{\Delta z}{2\pi R^2}\left(\frac{1}{c_0}\frac{\partial}{\partial t} + \frac{1}{R}\right)\delta(t - R/c_0) \qquad [154]$$

which is the time domain counterpart of eqn [152]. The equations presented here for the acoustic pressure may equally well be used for the forward stepping of the normal component of the particle velocity. For narrow beams, approximations are possible. This is further discussed in Section 2.19.5.3.

2.19.5.2.2 Attenuation substep

The attenuation substep is most easily performed in the frequency domain. For a given attenuation coefficient $\alpha(\omega)$ and corresponding phase coefficient $\beta(\omega)$, the attenuation substep is

$$\hat{p}(x, y, z + \Delta z, \omega) = \hat{p}(x, y, z, \omega)\hat{g}(\Delta z, \omega) \qquad [155]$$

with

$$\hat{g}(\Delta z, \omega) = \exp(-[\alpha(\omega) + j\beta(\omega) - jk]\Delta z) \qquad [156]$$

The term jk is subtracted because lossless propagation has already been accounted for in the diffraction substep. Sometimes, the frequency-domain attenuation substep is combined with the diffraction substep in eqns [151]–[152].

The time-domain version of the procedure mentioned earlier is described in Tavakkoli et al. (1998). In this case, the attenuation substep is

$$p(x, y, z + \Delta z, t) = \int_{-\infty}^{\infty} g\left(\Delta z, t - t'\right) p\left(x, y, z, t'\right) \mathrm{d}t' \qquad [157]$$

where $g(\Delta z, t)$ is the time-domain counterpart of $\hat{g}(\Delta z, \omega)$. This substep may be combined with the diffraction substep in eqns [153] and [154].

2.19.5.2.3 Nonlinear substep

In the time domain, the nonlinear substep is usually obtained by first transforming the field $p(x,y,z,t)$ into the comoving field $\bar{\bar{p}}(x, y, z, \tau)$, where $\tau = t - z/c_0$ is retarded time, and then numerically solving the lossless version of the Burgers equation (see Chapter 2.16, eqn [58]):

$$\frac{\partial \bar{\bar{p}}}{\partial z} = \frac{\beta \bar{\bar{p}}}{\rho_0 c_0^3}\frac{\partial \bar{\bar{p}}}{\partial \tau} \qquad [158]$$

Equation [64] of the same chapter shows that $\bar{\bar{p}}(z)$ can be stepped forward over Δz by using

$$\bar{\bar{p}}(z + \Delta z, \tau) = \bar{\bar{p}}\left[z, \tau + \frac{\beta \bar{\bar{p}}(z, \tau)}{\rho_0 c_0^3}\Delta z\right] \qquad [159]$$

This equation shows that the nonlinear substep can be implemented as a deformation of the retarded time axis. The most frequently used algorithm to numerically solve eqn [158]

is based on this idea and may be found in Cleveland et al. (1996) and Ginsberg and Hamilton (2008). It can be derived as follows. Equation [159] is rewritten as

$$\bar{\bar{p}}\left[z+\Delta z,\tau-\frac{\beta\bar{\bar{p}}(z,\tau)}{\rho_0 c_0^3}\Delta z\right]=\bar{\bar{p}}(z,\tau) \qquad [160]$$

Suppose that for a spatial distance z^k (k being the space index) and a number of retarded times τ_i^k (i being the time index), the pressure values $\bar{\bar{p}}(z^k,\tau_i^k)$ are known. Note that successive τ_i^k need not differ by a constant time interval. According to eqn [160], the pressure at the spatial distance $z^{k+1}=z^k+\Delta z$ satisfies

$$\bar{\bar{p}}\left[z^{k+1},\tau_i^k-\frac{\beta\bar{\bar{p}}(z^k,\tau_i^k)}{\rho_0 c_0^3}\Delta z\right]=\bar{\bar{p}}(z^k,\tau_i^k) \qquad [161]$$

Introduction of a new set of retarded times

$$\tau_i^{k+1}=\tau_i^k-\frac{\beta\bar{\bar{p}}(z^k,\tau_i^k)}{\rho_0 c_0^3}\Delta z \qquad [162]$$

makes it possible to write eqn [161] as

$$\bar{\bar{p}}(z^{k+1},\tau_i^{k+1})=\bar{\bar{p}}(z^k,\tau_i^k) \qquad [163]$$

This implies that the pressure values at z^{k+1} may easily be found by taking the pressure values at z^k and assigning these to new retarded time instants τ_i^{k+1}. Equation [162] defines the required time base transformation. To ensure causality, the spatial step must be chosen sufficiently small to avoid the time instants 'crossing over each other' during the deformation of the time axis, that is, to ensure that always $\tau_{i+1}^{k+1}>\tau_i^{k+1}$. The described algorithm appears in virtually all time-domain split-step methods for the simulation of nonlinear ultrasound.

There exists also a frequency-domain equivalent of the nonlinear substep that is based on the Burgers equation. A derivation of this may be found in Ginsberg and Hamilton (2008). In this case, it is assumed that the pressure that is to be stepped forward may be approximated by

$$\bar{\bar{p}}(x,y,z,\tau)=\frac{1}{2}\sum_{n=-M}^{M}P_n(x,y,z)\exp(jn\omega_0\tau)$$
$$\text{with } P_0(x,y,z)=0 \qquad [164]$$

Substitution into eqn [158] gives, after several manipulations,

$$\frac{\partial P_n}{\partial z}=\frac{j\beta\omega_0}{2c_0^2}\left(\sum_{i=1}^{n-1}iP_iP_{n-i}+\sum_{i=n+1}^{M}nP_iP_{i-n}^*\right) \qquad [165]$$

where the asterisk indicates the complex conjugate. This equation is integrated over Δz by approximating the differentiation at the left-hand side by an FD and reordering terms. This yields

$$P_n(z+\Delta z)=P_n(z)$$
$$+\Delta z\frac{j\beta\omega_0}{2c_0^2}\left[\sum_{i=1}^{n-1}iP_i(z)P_{n-i}(z)+\sum_{i=n+1}^{M}nP_i(z)P_{i-n}^*(z)\right] \qquad [166]$$

2.19.5.3 KZK Methods

For a relatively narrow beam of quasiplanar waves, the omnidirectional Westervelt equation may be approximated by the directional KZK equation. The derivation of this equation is given in Hamilton and Morfey (2008) and goes in two steps. First, the retarded time coordinate $\tau=t-z/c_0$ is used to replace the ordinary time coordinate t. Here, the positive z-axis is assumed to be the predominant direction of propagation, that is, the beam axis. In the retarded time frame, the acoustic pressure is indicated by $\bar{\bar{p}}(x,y,z,\tau)$. Because the acoustic pressure does not change when transforming from one time frame to another, the pressure in the retarded time frame should equal the pressure in the normal time frame, so $\bar{\bar{p}}(x,y,z,\tau)=p(x,y,z,t)$. These substitutions turn the Westervelt equation with thermoviscous losses (eqn [25] with $\mathcal{L}=0$) into

$$\nabla^2\bar{\bar{p}}-\frac{2}{c_0}\frac{\partial^2\bar{\bar{p}}}{\partial z\partial\tau}+\frac{\delta}{c_0^4}\frac{\partial^3\bar{\bar{p}}}{\partial\tau^3}=-\frac{\beta}{\rho_0 c_0^4}\frac{\partial^2\bar{\bar{p}}^2}{\partial\tau^2} \qquad [167]$$

Second, it is recognized that in the retarded time frame, the second derivative of $\bar{\bar{p}}$ with respect to the axial coordinate z is much smaller than the second derivatives with respect to the lateral coordinates x and y. This leads to the paraxial approximation

$$\nabla^2\bar{\bar{p}}=\frac{\partial^2\bar{\bar{p}}}{\partial x^2}+\frac{\partial^2\bar{\bar{p}}}{\partial y^2}+\frac{\partial^2\bar{\bar{p}}}{\partial z^2}\approx\frac{\partial^2\bar{\bar{p}}}{\partial x^2}+\frac{\partial^2\bar{\bar{p}}}{\partial y^2}=\nabla_\perp^2\bar{\bar{p}} \qquad [168]$$

where $\nabla_\perp^2$ is the Laplacian in the lateral plane. Using this in eqn [167] and multiplying all terms with $-c_0/2$, it is found that a narrow beam may be described by

$$\frac{\partial^2\bar{\bar{p}}}{\partial z\partial\tau}-\frac{c_0}{2}\nabla_\perp^2\bar{\bar{p}}-\frac{\delta}{2c_0^3}\frac{\partial^3\bar{\bar{p}}}{\partial\tau^3}=\frac{\beta}{2\rho_0 c_0^3}\frac{\partial^2\bar{\bar{p}}^2}{\partial\tau^2} \qquad [169]$$

This is the KZK equation. The second term at the left-hand side of this equation represents the diffraction of the beam, and the term at the right-hand side represents its nonlinear propagation. The parabolic equation is only accurate for waves that propagate in directions close to the z-direction. Consequently, the KZK equation is not valid near the source (where the field is not yet directed) and for propagation directions that deviate more than 20° from the z-direction (Lee and Pierce, 1995).

Usually, coordinate transformations are used to improve the performance in the far field or for specific types of focused beams. This will result in alternatives of the KZK equation. Because equations like [169] are used to describe the propagation of a beam away from the transducer, these are collectively called beam equations (also known as progressive or evolution equations). For example, the nonlinear spheroidal beam equation described by Kamakura et al. (2000) uses oblate spheroidal coordinates to specifically deal with spherical or elliptical transducers with a wide opening angle. As another example, Fox et al. (2005) have applied coordinate rotations to match the preferred direction of the KZK equation with the direction of a steered narrow beam.

2.19.5.3.1 Texas code

The Texas code (Cleveland et al., 1996; Lee and Hamilton, 1995) is intended for generating solutions of the KZK equation in the time domain. It is based on the equation that is obtained by integrating eqn [169] with respect to τ:

$$\frac{\partial\bar{\bar{p}}}{\partial z}=\frac{c_0}{2}\int_{-\infty}^{\tau}\nabla_\perp^2\bar{\bar{p}}(\tau')\,d\tau'+\frac{\delta}{2c_0^3}\frac{\partial^2\bar{\bar{p}}}{\partial\tau^2}+\frac{\beta\bar{\bar{p}}}{\rho_0 c_0^3}\frac{\partial\bar{\bar{p}}}{\partial\tau} \qquad [170]$$

The code solves this equation using the split-step approach as indicated in Figure 15(a).

In the first substep, the diffraction over Δz is computed. The input of this substep is $\bar{\bar{p}}_{\mathrm{d}}(z) = \bar{\bar{p}}(z)$, where $\bar{\bar{p}}(z)$ is the known pressure distribution that needs to be stepped forward. At the start of the scheme, this is the given pressure distribution in the transducer plane, and when the scheme is running, this is the pressure distribution resulting from the previous step. The output of the diffraction substep is $\bar{\bar{p}}_{\mathrm{d}}(z + \Delta z)$, which is obtained by numerically solving the diffraction part from eqn [170]:

$$\frac{\partial \bar{\bar{p}}_{\mathrm{d}}}{\partial z} = \frac{c_0}{2} \int_{-\infty}^{\tau} \nabla_{\perp}^2 \bar{\bar{p}}_{\mathrm{d}}\left(\tau'\right) \mathrm{d}\tau' \qquad [171]$$

Application of the first-order FD approximation of the derivative yields

$$\bar{\bar{p}}_{\mathrm{d}}(z + \Delta z, \tau) = \bar{\bar{p}}_{\mathrm{d}}(z, \tau) + \Delta z \frac{c_0}{2} \int_{-\infty}^{\tau} \nabla_{\perp}^2 \bar{\bar{p}}_{\mathrm{d}}\left(z, \tau'\right) \mathrm{d}\tau' \qquad [172]$$

The integral is computed using the trapezoidal rule, and the second-order spatial derivatives due to the $\nabla_{\perp}^2$ operator are evaluated using FDs.

The second substep over Δz concerns the computation of the attenuation. The input of this substep is $\bar{\bar{p}}_{\mathrm{a}}(z) = \bar{\bar{p}}_{\mathrm{d}}(z + \Delta z)$ and the output is $\bar{\bar{p}}_{\mathrm{a}}(z + \Delta z)$. This is obtained by numerically solving the attenuation part from eqn [170]:

$$\frac{\partial \bar{\bar{p}}_{\mathrm{a}}}{\partial z} = \frac{\delta}{2c_0^3} \frac{\partial^2 \bar{\bar{p}}_{\mathrm{a}}}{\partial \tau^2} \qquad [173]$$

The same approach as for the diffraction substep now yields

$$\bar{\bar{p}}_{\mathrm{a}}(z + \Delta z, \tau) = \bar{\bar{p}}_{\mathrm{a}}(z, \tau) + \Delta z \frac{\delta}{2c_0^3} \frac{\partial^2 \bar{\bar{p}}_{\mathrm{a}}(z, \tau)}{\partial \tau^2} \qquad [174]$$

The second-order temporal derivative at the right-hand side is computed using FDs.

To focus on the basics of the applied approach, the diffraction and attenuation substeps have been described here in their simplest form. In actual implementations of the Texas code, these steps are more elaborate. Commonly, coordinate transformations and normalization of quantities are employed. In one particular version, eqn [173] is supplemented by a number of equations that represent separate relaxation processes (Cleveland et al., 1996). Moreover, to reduce numerical oscillations in the near field of the transducer, in this zone, eqns [171] and [173] are usually solved using an implicit backward FD scheme, and to allow for larger steps Δz, outside the near field, a Crank–Nicolson scheme is commonly applied (Lee and Hamilton, 1995). Sometimes, an alternating direction implicit scheme is used for the integration of eqn [171] (Yang and Cleveland, 2005). Also, the step size Δz is often chosen in an adaptive way.

In the third substep, the nonlinear distortion over Δz is computed. The input of this substep is $\bar{\bar{p}}_{\mathrm{n}}(z) = \bar{\bar{p}}_{\mathrm{a}}(z + \Delta z)$ and the output is $\bar{\bar{p}}_{\mathrm{n}}(z + \Delta z)$, which follows from numerically solving the nonlinear part from eqn [170]:

$$\frac{\partial \bar{\bar{p}}_{\mathrm{n}}}{\partial z} = \frac{\beta \bar{\bar{p}}_{\mathrm{n}}}{\rho_0 c_0^3} \frac{\partial \bar{\bar{p}}_{\mathrm{n}}}{\partial \tau} \qquad [175]$$

This is performed with the time base transformation described in Section 2.19.5.2.3. The output $\bar{\bar{p}}_{\mathrm{n}}(z + \Delta z, \tau) = \bar{\bar{p}}(z + \Delta z, \tau)$ is the final result of the forward stepping over Δz.

2.19.5.3.2 Bergen code

The Bergen code (Aanonsen et al., 1984; Baker et al., 1995) provides solutions of the KZK equation in the frequency domain. It is based on a finite Fourier sum that approximates the ultrasound field of a periodic source with frequency ω_0 by

$$\bar{\bar{p}}(x, y, z, \tau) = \sum_{n=1}^{M} a_n(x, y, z) \sin\left(n\omega_0\tau\right) + b_n(x, y, z) \cos\left(n\omega_0\tau\right) \qquad [176]$$

in which the coefficients a_n and b_n represent the local amplitudes of the harmonics. Substitution of eqn [176] into eqn [169] provides a system of coupled differential equations that relate a_n and b_n through

$$\frac{\partial a_n}{\partial z} = A_{1,n} a_n + D_{1,n} \nabla_{\perp} b_n + N_{1,n} \left[\frac{1}{2} \sum_{p=1}^{n-1} \left(a_p a_{n-p} - b_p b_{n-p}\right) - \sum_{p=n+1}^{M} \left(a_{p-n} a_p - b_{p-n} b_p\right) \right] \qquad [177]$$

$$\frac{\partial b_n}{\partial z} = A_{2,n} b_n + D_{2,n} \nabla_{\perp} a_n + N_{2,n} \left[\frac{1}{2} \sum_{p=1}^{n-1} \left(b_p a_{n-p} - a_p b_{n-p}\right) - \sum_{p=n+1}^{M} \left(b_{p-n} a_p - a_{p-n} b_p\right) \right] \qquad [178]$$

Here, the terms with constants A account for the attenuation, the terms with constants D represent the diffraction, and the terms with constants N include the nonlinear propagation. The system of equations is efficiently solved by employing an implicit backward FD scheme in the near field of the transducer and an alternating direction implicit scheme outside this zone.

2.19.5.4 INCS Method

The INCS method is an omnidirectional method for the simulation of nonlinear, pulsed ultrasound fields in media with realistic tissue attenuation and heterogeneity. It has been formulated in its original form by Huijssen (2008) and Huijssen and Verweij (2010), and later, extensions have been described by Demi et al. (2011), Demi (2013), and Verweij et al. (2013). The method is based on the IE for a nonlinear contrast source problem. In doing so, it avoids the limitations that are posed by the use of the 1-D Burgers equation. By filtering the relevant quantities in space and time, the numerical solution of the IE can be performed at a discretization that is close to two points per spatial wavelength and temporal period. Because of the coarse grid, simulations involving a computational domain that measures hundreds of wavelengths and periods of the maximum frequency of interest are nowadays possible on a moderate computer cluster. In view of the medical diagnostic application, the focus is on weak to moderate nonlinearity. First, the lossless and homogeneous case will be presented, and later, the inclusion of losses and inhomogeneities will be discussed. At that stage, it will also become clear that in the

absence of nonlinearity, the INCS method turns into an IE method for the simulation of linear ultrasound waves.

2.19.5.4.1 Contrast source formulation and iterative solution

The INCS method is based on the Westervelt equation. For the lossless and homogeneous case, this is given by eqn [17], and when the action of the transducer is explicitly taken into account, one obtains

$$\nabla^2 p - \frac{1}{c_0^2}\frac{\partial^2 p}{\partial t^2} = -S_{\mathrm{tr}} - \frac{\beta}{\rho_0 c_0^4}\frac{\partial^2 p^2}{\partial t^2} \qquad [179]$$

The basic idea behind the INCS method is that the nonlinear term at the right-hand side of this equation is considered as a distributed contrast source

$$S_{\mathrm{nl}}(p) = \frac{\beta}{\rho_0 c_0^4}\frac{\partial^2 p^2}{\partial t^2} \qquad [180]$$

In view of this, eqn [179] is rewritten as

$$\nabla^2 p - \frac{1}{c_0^2}\frac{\partial^2 p}{\partial t^2} = -S_{\mathrm{tr}} - S_{\mathrm{nl}}(p) \qquad [181]$$

Note that the terms on the left-hand side of this equation form the wave operator of a linear medium with wave speed c_0. Along the same line of thought, the terms on the right-hand side can be considered as two separate sources that generate waves in this linear 'background' medium. The primary source S_{tr} causes the linear acoustic field contribution

$$p^{(0)}(\boldsymbol{x},t) = S_{\mathrm{tr}}(\boldsymbol{x},t) *_{\boldsymbol{x},t} G(\boldsymbol{x},t) \qquad [182]$$

that is also present in the absence of nonlinearity, that is, if $S_{\mathrm{nl}}(p)=0$. Here, $G(\boldsymbol{x},t)$ is the 3-D Green's function defined in eqn [49]. The contrast source $S_{\mathrm{nl}}(p)$ causes a contribution

$$\delta p(\boldsymbol{x},t) = S_{\mathrm{nl}}[p(\boldsymbol{x},t)] *_{\boldsymbol{x},t} G(\boldsymbol{x},t) \qquad [183]$$

which accounts for the nonlinear distortion of the acoustic field. The total field is

$$\begin{aligned} p(\boldsymbol{x},t) &= p^{(0)}(\boldsymbol{x},t) + \delta p(\boldsymbol{x},t) \\ &= p^{(0)}(\boldsymbol{x},t) + S_{\mathrm{nl}}[p(\boldsymbol{x},t)] *_{\boldsymbol{x},t} G(\boldsymbol{x},t) \end{aligned} \qquad [184]$$

Because $p(\boldsymbol{x},t)$ appears on the left-hand side as well as on the right-hand side, this is an IE that needs to be solved for $p(\boldsymbol{x},t)$. A simple iterative scheme to do so is as follows:

1. Compute $p^{(0)}(\boldsymbol{x},t) = S_{\mathrm{tr}}(\boldsymbol{x},t) *_{\boldsymbol{x},t} G(\boldsymbol{x},t)$.
2. Set $j=1$.
3. Define $S^{(j)}(\boldsymbol{x},t) = S_{\mathrm{nl}}[p^{(j-1)}(\boldsymbol{x},t)]$.
4. Compute $p^{(j)}(\boldsymbol{x},t) = p^{(0)}(\boldsymbol{x},t) + S^{(j)}(\boldsymbol{x},t) *_{\boldsymbol{x},t} G(\boldsymbol{x},t)$.
5. If the answer is not accurate enough, set $j=j+1$ and go to step 3, otherwise stop.

This scheme is known as the Neumann iterative solution. It can be interpreted as a perturbation scheme, where $p^{(1)}(\boldsymbol{x},t)$ is identified as the quasilinear solution (Ginsberg, 2008). With increasing j, this quasilinear solution is iteratively improved towards the full nonlinear wave field.

The convergence of the scheme is illustrated in Figure 16 for a nonlinearly propagating pulsed plane wave in water. The iterations $p^{(j)}$ are compared to the solution of the Burgers equation, which serves as a benchmark. The convergence of the Neumann iterative solution is very fast. As a rule of thumb, to obtain a relative error in the order of a percent in the simulation of the hth harmonic, it is sufficient to compute iteration $j=h+1$ in the case of weak to moderate nonlinear distortion as encountered in medical diagnostics.

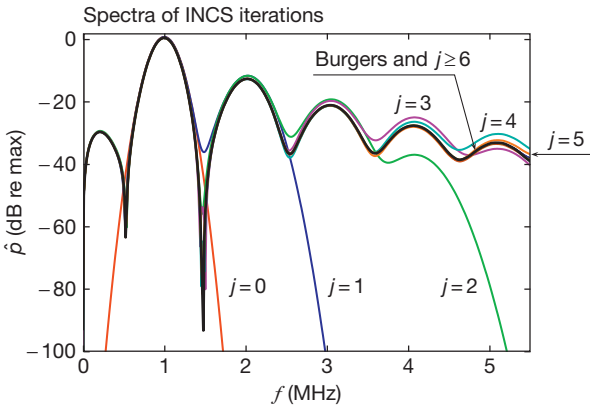

Figure 16 Frequency spectra of iterations $p^{(j)}$ as obtained by the iterative nonlinear contrast source (INCS) method for a plane acoustic wave showing nonlinear propagation. The iterations for $j=0$ to $j=6$ (thin colored lines) are compared to the solution of the Burgers equation (thick black line), which is considered as a benchmark. The medium is water, and the excitation pulse has an amplitude of 500 kPa, a center frequency of 1 MHz and a Gaussian envelope with a width of $2\sigma=2.12$ μs. The point of observation is at $x=100$ mm. Each successive iteration $p^{(j)}$ gives a better estimate for increasingly higher harmonics.

2.19.5.4.2 Discretization and evaluation of the convolution integral

Even in very simple situations, the convolution $S^{(j)}(\boldsymbol{x},t) *_{\boldsymbol{x},t} G(\boldsymbol{x},t)$ that appears in step 4 of the Neumann scheme mentioned earlier must be evaluated numerically. Because $S^{(j)}(\boldsymbol{x},t)$ and $G(\boldsymbol{x},t)$ are distributed over the entire spatial and temporal computational domain, the convolution integrals also run over this entire domain. For domains with realistically large dimensions, efficient computation and storage requires a grid that is as coarse as possible, preferably with only two points per shortest wavelength and period as demanded by the Nyquist criterion. This is achieved by using the filtered convolution method (Verweij and Huijssen, 2009).

For simplicity, the filtered convolution method is first explained for the one-dimensional temporal convolution integral:

$$F(t) = G(t) *_t S(t) = \int_{-\infty}^{\infty} G\left(t-t'\right) S\left(t'\right) \mathrm{d}t' \qquad [185]$$

This integral may be approximated by the convolution sum:

$$F_n = G_n *_n S_n = \Delta t \sum_m G_{n-m} S_m \qquad [186]$$

where $G_n = G(n\Delta t)$ and $S_n = S(n\Delta t)$ are samples of $G(t)$ and $S(t)$, F_n approximates $F(n\Delta t)$, and Δt is the applied sampling interval. For numerical computations, the number of samples must be limited. This corresponds to windowing of the functions in eqn [185]. When it is sufficient to consider S_n for $n \in$

$[0, N-1]$ and F_n is needed on that same interval, then G_n may be restricted to the interval $n \in [-N+1, N-1]$ without influencing the desired values of F_n. The convolution sum in eqn [186] is efficiently evaluated by using FFTs. Because this requires each function to have the same number of samples, for $n \in [-N+1, -1]$ extra samples $S_n = 0$ are added to the existing sequence. This zero-padding also cures the fact that by using FFTs, one actually performs a circular convolution that might spoil the desired F_n. The length of the involved FFTs is $2N$, which results in a computational effort per convolution in the order of $2N \log(2N)$. The main difference between the approximate F_n and the exact $F(n\Delta t)$ usually arises from the sampling of the involved functions. If no further precautions are taken, accurate results may necessitate a sampling with many (10 or more) points per period of the highest frequency that is expected in $F(t)$. In particular for higher-dimensional convolutions, this may lead impractically large grid sizes.

However, it may be assumed that there is a maximum angular frequency of interest Φ such that all the relevant components of $F(t)$ have angular frequencies $|\omega| \leq \Phi$ and all the components with $|\omega| > \Phi$ may be discarded. This fact will now be employed to reduce the number of points per wavelength without risking large sampling errors. First, $G(t)$ and $S(t)$ are subjected to an ideal low-pass filter with an angular cutoff frequency $\Omega \geq \Phi$. The cutoff frequency may be chosen larger than the maximum frequency of interest to keep in some more frequencies 'for safety.' Because $F(t)$ is the convolution of these functions, the filtering will not remove any components of interest. Next, $G(t)$ and $S(t)$ are sampled using a sampling interval $\Delta t = \pi/\Omega$. Since this yields at least two points per period for all frequencies that have remained after the filtering, the Nyquist criterion is satisfied and aliasing will not occur. Subsequently, the numerical convolution is performed using FFTs. Due to the absence of aliasing, the resulting F_n will in fact be equal to the samples of the filtered version of the exact $F(t)$. In other words, the only approximation error that will be made is due to the applied filtering, and this will only affect components that have been considered to be of no interest. By discarding the components with frequencies $|\omega| > \Omega$, the procedure mentioned earlier avoids aliasing errors to occur in the components with frequencies $|\omega| \leq \Omega$.

From the explanation mentioned earlier, it follows that the 1-D filtered convolution method consists of the following steps:

1. Filter $G(t)$ and $S(t)$ with an ideal low-pass filter with an angular cutoff frequency $\Omega \geq \Phi$, and apply a window that contains $2N$ sampling points with mutual distance $\Delta t = \pi/\Omega$. The number of sampling points determines the window width $2T = (2N-1)\pi/\Omega$, which must be long enough to contain the significant parts of the functions involved.
2. Sample the filtered and windowed versions of $G(t)$ and $S(t)$ with a sampling distance $\Delta t = \pi/\Omega$, to obtain G_n and S_n. Apply zero-padding to extend the sequence S_n. For both functions, this yields $2N$ sampling points with index $n \in [-N, N-1]$.
3. Apply $2N$-point FFTs to G_n and S_n.
4. Multiply the obtained transforms and perform a $2N$-point inverse FFT.

The numerical computation of the convolution integral $S^{(j)}(\boldsymbol{x},t) * _{\boldsymbol{x},t} G(\boldsymbol{x},t)$ in step 4 of the Neumann scheme requires that the filtered convolution method is applied to each of the four coordinates involved. Besides a maximum temporal angular frequency Φ, also a maximal spatial angular frequency Φ/c_0 is introduced. The latter implies that only wave components with spatial angular frequencies $||\boldsymbol{k}|| = \sqrt{k_x^2 + k_y^2 + k_z^2} \leq \Phi/c_0$ are considered to be interesting. In the first step of the filtered convolution method, $G(\boldsymbol{x},t)$ and $S^{(j)}(\boldsymbol{x},t)$ are filtered and windowed. In the time domain, all frequencies $|\omega| > \Omega$ are removed, where Ω is chosen equal or larger than Φ. In the space domain, all spatial frequencies $||\boldsymbol{k}|| > K = \Omega/c_0$ are filtered out. Next, the functions $G(\boldsymbol{x},t)$ and $S^{(j)}(\boldsymbol{x},t)$ are sampled using a sampling distance $\Delta t = \pi/\Omega$ for the time coordinate and $\Delta x = \pi/K$ for the space coordinates. In this way, the sampling occurs with at least two points per wavelength and period for all frequencies involved, and no temporal or spatial aliasing will occur. Subsequently, the four-dimensional numerical convolution is performed using FFTs.

Because the contrast source $S^{(j)}(\boldsymbol{x},t)$ contains the square of the pressure $p^{(j-1)}(\boldsymbol{x},t)$, the temporal and spatial spectra of the contrast source in step j of the Neumann scheme are twice as wide as the corresponding spectra of the acoustic pressure field obtained at step $j-1$. This doubling of the spectra for each step of the scheme means that the temporal and spatial spectra of the acoustic pressure field reach their limits Ω and K, respectively, after only a few steps of the scheme. At the next step of the scheme, the spectra of the contrast source would pass the limits Ω and K, and aliasing would occur if no precautions were taken. This is why the INCS method consequently applies the filtered convolution for each step of the scheme and in doing so limits the spectra of a newly computed contrast source before the numerical convolution is performed. Further details of the filtering of the contrast source are given in Verweij and Huijssen (2009).

2.19.5.4.3 Inclusion of attenuation and heterogeneity

With the INCS method, attenuation and heterogeneity of the speed of sound and the density of mass can easily be accounted for by additional contrast sources.

Attenuation is introduced by giving the medium a certain relaxation behavior, which may also depend on position (Demi et al., 2011). In this way, very realistic biomedical loss models can be employed. The relaxation function is written as (cf. eqn [28])

$$m(\boldsymbol{x},t) = \delta(t) + A(\boldsymbol{x},t) \qquad [187]$$

Substitution into eqn [29] yields

$$\nabla^2 p(\boldsymbol{x},t) - \frac{1}{c_0^2}\frac{\partial^2 p(\boldsymbol{x},t)}{\partial t^2} = -S_{\text{at}}[p(\boldsymbol{x},t)] \qquad [188]$$

with

$$S_{\text{at}}[p(\boldsymbol{x},t)] = -\frac{1}{c_0^2}\frac{\partial^2}{\partial t^2}[A(\boldsymbol{x},t) *_t p(\boldsymbol{x},t)] \qquad [189]$$

This is a contrast source that will account for the attenuation of the ultrasound wave.

Heterogeneity of the speed of sound and the density of mass is introduced by replacing c_0 by $c_0(\boldsymbol{x})$ and ρ_0 by $\rho_0(\boldsymbol{x})$.

These changes are applied to eqns [180] and [189] in a straightforward manner. Further consequences for the right-hand side of eqn [179] may be assessed by making corresponding changes to eqns [18] and [19]. The equivalent of eqn [20] then becomes

$$\nabla^2 p - \frac{1}{c_0^2}\frac{\partial^2 p}{\partial t^2} = -S_{\mathrm{ss}}[p(\boldsymbol{x},t)] - S_{\mathrm{dm}}[p(\boldsymbol{x},t)] \qquad [190]$$

with

$$S_{\mathrm{ss}}[p(\boldsymbol{x},t)] = \left(\frac{1}{c_0^2} - \frac{1}{c_0^2(\boldsymbol{x})}\right)\frac{\partial^2 p(\boldsymbol{x},t)}{\partial t^2} \qquad [191]$$

$$S_{\mathrm{dm}}[p(\boldsymbol{x},t)] = -\frac{\nabla\rho(\boldsymbol{x})\cdot\nabla p(\boldsymbol{x},t)}{\rho(\boldsymbol{x})} \qquad [192]$$

These are the contrast sources that will account for the heterogeneity of the speed of sound and the density of mass.

The appearance of new contrast sources does not make the INCS method more complex because all contrast terms can just be added to form a total contrast source:

$$S_{\mathrm{cs}}[p(\boldsymbol{x},t)] = S_{\mathrm{nl}}[p(\boldsymbol{x},t)] + S_{\mathrm{at}}[p(\boldsymbol{x},t)] + S_{\mathrm{ss}}[p(\boldsymbol{x},t)] + S_{\mathrm{dm}}[p(\boldsymbol{x},t)] \qquad [193]$$

which may replace the original nonlinear contrast source. However, the extra terms can influence the convergence of the Neumann iterative solution.

2.19.5.5 Comparison between INCS and the *k*-Space Pseudospectral Method

It has been stated earlier that methods described in Section 2.19.4 can, with some extensions, be used to compute nonlinear ultrasound fields. Moreover, methods from Section 2.19.5 may, with some simplifications, be applied to simulate linear acoustic propagation. As a demonstration of the first statement, here, the *k*-space method and the IE method are both used to simulate nonlinear ultrasound fields. The applied methods are the *k*-space method as implemented in the k-Wave toolbox and applied to nonlinear propagation (Treeby et al., 2012b) and the INCS method (Demi et al., 2011). Both methods, although being quite different, use no approximations apart from those related to the discretization of the problem. In particular, both methods are able to compute in an omnidirectional manner the nonlinear ultrasound field in a heterogeneous medium with frequency-dependent attenuation. These facts allow for accurate comparisons between both methods.

Two numerical comparisons between the INCS method and k-Wave are shown in Figures 17 and 18. The plots in both panels (a) are based on the maximum of the computed total time-domain signal for a given location. The plots in each of the panels (b), (c), and (d) show the maxima of the time-

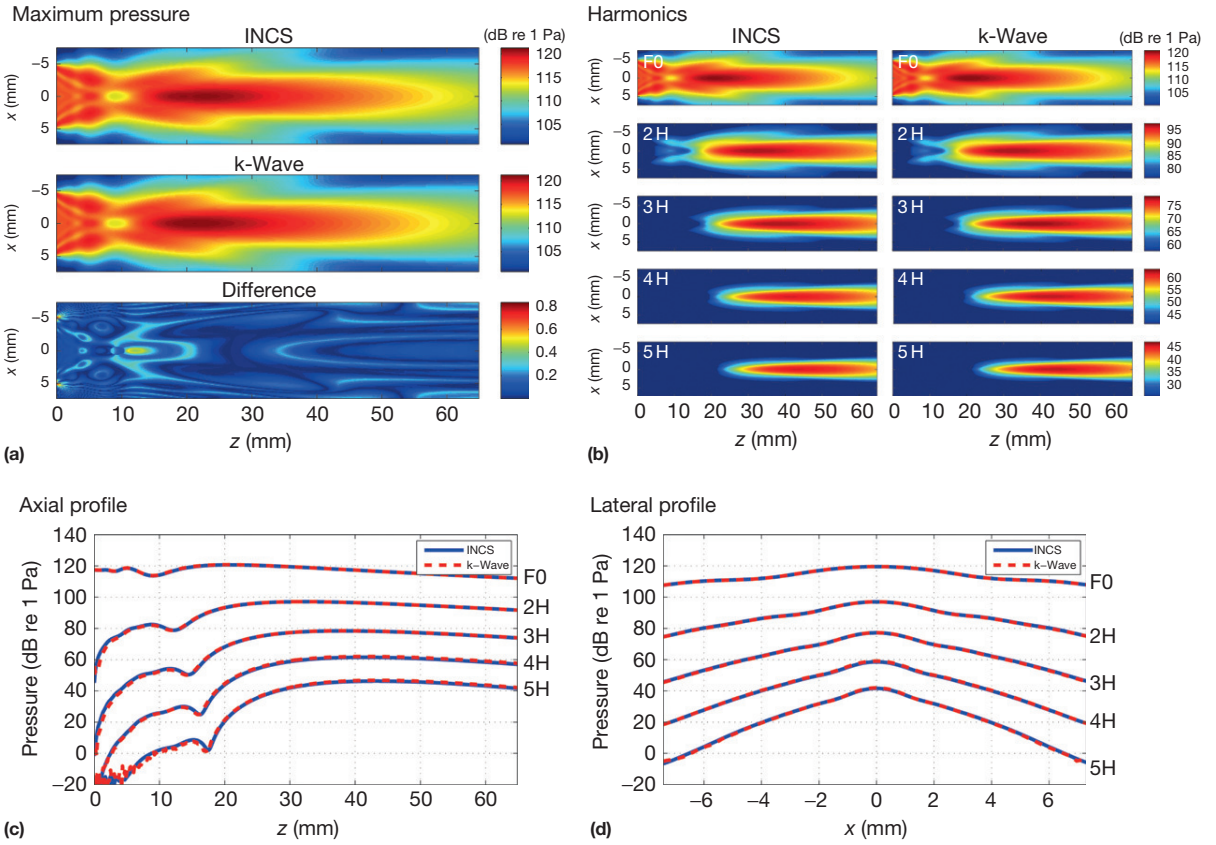

Figure 17 Comparison between INCS and k-Wave for a simulation in a homogeneous, nonlinear, and attenuating medium. (a) Maximum pressure in the central *x*–*z* plane. (b) Maximum pressure at the first five harmonics in the central *x*–*z* plane. (c) Maximum pressure at the first five harmonics along the source axis. (d) Maximum pressure at the first five harmonics in the lateral direction through the peak of the wave field. In panels (a) and (b), the piston transducer is located at the left side between $x = -5$ mm and $x = 5$ mm.

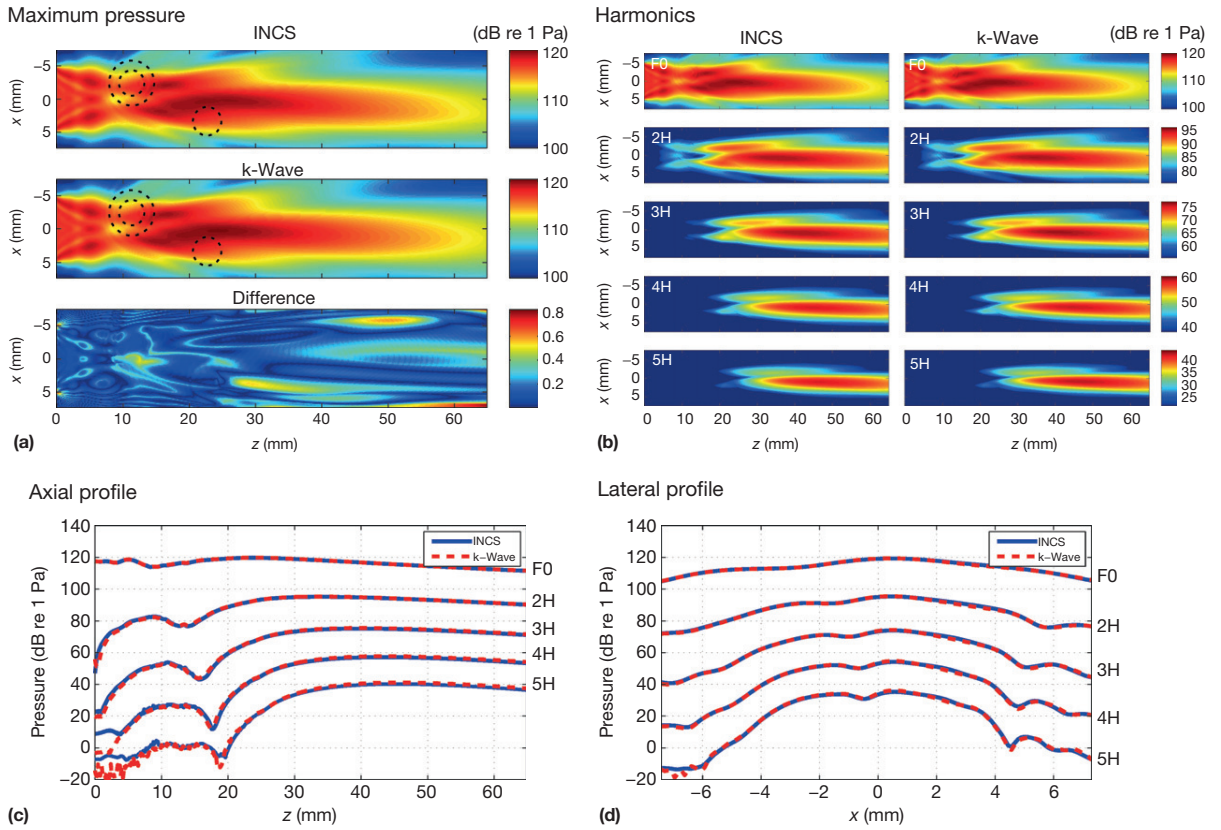

Figure 18 Comparison between INCS and k-Wave for a simulation in a heterogeneous, nonlinear, and attenuating medium. (a) Maximum pressure in the central x–z plane. (b) Maximum pressure at the first five harmonics in the central x–z plane. (c) Maximum pressure at the first five harmonics along the source axis. (d) Maximum pressure at the first five harmonics in the lateral direction through the peak of the wave field. The heterogeneities are indicated in panel (a) by dashed circles. In panels (a) and (b), the piston transducer is located at the left side between $x=-5$ mm and $x=5$ mm.

domain signals related to the separate harmonics that are present at a certain position. These harmonics are extracted from the computed total time-domain signal by applying numerical band-pass filters. The simulations were done in such a way that five harmonics could be extracted. This is, for instance, required when dealing with superharmonic imaging (Van Neer et al., 2011). In both simulations and for both methods, the computational domain was set to $160\times160\times600$ grid points with a grid point spacing (i.e., sampling interval) in each Cartesian direction of 114 μm. At the Nyquist limit of two grid points per wavelength, this corresponds to a maximum supported frequency of 6.5 MHz for a medium with a speed of sound $c_0=1482\ \mathrm{m\,s^{-1}}$ as mostly used in the comparisons. The source was defined as a volume injection source in the shape of a square piston facing in the z-direction and covering 87×87 grid points. The source signal was defined as a Gaussian-modulated tone burst:

$$p_{\mathrm{source}}=P_0\exp\left[-\left(\frac{2t}{t_{\mathrm{w}}}\right)^2\right]\sin\left(2\pi f_0 t\right) \qquad [194]$$

with a source amplitude $P_0=750$ kPa, source frequency $f_0=1$ MHz, and tone-burst length of $t_{\mathrm{w}}=3/f_0$.

For the first comparison, shown in Figure 17, a homogeneous, attenuative, and nonlinear medium was considered with a speed of sound $c_0=1482\ \mathrm{m\,s^{-1}}$, density of mass $\rho_0=1000\ \mathrm{kg\,m^{-3}}$, nonlinearity parameter $B/A=4.96$ (equal to a coefficient of nonlinearity $\beta=3.48$), and power-law attenuation of the form $\alpha=\alpha_0 f^b$ with parameters $\alpha_0=0.75$ dB $\mathrm{MHz}^{-b}\,\mathrm{cm}^{-1}$ and $b=1.5$. For the INCS method, a comoving time window of 399 points was applied with two grid points per period at 6.5 MHz (implying a CFL = 1), and the Neumann scheme was used with six iterations to compute the numerical solution. For the k-Wave simulation, a comoving time window is not used (only the current time step is stored in memory), and a CFL = 0.25 was applied. Figure 17 shows that there is excellent qualitative and quantitative agreement between the two methods, and the maximum difference in the total field shown in Figure 17(a) is on the order of 0.8 dB.

For the second comparison, presented in Figure 18, two objects with contrasting material properties were included in the previously described medium. These objects are a hollow cylinder and a sphere and are indicated in Figure 18 by dashed circles. The contrasting property of the hollow cylinder was its speed of sound of $1540\ \mathrm{m\,s^{-1}}$, while the ball had a nonlinearity parameter of $B/A=0$ (equal to a coefficient of nonlinearity of $\beta=1$) and power-law attenuation parameters of $\alpha_0=1.50$ dB $\mathrm{MHz}^{-b}\,\mathrm{cm}^{-1}$ and $b=1.5$. Other parameters were matched to the background medium parameters used in the first comparison. For the INCS method, a comoving time window of 709 points was used with an implied CFL = 1, and the Neumann scheme was used with 13 iterations to compute

the numerical solution. For the k-Wave simulation, a CFL = 0.25 was again applied. Figure 18 shows that there is again excellent qualitative and quantitative agreement between the two methods.

Both comparisons show that the applied methods are quite able to simulate nonlinear ultrasound propagation in media with tissue-realistic attenuation and, as demonstrated by the second comparison, that both methods can do so for media having heterogeneous medium parameters. Moreover, numerical confidence in both methods is established from the observation that although the methods are computationally quite different, the results are in excellent agreement.

In conclusion, the current availability of computer power and advanced simulation methods have already brought great possibilities for simulating ultrasound wave fields in realistic biological media. On the other hand, there are many aspects that are not yet fully addressed (shear waves in bone, media with contrast bubbles, multiphase media, etc.) and that open up opportunities for further research in the field of numerical simulation of medical ultrasound.

References

Aanonsen SI, Barkve T, Naze Tjøtta J, and Tjøtta S (1984) Distortion and harmonic generation in the nearfield of a finite amplitude sound beam. *Journal of the Acoustical Society of America* 75: 749–768.

Aubry J-F, Tanter M, Pernot M, Thomas J-L, and Fink M (2003) Experimental demonstration of noninvasive transskull adaptive focusing based on prior computed tomography scans. *Journal of the Acoustical Society of America* 113: 84–93.

Baker AC, Berg AM, Sahin A, and Naze Tjøtta J (1995) The nonlinear pressure field of plane, rectangular apertures: Experimental and theoretical results. *Journal of the Acoustical Society of America* 97: 3510–3517.

Baker AC and Humphrey VF (1992) Distortion and high-frequency generation due to nonlinear propagation of short ultrasonic pulses from a plane circular piston. *Journal of the Acoustical Society of America* 92: 1699–1705.

Bamber JC (1998) Ultrasonic properties of tissues. In: Duck FA, Baker AC, and Starritt HC (eds.) *Ultrasound in Medicine*, pp. 57–88. Bristol, UK: Institute of Physics Publishing.

Bamber JC (2004) Attenuation and absorption. In: Hill CR, Bamber JC, and Ter Haar GR (eds.) *Physical Principles of Medical Ultrasound*, 2nd ed., pp. 118–199. Chichester, UK: Wiley.

Barton G (1995) *Elements of Green's Functions and propagation – Potentials, Diffusion and Waves*. New York, NY: Oxford University Press.

Bérenger J-P (1994) A perfectly matched layer for the absorption of electromagnetic waves. *Journal of Computational Physics* 114: 185–200.

Bérenger J-P (2007) Perfectly matched layer (PML) for computational electromagnetics. In: Balanis CA (ed.) *Synthesis Lectures on Computational Electromagnetics*, vol. 2, pp. 1–117. San Rafael, CA: Morgan and Claypool.

Bojarski NN (1982) The k-space formulation of the scattering problem in the time domain. *Journal of the Acoustical Society of America* 72: 570–584.

Bojarski NN (1985) The k-space formulation of the scattering problem in the time domain: An improved single propagator formulation. *Journal of the Acoustical Society of America* 77: 826–831.

Boyd JP (2001) *Chebyshev and Fourier Spectral Methods*. Mineola, NY: Dover Publications.

Charney JG, Fjörtoft R, and Neumann JV (1950) Numerical integration of the barotropic vorticity equation. *Tellus* 2: 237–254.

Christopher PT and Parker KJ (1991a) New approaches to nonlinear diffractive field propagation. *Journal of the Acoustical Society of America* 90: 488–499.

Christopher PT and Parker KJ (1991b) New approaches to the linear propagation of acoustic fields. *Journal of the Acoustical Society of America* 90: 507–521.

Cleveland RO, Hamilton MF, and Blackstock DT (1996) Time-domain modeling of finite-amplitude sound in relaxing fluids. *Journal of the Acoustical Society of America* 99: 3312–3318.

Cobbold RSC (2007) *Foundations of Biomedical Ultrasound*. New York, NY: Oxford University Press.

Courant R, Friedrichs K, and Lewy H (1967) On the partial difference equations of mathematical physics. *IBM Journal of Research and Development* 11: 215–234.

De Hoop AT (1995) Handbook of Radiation and Scattering of Waves. London, UK: Academic Press. (http://www.atdehoop.com).

Demi L (2013) Modeling Nonlinear Propagation of Ultrasound through Inhomogeneous Biomedical Media, PhD Thesis Delft University of Technology (http://www.repository.tudelft.nl).

Demi L, Van Dongen KWA, and Verweij MD (2011) A contrast source method for nonlinear acoustic wave fields in media with spatially inhomogeneous attenuation. *Journal of the Acoustical Society of America* 129: 1221–1230.

Duck FA (1990) *Physical Properties of Tissue*. London, UK: Academic Press.

FOCUS Quick Start Guide (2013) Michigan State University, August 27, 2013. (http://www.egr.msu.edu/~fultras-web).

Fokkema JT and Van den Berg PM (1993) *Seismic Applications of Acoustic Reciprocity*. Amsterdam, The Netherlands: Elsevier.

Fornberg B (1988) Generation of finite difference formulas on arbitrarily spaced grids. *Mathematics of Computation* 51: 699–706.

Fornberg B (1996) *A Practical Guide to Pseudospectral Methods*. Cambridge: Cambridge University Press.

Fox PD, Bouakaz A, and Tranquart F (2005) Computation of steered nonlinear fields using offset KZK axes. In: Proceedings of the IEEE Ultrasonics Symposium, pp. 1984–1987. IEEE.

Frijlink ME, Kaupang H, Varslot T, and Måsøy S-E (2008) Abersim: A simulation program for 3D nonlinear acoustic wave propagation for arbitrary pulses and arbitrary transducer geometries. In: Proceedings of the IEEE Ultrasonics Symposium, pp. 1282–1285. IEEE.

Gélat P, Ter Haar G, and Saffari N (2011) Modelling of the acoustic field of a multi-element HIFU array scattered by human ribs. *Physics in Medicine and Biology* 56: 5553–5581.

Ginsberg JH (2008) Perturbation methods. In: Hamilton MF and Blackstock DT (eds.) *Nonlinear Acoustics*, pp. 279–308. Melville, NY: Acoustical Society of America.

Ginsberg JH and Hamilton MF (2008) Computational methods. In: Hamilton MF and Blackstock DT (eds.) *Nonlinear Acoustics*, pp. 309–341. Melville, NY: Acoustical Society of America.

Ginter S, Liebler M, Steiger E, Dreyer T, and Riedlinger RE (2002) Full-wave modeling of therapeutic ultrasound: Nonlinear ultrasound propagation in ideal fluids. *Journal of the Acoustical Society of America* 111: 2049–2059.

Gottlieb D and Hesthaven JS (2001) Spectral methods for hyperbolic problems. *Journal of Computational and Applied Mathematics* 128: 83–131.

Hallaj IM and Cleveland RO (1999) FDTD simulation of finite-amplitude pressure and temperature fields for biomedical ultrasound. *Journal of the Acoustical Society of America* 105: L7–L12.

Hamilton MF and Blackstock DT (eds.) (2008) *Nonlinear Acoustics*. Melville, NY: Acoustical Society of America.

Hamilton MF and Morfey CL (2008) Model equations. In: Hamilton MF and Blackstock DT (eds.) *Nonlinear Acoustics*, pp. 41–63. Melville, NY: Acoustical Society of America.

Harris GR (1981) Review of transient field theory for a baffled planar piston. *Journal of the Acoustical Society of America* 70: 10–20.

Hesthaven JS, Gottlieb S, and Gottlieb D (2007) *Spectral Methods for Time-Dependent Problems*. Cambridge, UK: Cambridge University Press.

Hoffelner J, Landes H, Kaltenbacher M, and Lerch R (2001) Finite element simulation of nonlinear wave propagation in thermoviscous fluids including dissipation. *IEEE Transactions on Ultrasonics, Ferroelectrics, and Frequency Control* 48: 779–786.

Huang D-H, Liao C-K, Wei C-W, and Li P-C (2005) Simulations of optoacoustic wave propagation in light-absorbing media using a finite-difference time-domain method. *Journal of the Acoustical Society of America* 117: 2795–2801.

Huijssen J (2008) Modeling of Nonlinear Medical Diagnostic Ultrasound. PhD Thesis, Delft University of Technology. (http://www.repository.tudelft.nl).

Huijssen J and Verweij MD (2010) An iterative method for the computation of nonlinear, wide-angle, pulsed acoustic fields of medical diagnostic transducers. *Journal of the Acoustical Society of America* 127: 33–44.

Huijssen J, Verweij MD, and De Jong N (2008) Green's function method for modeling nonlinear three dimensional pulsed acoustic fields in diagnostic ultrasound including tissue-like attenuation. In: Proceedings of the IEEE Ultrasonics Symposium, pp. 375–378. IEEE.

Jensen JA (1991) A model for the propagation and scattering of ultrasound in tissue. *Journal of the Acoustical Society of America* 89: 182–190.

Jensen JA (1999) A new calculation procedure for spatial impulse responses in ultrasound. *Journal of the Acoustical Society of America* 105: 3266–3274.

Jensen JA (2001) Speed-accuracy trade-offs in computing spatial impulse responses for simulating medical ultrasound imaging. *Journal of Computational Acoustics* 9: 731–744.

Jensen JA (2011) Users' guide for the Field II program – Release 3.20, (http://field-ii.dk).

Jensen JA, Gandhi D, and O'Brien WD (1993) Ultrasound fields in an attenuating medium. *Proceedings of the IEEE Ultrasonics Symposium*, vol. 2, pp. 943–946. IEEE.
Jensen JA and Nikolov SI (2000) Fast simulation of ultrasound images. In: Proceedings of the IEEE Ultrasonics Symposium, pp. 1721–1724. IEEE.
Jensen JA and Svendsen NB (1992) Calculation of pressure fields from arbitrarily shaped, apodized, and excited ultrasound transducers. *IEEE Transactions on Ultrasonics, Ferroelectrics, and Frequency Control* 39: 262–267.
Kamakura T, Ishiwata T, and Matsuda K (2000) Model equation for strongly focused finite-amplitude sound beams. *Journal of the Acoustical Society of America* 107: 3035–3046.
Karamalis A, Wein W, and Navab N (2010) Fast ultrasound image simulation using the Westervelt equation. In: Jiang T, Navab N, Pluim JPW, and Viergever MA (eds.) *MICCAI 2010, Part I. Lecture Notes in Computer Science*, vol. 6361, pp. 243–250. Heidelberg, Germany: Springer-Verlag.
Kelly JF and McGough RJ (2006) A time–space decomposition method for calculating the nearfield pressure generated by a pulsed circular piston. *IEEE Transactions on Ultrasonics, Ferroelectrics, and Frequency Control* 53: 1150–1159.
Kleinman RE and Van den Berg PM (1991) Iterative methods for solving integral equations. *Radio Science* 26: 175–181.
Lee Y-S and Hamilton MF (1995) Time-domain modeling of pulsed finite-amplitude sound beams. *Journal of the Acoustical Society of America* 97: 906–917.
Lee D and Pierce AD (1995) Parabolic equation development in recent decade. *Journal of Computational Acoustics* 3: 95–173.
Lines LR, Slawinski R, and Bording RP (1999) A recipe for stability of finite-difference wave-equation computations. *Geophysics* 64: 967–969.
Manry CW and Broschat SL (1996) FDTD simulations for ultrasound propagation in a 2-D breast model. *Ultrasonic Imaging* 18: 25–34.
Mast TD (2000) Empirical relationships between acoustic parameters in human soft tissues. *Acoustics Research Letters* 1: 37–42.
Mast TD, Hinkelman LM, Orr MJ, Sparrow VW, and Waag RC (1997) Simulation of ultrasonic pulse propagation through the abdominal wall. *Journal of the Acoustical Society of America* 102: 1177–1190.
McGough RJ (2004) Rapid calculations of time-harmonic nearfield pressures produced by rectangular pistons. *Journal of the Acoustical Society of America* 115: 1934–1941.
McGough RJ, Samulski TV, and Kelly JF (2004) An efficient grid sectoring method for calculations of the near-field pressure generated by a circular piston. *Journal of the Acoustical Society of America* 115: 1942–1954.
Nachman AI, Smith JF, and Waag RC (1990) An equation for acoustic propagation in inhomogeneous media with relaxation losses. *Journal of the Acoustical Society of America* 88: 1584–1595.
Nassiri DK and Hill CR (1986) The differential and total bulk scattering acoustic cross sections of some human and animal tissues. *Journal of the Acoustical Society of America* 79: 2034–2047.
O'Donnell M, Janes ET, and Miller JG (1981) Kramers-Kronig relationship between ultrasonic attenuation and phase velocity. *Journal of the Acoustical Society of America* 69: 696–701.
Pierce AD (1989) *Acoustics: An Introduction to Its Physical Principles and Applications*. Woodbury, NY: Acoustical Society of America.
Pinton GF, Dahl J, Rosenzweig S, and Trahey GE (2009) A heterogeneous nonlinear attenuating full-wave model of ultrasound. *IEEE Transactions on Ultrasonics, Ferroelectrics, and Frequency Control* 56: 474–488.
Qi Q and Geers TL (1998) Evaluation of the perfectly matched layer for computational acoustics. *Journal of Computational Physics* 139: 166–183.
Rayleigh JWS (1945) *The Theory of Sound*, vol. 2: New York, NY: Dover Publications.
Sacks ZS, Kingsland DM, Lee R, and Lee JF (1995) A perfectly matched anisotropic absorber for use as an absorbing boundary condition. *IEEE Transactions on Antennas and Propagation* 43: 1460–1463.
Sparrow VW and Raspet R (1991) A numerical method for general finite amplitude wave propagation in two dimensions and its application to spark pulses. *Journal of the Acoustical Society of America* 90: 2683–2691.
Stepanishen PR (1971) Transient radiation from pistons in an infinite planar baffle. *Journal of the Acoustical Society of America* 49: 1629–1638.
Strikwerda J (2004) *Finite Difference Schemes and Partial Differential Equations*. Philadelphia, PA: SIAM.
Szabo TL (1995) Causal theories and data for acoustic attenuation obeying a frequency power law. *Journal of the Acoustical Society of America* 97: 14–24.
Tabei M, Mast TD, and Waag RC (2002) A k-space method for coupled first-order acoustic propagation equations. *Journal of the Acoustical Society of America* 111: 53–63.
Tavakkoli J, Cathignol D, Souchon R, and Sapozhnikov OA (1998) Modeling of pulsed finite-amplitude focused sound beams in time domain. *Journal of the Acoustical Society of America* 104: 2061–2072.
Temkin S (2001) *Elements of Acoustics*. Melville, NY: Acoustical Society of America.
Thomas JW (2010) *Numerical Partial Differential Equations: Finite Difference Methods*. New York: Springer-Verlag.
Treeby BE and Cox BT (2010a) k-Wave: MATLAB toolbox for the simulation and reconstruction of photoacoustic wave fields. *Journal of Biomedical Optics* 15: 021314-1–021314-12.
Treeby BE and Cox BT (2010b) Modeling power law absorption and dispersion for acoustic propagation using the fractional Laplacian. *Journal of the Acoustical Society of America* 127: 2741–2748.
Treeby BE, Cox BT, and Jaros J (2012a) *k-Wave—A MATLAB Toolbox for the Time Domain Simulation of Acoustic Wave Fields: User Manual*. (http://www.k-wave.org).
Treeby BE, Jaros J, Rendell AP, and Cox BT (2012b) Modeling nonlinear ultrasound propagation in heterogeneous media with power law absorption using a k-space pseudospectral method. *Journal of the Acoustical Society of America* 131: 4324–4336.
Treeby BE, Zhang EZ, Thomas AS, and Cox BT (2011) Measurement of the ultrasound attenuation and dispersion in whole human blood and its components from 0–70 MHz. *Ultrasound in Medicine and Biology* 37: 289–300.
Van Neer PMLJ, Danilouchkine MG, Verweij MD, et al. (2011) Comparison of fundamental, second harmonic, and superharmonic imaging: A simulation study. *Journal of the Acoustical Society of America* 130: 3148–3157.
Varslot T and Måsøy S-E (2006) Forward propagation of acoustic pressure pulses in 3D soft biological tissue. *Modeling, Identification and Control* 27: 181–200.
Varslot T and Taraldsen G (2005) Computer simulation of forward wave propagation in soft tissue. *IEEE Transactions on Ultrasonics, Ferroelectrics, and Frequency Control* 52: 1473–1482.
Verweij MD (1995) Modeling space-time domain acoustic wave fields in media with attenuation: The symbolic manipulation approach. *Journal of the Acoustical Society of America* 97: 831–843.
Verweij MD, Demi L, and Van Dongen KWA (2013) Computation of nonlinear ultrasound fields using a linearized contrast source method. *Journal of the Acoustical Society of America* 134: 1442–1453.
Verweij MD and Huijssen J (2009) A filtered convolution method for the computation of acoustic wave fields in very large spatiotemporal domains. *Journal of the Acoustical Society of America* 125: 1868–1878.
Wells PNT (1975) Absorption and dispersion of ultrasound in biological tissue. *Ultrasound in Medicine and Biology* 1: 369–376.
Westervelt PJ (1963) Parametric acoustic array. *Journal of the Acoustical Society of America* 35: 535–537.
Wojcik G, Fornberg B, Waag R, et al. (1997) Pseudospectral methods for large-scale bioacoustic models. In: Proceedings of the IEEE Ultrasonics Symposium, pp. 1501–1506. IEEE.
Yang X and Cleveland RO (2005) Time domain simulation of nonlinear acoustic beams generated by rectangular pistons with application to harmonic imaging. *Journal of the Acoustical Society of America* 117: 113–123.
Yano T and Inoue Y (1996) Strongly nonlinear waves and streaming in the near field of a circular piston. *Journal of the Acoustical Society of America* 96: 3353–3372.
Yee K (1966) Numerical solution of initial boundary value problems involving Maxwell's equations in isotropic media. *IEEE Transactions on Antennas and Propagation* 14: 302–307.
Yuan X, Borup D, Wiskin J, Berggren M, and Johnson SA (1999) Simulation of acoustic wave propagation in dispersive media with relaxation losses by using FDTD method with PML absorbing boundary condition. *IEEE Transactions on Ultrasonics, Ferroelectrics, and Frequency Control* 46: 14–23.
Zemp RJ, Tavakkoli J, and Cobbold RSC (2003) Modeling of nonlinear ultrasound propagation in tissue from array transducers. *Journal of the Acoustical Society of America* 113: 139–152.
Zeng X and McGough RJ (2008) Evaluation of the angular spectrum approach for simulations of near-field pressures. *Journal of the Acoustical Society of America* 123: 68–76.

Relevant Websites

Field II – http://field-ii.dk.
FOCUS – http://www.egr.msu.edu/~fultras-web.
Handbook of Radiation and Scattering of Waves – http://www.atdehoop.com.
k-Wave – http://www.k-wave.org.
Repository Delft University of Technology – http://repository.tudelft.nl.